Development of Aqueous Quantum Dots and Hybrid Nanoparticles

by

Süleyman Sinan Öztürk

A Thesis Submitted to the
Graduate School of Engineering
in Partial Fulfillment of the Requirements for
the Degree of
Master of Science
in
Materials Science and Engineering
Koç University

September 2008

Koç University

Graduate School of Sciences and Engineering

This is to certify that I have examined this copy of a master's thesis by

Süleyman Sinan Öztürk

and have found that it is complete and satisfactory in all respects,
and that any and all revisions required by the final
examining committee have been made.

Committee Members:

_____

H.Funda Yağcı Acar, Ph. D. (Advisor)

_____

Mehmet Suat Somer, Ph. D.

_____

Alphan Sennaroğlu, Ph. D.

Date: _____

ABSTRACT

Nanoparticles are one of the major areas of nanotechnology where size confinement provided a dramatic differentiation in material properties enabling numerous applications for many disciplines. Among these superparamagnetic iron oxides and semiconductor quantum dots are possibly the most widely studied nanoparticles due to their great potential in broad application areas, most significantly in health, defense and energy. The target area for the nanoparticles described in this thesis is the biotechnology and medicine.

The premise of this thesis is to synthesize aqueous magnetic luminescent hybrid nanoparticles. To achieve such a goal, highly luminescent, water soluble and biocompatible colloidal CdS and CdTe QDs were synthesized first. Then, as prepared colloidal QD solution was used to coat and stabilize magnetic iron oxide nanoparticles in a unique, safe and economical one-pot reaction. The approach involves utilization of biocompatible multifunctional coating molecule, primarily L-cysteine, which can stabilize both nanoparticles and keep them in water simultaneously. The cell uptake and cell viability studies confirmed suitability for bio applications.

Development of such a multi-functional single entity will provide dual sensing modes (optical and magnetic detection) as well as combined sensing and separation capabilities.

ÖZET

Büyüklük sınırlamasının malzeme özelliklerine sağladığı dramatik değişiklikler nedeniyle nanoparçacıklar nanoteknolojinin ana konularından biri olmuştur. Bu yeni özellikler birçok disiplinde yeni teknolojinin gelişmesine olanak sağlamıştır. Bunların içinden en fazla çalışılanlar, geniş bir kullanım alanında özellikle sağlıkta, ulusal güvenlikte ve enerjide önemli potansiyele sahip olan süperparamanyetik demir oksitler ve yarı iletken kuantum noktacıklarıdır. Bu teze konu olan nanoparçacıkların hedef kullanım alanı biyoteknoloji ve tıp bilimidir.

Bu tezdeki öncül hedef manyetik ışıyan nano parçacıklar sentezlemektir. Bu hedefi mümkün kılmak için, ışıyan, suda asılı kalan ve biyo-uyumlu CdS ve CdTe nanoparçacıklar sentezlendi. Daha sonra, bu kolloidal kuantum noktacıkları ihtiva eden çözelti, manyetik demir oksit nanoparçacıklarını kaplamak ve kararlı hale getirmek için kullanıldı. Bu işlem biyo-uyumlu, öncelikle L-sistin gibi çok fonksiyonlu, her iki tip nanoparçacığı da kaplayabilecek özellikte moleküller kullanılarak başarıldı. Bu sayede manyetik ve ışıyan hibrid nanoparçacıklar kararlı ve suda asılı hale getirildi. Parçacıkların hücre içi alım ve hücre toksisitesi araştırmaları, bu parçacıkların biyolojik uygulamalar için elverişli olduğunu gösterdi.

Manyetik alanda taşınabilen ve optik ve manyetik yöntemlerle tanınabilen çok fonksiyonlu parçacıklar bu sayede üretilmiştir.

ACKNOWLEDGEMENTS

I will do my best to make this thesis as just as possible. I have not walked alone in this path leading to a success story and I fell lucky whoever opened their generous heart in my way. From the beginning, my family has supported me most of all. My mother and father always were a good friend and parent that a child can not ask for more. I will be their last and most satisfactory child that transfers the inherited kindness to posterity. My eldest sister Yasemin Şen is like my personality coach and supported me most by financial aids. Nilgün Ersoy was more like a second mother in my life who loved me with a precious smile. My little sister Gül Vardar calmed me in my ambiguous moments and provided her best without any doubts. I should also admit that my love Zilha is nothing but my family. She has never failed to love and forgive.

The results presented in here can not be possible without the hard work of my colleagues. Without any doubts, my graduated lab-mate Serdar Çelebi, the father of many implementations in the laboratory, was so generous in helping my projects. We have clashed ideas almost everyday with victorious results for both sides, at the end we have learned too many from each other in a limited time.

My life in Nanomaterials and Polymers Laboratory has never been as colorful as before with people shaped my life. It is impossible to pay my dues to my cheerful friends who have enriched my career and brightened my days when everything was ordinary. It was very enjoyable to have fun in our most desperate time when we were lost in the edge of long and hard cliffs. At the moment, I should admit that Muharrem Güler was more like

a Master of Experience in the technical difficulties with endless endurance. Without him, the bureaucracy will burden to achieve simple solutions. The main credits are deserved by Recep Kaş, a unique personality who is very open to improve his knowledge. However I never treat him the way he deserves, he helped to cheer my motivation every time. My office partners Bilinç Barçın, Ceren Yılmaz and Esra Sevinç created such an atmosphere with their rare sense of humor. Our fun screams from the lab always created curiosities for the outsiders. Although we were like competing each time, we never forget the fact that we were on the same side at least against corrupted personalities. I have found little chance to deepen my knowledge from Gökhan Çaylı who has incredibility fast adapted to our fun tech laboratory. I really enjoyed the time I shared and spent in the laboratory.

My life for the last seven years has largely shaped by my KU friends; Ilkin Kokal, Kamil Kiraz and Semih Afyon. These people might not come together again with such a combination full of memories to share. It is always hard to find real friends that you will call them as “the king”. Behind the curtains has never been so clear and realistic when I spend times with these people and I hope to have a lifelong friendship.

I must also thank to other members of inorganic department who helped me in utilizing my measurements. Selçuk Acar, a very famous personality who is full of enjoy that deserves more than he has. Atilla Aşar will be remembered by his everlasting luck. It is always appreciated that somebody cares about what you have done at weekends. Cevriye Koz taught me that there is always a brighter side in life and when people are appraised, life is easier. Ali Baş, Ahmet Topçu and Zeliha Şentürk were always been there when help was needed.

Mehmet Somer was of course the most important faculty member who is hard to forget. He acted his beloved students more like a friend and it was very valuable to have a cup of coffee with him. The simplistic way of looking into a sophisticated life and sophisticated conversation about a simple soccer game will be remembered forever.

I am also grateful to my instructors and professors who provided me essential and important concepts during my stay at Koç. I would like to thank for their contributions on my thesis especially Feyza Selçuk on her help in the toxicology studies, Emel Yılgör for using FT-IR instrument once to collect data when needed, Hüseyin Çankaya and his coworkers in Laser photonics laboratory for providing me the keys to collect absorption spectra data, Can Özen from METU for using microscopy, Ingo Lieberwirt from Max-Planck Institute in Mainz for TEM images, Levent Demirel for opening the wide range possibilities in his laboratory and Durata Haciu for cheering my motivation every time.

I do respect to my professor Funda Acar who made this thesis possible. She has never given up on us and watched over our every individual problem. We do like her even she pushed us really hard. The deep sorrow of my heart will never cheer up again because I will never find a coach with full of patience to perform my sarcastic sense of humor.

I also would like to thank all the people that I shared informal conversations in social event activities about my thesis.

Finally, I would like to thank God, the Almighty, for having made everything possible with all the blessing and courage, He has given me.

TABLE OF CONTENTS

LIST OF TABLES

LIST OF FIGURES

NOMENCLATURE

m_e	effective mass of electron
m_h	effective mass of hole
E_g	band gap energy
h	Planck constant
$\Psi(x)$	wavefunction
$V(x)$	varying potential
E^*_{Ry}	effective Rydberg energy
CdS	cadmium sulfide
CdTe	cadmium telluride
-COOH	carboxylic acid group
-SH	thiol group
R_3PE	organophosphine chalcogenides
TMS_2E	bistrimethylsilylchalcogenides
TOPO	trioctylphophine oxide
PVP	polyvinylpyrrolidone
PEG	polyethylene glycol
PAA	poly(acrylic acid)
PVA	poly(vinyl alcohol)

MAA	mercaptoacetic acid
DLS	dynamic light scattering
PLGA	poly(lactic-co-glycolic acid)
FDA	Food and Drug Administration
QDs	quantum dots
MNs	magnetic nanoparticles
DMSA	dimercapto succinic acid
TGA	thioglycolic acid
pH	the potential hydronium ion concentration
IPA	isopropyl alcohol
EBR	electron Bohr radius
SPIONs	superparamagnetic iron oxide nanoparticles
Fe_3O_4	iron oxide (magnetite)
γ-Fe_2O_3	iron oxide (maghemite)
FT-IR	Fourier transform infrared
FWHM	full width at half maximum
UV-Vis-NIR	ultraviolet visible near infrared
TEM	transmission electron microscopy
p-XRD	powder x-ray diffraction
Nd:YAG	neodymium-doped yttrium aluminium garnet
DAPI	4’,6-diamidino-2-phenylindole filter

MRI	magnetic resonance imaging
K_{sp}	solubility constant
N_{QD}	number of quantum dots
nm	nanometer
ζ	zeta-potential
PL	photoluminescence
QY	quantum yield
VSM	vibrating sample magnetometer
ZFC/FC	zero field cooled/field cooled
Oe	Oersted
XPS	X-ray photoelectron spectroscopy
ICP	inductively coupled plasma
V_m	molar volume of solid
D	diffusion coefficient of monomer
$[M]_{bulk}$	monomer concentration in the bulk of solution
C^0_{flat}	solubility of bulk material
γ	specific surface energy of particle
$k_g{}^{flat}$	rate constant for the growth of a flat surface

Chapter 1

INTRODUCTION

1.1 What is a quantum dot?

After the invention of the transistors in 1947 at Bell Laboratories, transistors have played an important role in the technological revolution. As Richard P. Feynman has stated at the annual meeting of the American Physical Society at the California Institute of Technology on December 29th, 1959, "There's plenty of room at the bottom". In his speech, he pointed out the nanotechnology and in 60 years period we have witnessed the production of 45nm transistors.

Nano-revolution which has been ruled by nanocrystalline materials has developed into a large field in material science. Their unique physical and chemical properties which differ from those of the bulk materials have been investigated since early 80's. These special properties of nanostructures can be explained in terms of two characteristics:

Firstly, the surface to volume ratio of nanomaterials is higher than that of bulk solid. To visualize the situation we can consider a cube with 4 atoms in each dimension. The number of atoms at the surface is 88 % of the total number of atoms in the structure whereas, when we have 8 atoms in each dimension, the percentage of the surface atom decreases to 58%. The physical and chemical properties are different at small scale due to the formation of defects in the structure. For example, melting point of nanoparticles is lower than that of bulk material due to a lower cohesive energy [1, 2]. Another example is the color of the nano gold particles with red color rather than yellow [3].

Secondly, the quantum mechanics is different. The wave character of the electron restricts electronic motion into discrete energy states rather than a continuum in case of nanoparticles. The forbidden energy levels are stated as band gap which is a distinguishing property of bulk materials lies in between the valance band and the conduction band. Electrons allocated in the valance band jumps to the conduction band with an external stimulus such as heat, voltage, or a photon by leaving a positive hole in the valance band. The excited electron and the positively charged hole are taken as a pair called *the exciton*. In bulk semiconductors, the electron stays momentarily in the conduction band before falling down to the valance band (Figure 1. 1). Since the band gap of the bulk material is fixed, the resulting emission frequency is also a fixed value. The distance between the excited electron and the hole is called as *Exciton Bohr Radius (EBR)* which is also the smallest radius for a quantum dot having a continuous energy bands. Table 1.1 summarizes the band gap energy and corresponding absorbance cutoff limit for the fluorescent nanoparticles. When the size of the crystal is as small as the EBR, the energy states are quantized and no longer continuous which is referred as the *quantum confinement*. QDs differentiate from the bulk material with the quantum confinement effect. The exciton behaves like free particles in the vacuum to the applied field with different mass which is called as the *effective mass* (m_e, in the units of the mass of an electron).

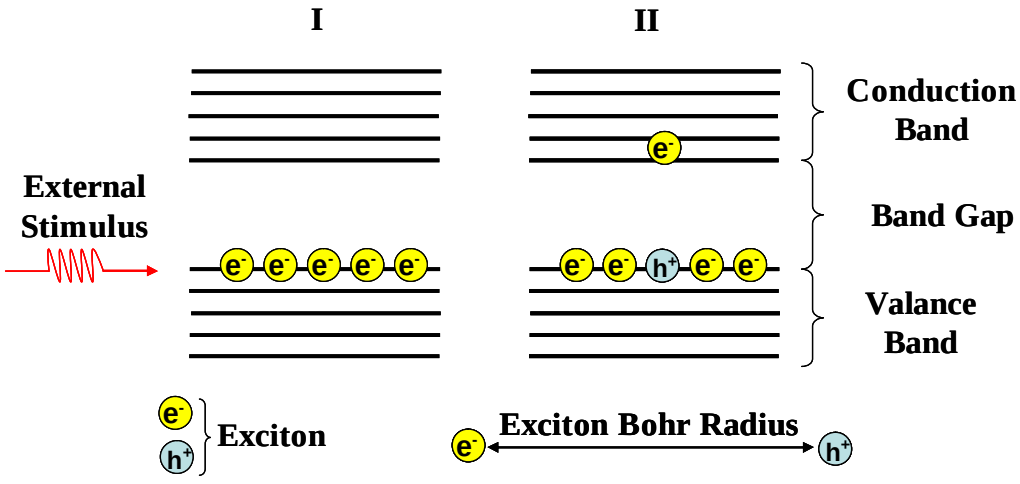

Figure 1. 1 Semiconductor band theory.[4]

Table 1. 1 Band gap and cutoff emission limit of some nanoparticles [5].

Semiconductors	Band-gap energy (eV)	Approximated bulk threshold wavelength (nm)
Si	1.12	1107
Ge	0.66	1879
CdS	2.42	512
CdSe	2.70	729
CdTe	1.50	827
ZnS	3.20	388
ZnSe	2.58	481
PbS	0.50	2480
HgS	0.50	2480
HgTe	0.14	8857
GaAs	1.43	867

The spatial confinement of nanoparticles occurs in three dimensions which produce two, one and zero dimensional shapes (Figure 1. 2). Three dimensional confinement leads to quantum dots, two dimensional confinement produces quantum wires and finally one dimensional confinement leads to quantum wells. When we look for the density of states for the corresponding confinements, each produces a non-continuous function. The density of state is a step function for quantum wells and a series of quantized values for the quantum dots. On the other hand, quantum wire has an intermediate density of state function compared to quantum wells and quantum dots.

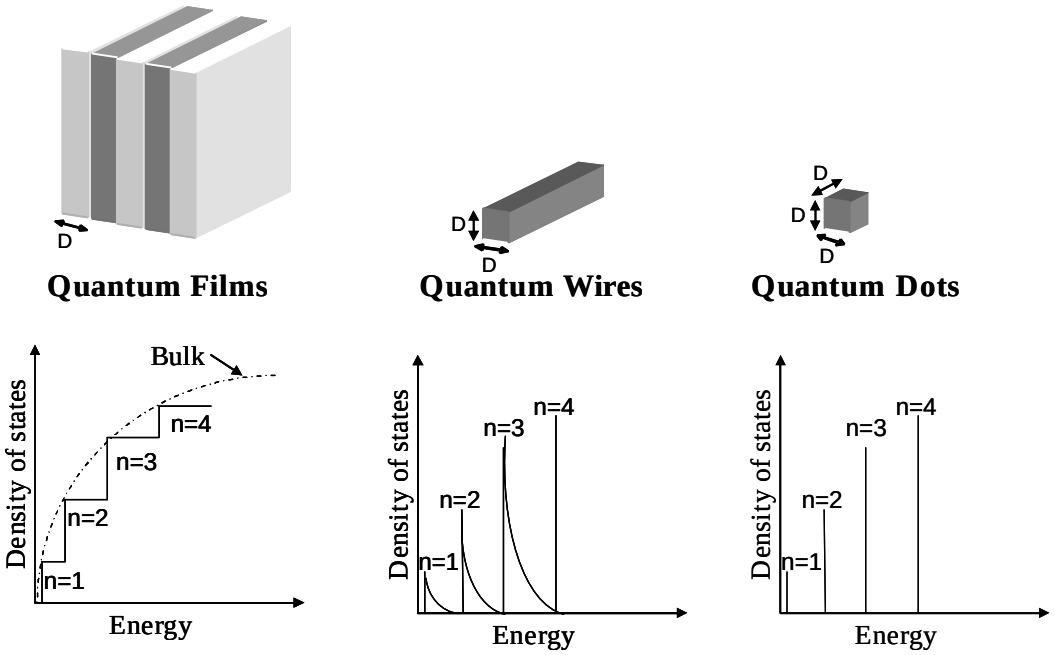

Figure 1. 2 Dimensional quantum confinements and its effect on density of states [6].

1.1.1 Size tunable optical properties

The band gap of a quantum dot is a size dependent property which is larger than the band gap of the bulk material. When the nanoparticles get smaller, the band gap becomes more pronounceable with respect to the size of the nanoparticles. This phenomenon also referred as a blue shift with a lower wavelength and higher frequency that result in a larger band gap than its bulk.

The transportation of electrons through different excitonic energy levels produces absorption spectra. The region where the relatively bigger particles start to absorb energy is referred as *absorption edge*. The overlapping of excitonic absorptions produces a peak maximum at the highest distribution of average particle size which is called as *absorption onset*. The higher the slope of the absorption onset, the lower is the size distribution of the particles.

The electrons in the conduction band returns to the valance band either by radiative recombinations or non-radiative recombinations. The combination of electron with the hole generates a photon in the form of electromagnetic radiation in radiative recombinations and a phonon in the form of energy of the lattice vibrational wave for the non-radiative recombinations. The photon energy depends on the band gap of the nanoparticles which determine the color of the radiation in the emission (Figure 1. 3). Eventually, there is always an energy loss in such spontaneous recombinations where the emission wavelength is longer than the absorption onset. This energy loses occurring at higher wavelengths is referred as *Stoke's shift* (Figure 1. 4). There are numerous factors for the occurrence of the energy trap sites that causes non-radiative recombinations. Most common ones are the surface defects, structural defects, atomic vacancies, dangling bonds, and adsorbents of the proximity molecule at the interface.

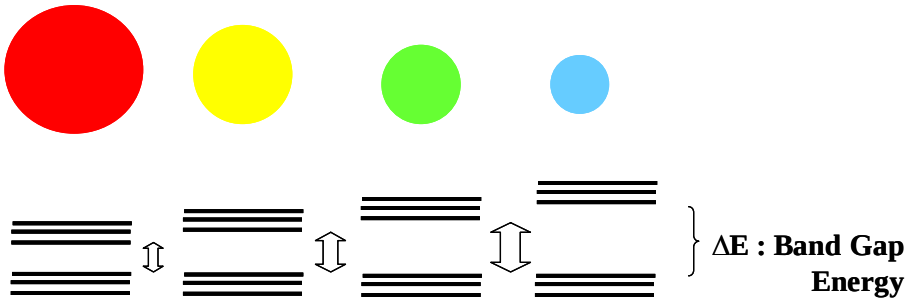

Figure 1. 3 The change in the color emission and particle size with band gap energy. (www.evidenttech.com)

The emission spectra of the quantum dots are independent of the excitation wavelength. The higher energy photon increase the number of electronic and vibrational levels involved which rapidly loses excess energy to fall back to the lowest vibrational levels of the first excited state. Consequently, although other transitions to higher excited states exist, the emission spectrum is only the mirror image of the ground state to lowest excited state transitions (Figure 1. 4) [7]. The main advantage of quantum dots compared to the organic fluorophores is their narrow emission spectra. The excitation at a specific wavelength can result into different color emissions for a quantum dot mixture of different sizes.

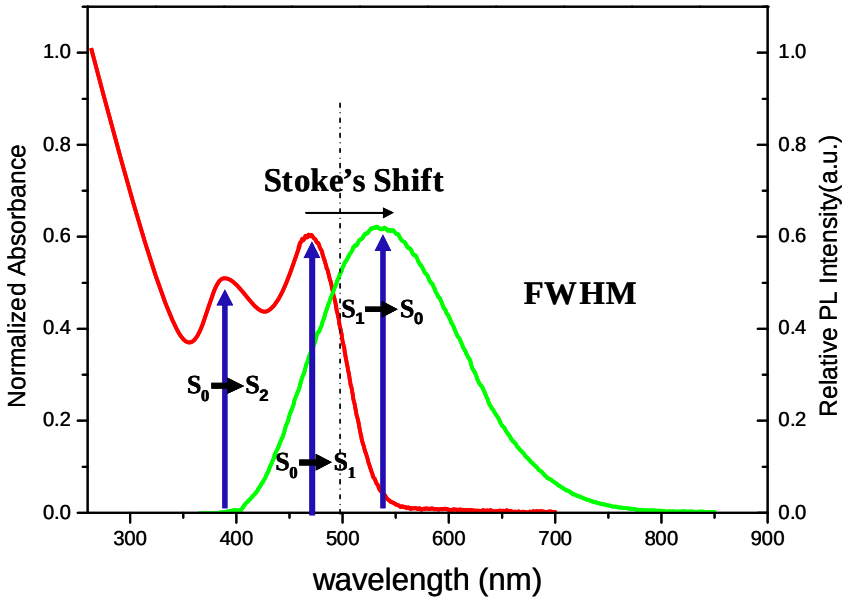

Figure 1. 4 The relation between the absorption and emission spectra of fluorescent nanoparticle [8].

Typically the emission spectra of the quantum dots have a Gaussian curve and the width of this curve determines the value of full width at half-maximum (FWHM). FWHM gives a relative measure for the size distribution of the particles where a smaller width corresponds to a narrower size distribution. The distribution is temperature dependent where increasing temperature creates an order in the excitons of the larger particles and results in a narrower FWHM [9].

1.1.2 Effective Mass Approximation

The first theoretical studies about the quantum confinement in quantum dots were published by Brus et al in 1984 [10]. The molecular quantum chemistry was the model to establish a new framework for such systems which was practically a modulated particle in a box problem. Group II-VI and III-V semiconductors behave like a hydrogen-like model due to the confined electron-hole pairs in the nanocrystalline structure. The exciton can not pass the potential energy barriers at the electronic states and Schrödinger equation can be

used to solve this one-dimensional problem. The equation for a particle of mass m, in one-dimensional box of length L in the direction of the confinement can be stated as:

$$-\frac{\hbar^2}{2m}\frac{\partial^2\Psi(x)}{\partial x^2}+V(x)\Psi(x)=E\Psi(x) \qquad (1.1)$$

where ħ is the reduced Planck constant, m is the mass of the particle, Ψ(x) is the wavefunction to be solved, V(x) varying potential and E is the energy.

The value of the Ψ(x) outside the box is zero and inside the box relation can be found from the combined solution of a differential equation and Eigen value problem which reduces to the following equation:

$$\Psi_n(x)=\sqrt{\frac{2}{L}}\sin(\frac{n\pi x}{L}) \qquad (1.2)$$

The solution of 1.1 by using 1.2 is:

$$E_n=\frac{n^2\hbar^2\pi^2}{2mL^2}=\frac{n^2h^2}{8mL^2} \qquad (1.3)$$

where n is a positive integer, m is the mass of the particle, h is the Planck constant and L is the length of the box.

This treatment has been used for the excitonic energy levels in the semiconductor clusters and the energy of the lowest excited state has been stated by solving the wavefunction. The energy of the exciton depends on the band gap of the bulk material, quantum energy localization (kinetic energy), Coulomb attraction and finally the correlation effect. These three contributions form the final Brus equation [10] which is:

$$E_{(R)}=E_g+\frac{h^2}{8R^2}\left[\frac{1}{m_e}+\frac{1}{m_h}\right]-1.786\frac{e^2}{\varepsilon R}-0.248E^*_{Ry} \qquad (1.4)$$

where R is the cluster radius, m_e is the electron effective mass, m_h is the hole effective mass, ϵ is the dielectric constant, E_g is the band gap of the bulk material, and E^*_{Ry} is the effective Rydberg energy.

It can be seen that E is inversely proportional to R^2 and R in the confinement energy term and Coulomb attraction, respectively.

The breakdown of the effective mass approximation for particles smaller than 10nm made Wang et al to modify the equation by considering the electron transfer from the anion to the cation part of the particle[11]. A tight-binding model was formed for a better band structure for individual semiconductors. For CdS, a 13-parameter tight-binding model has been developed to give a satisfactory result for the band structure that does not deviate from the bulk. A further development in the formula can be obtained by taking account the effects of finite well depth, surfaces and defects [12, 13].

1.2 Synthesis of Quantum Dots

Since the last few decades, quantum dot related researches became popular in theoretical and practical applications. After the preliminary synthesis of quantum dots in colloidal solutions, many techniques were applied to obtain ordered arrays of nanocrystals by lithography, dip-coating, chemical bath deposition and epitaxial growth [14-17]. A review about the colloidal synthesis will be presented here.

High temperature colloidal synthesis yields uniform semiconductor nanoparticles in terms of size, chemical composition, shape and surface chemistry. The size and composition of such nanoparticles can be tailored by choosing an appropriate capping layer and amount. During the crystal growth, the capping agent adheres to the surface of the nanocrystals and provides a dynamic shell that stabilizes the nanocrystals in solution and controls the reaction kinetics after nucleation. The steric hindrance of the capping agent on the surface determines the rate of the reaction and consequently average size of the nanocrystals. A weak hindrance of nanoparticles looses the energy barrier to counteract the van der Waals attractions which causes the flocculation of the particles. The solubility of the nanoparticles in the synthesis environment depends on the functionality of the capping agent which can be hydrophilic or hydrophobic or both. Therefore, there are two methods in the synthesis of nanoparticles either in an organic solvent or in an aqueous medium.

In 1993, Bawendi et al presented an organometallic approach in synthesizing high quality nearly monodisperse (%5 rms in diameter) CdE (E = S, Se, Te) nanoparticles [18]. A discrete homogenous nucleation was started by decomposing the organometallic precursors at high temperatures (300 ºC) in a coordinating solvent. Slow growth and annealing in the coordinating solvent resulted in a uniform surface passivization and regularity in the core structure. A size selective process was used to obtain nearly monodisperse nanoparticles where the average crystal size can be obtained from ~12 to ~115 A°. In the synthesis of group II-VI nanocrystals, metal alkyls (dimethylcadmium and diethylcadmium) are chosen as the group II source. Group VI sources are generally organophosphine chalcogenides (R_3PE) or bistrimethylsilylchalcogenides (TMS_2E) [19]. The R_3PE type reagents are used as Se and Te source whereas; TMS_2E is used as S source due to its higher reactivity than R_3PS. The coordinating solvent is not limited to long chain alkylphosphine or alkylphosphine oxides but also alkylphosphite, alkylphosphate, pyridines, alkylamines, quinoline and triglyme can be used to produce large volumes of nanoparticles [20]. Main drawbacks of such systems were the toxicity, pyrophoric and explosive behavior of the expensive chemicals. In the recent studies of Peng et al, CdO has been chosen as the source for a desirable greener route [21]. In the recent developments, surface ligands are known to be coordinating the surface Cd^{2+} ions. In the context of hard-soft acid-base theory, Cd^{2+} is a soft acid and base conjugates of phosphonic acid and carboxylic acid where the lone pairs of the O atom provides the ligand interaction can be used to coordinate particle surface. In the frame of the theory; amines, sulfonates, sulfoxides, ketones, aldehydes and esters can also be chosen [22]. The coordination of the nanoparticle surface decreases the non-radiative exciton recombination by eliminating the surface defects which results in better luminescence.

Although, a predominant method to produce highly luminescent and nearly monodisperse nanoparticles is to follow an organic route, many of the biological applications require nanoparticles that form stable colloidal solutions in water. The nanoparticles that are synthesized in organic solvents with hydrophobic groups can be transferred into water by ligand exchange [23-26] or micellar encapsulation [27-29]. The

nanoparticles in an aqueous solvent after the ligand exchange have lower photoluminescence, colloidal stability and surface passivization due to strong polar property of the water. Kuno et al reported that surface exchange reaction of nanoparticles capped with trioctylphosphine oxide (TOPO) by thiophenol and pyridine decreased the quantum yield by ten-fold [30]. Talapin et al reported a roughly better luminescence upon the exchange of TOPO with amines such as n-hexadecylamine, n-dodecylamine and allylamine [31]. Schmelz et al reported that the PL of the TOPO capped CdSe nanocrystals disappears upon exchange the with 1,12-diazaperylene [32].

Another way to prepare water soluble nanoparticles is to perform the synthesis directly in the aqueous environment by using hydrophilic capping agent to sustain colloidal stability. There is more than one approach to prepare water dispersed nanoparticles varying from hydrothermal synthesis to microwave-assisted preparation.[33, 34] The common route is to use thiol (-SH) groups where a strong covalent bond with cadmium can be obtained. The capping agent is chosen such that thiol groups bind to the surface and other functional groups provide the solubility in water and colloidal stability. Thioglycolic acid [35, 36], cysteine[37, 38], mercaptopropionic acid [39] , mercaptoethanol [40], mercaptoethylamine [41] are used by many research groups where the investigation were focused on the luminescence as a response to the ratio of the precursors, reaction time, concentrations and pH.

1.3 Superparamagnetism

Superparamagnetism is the phenomenon where magnetic material behaves similar to paramagnetism below Curie temperature. Above the Curie temperature, lattice vibrations become more energetic, which disrupts the alignment of the spins. The spins in the crystal domains can not align perfectly with each other and after the energy in the vibration is sufficient, the spin of the atom disorient itself and the crystal behaves as paramagnetic. For example oxygen is paramagnetic at atmospheric pressure and room temperature. Each oxygen molecule has a net magnetic dipole moment but due to thermal agitation there is no

average moment per molecule. Nevertheless, in the presence of an external field, molecular magnetic moments take various alignments with the field and the net magnetization increases with the applied field. Moreover, unlike ferromagnetism, magnetization disappears when the field is removed. In superparamagnetism, magnetic material confined at small scale (1-10 nm) has no individual magnetic domains. The thermal energy even below Curie temperature is sufficient enough to change the magnetization of the entire crystal to produce a zero net magnetization. In superparamagnetic materials, the crystal as a whole responds to the external field with a higher net magnetization than paramagnetic materials. This size dependent property has been observed for ferromagnetic materials like Fe_3O_4 and γ-Fe_2O_3. The derivative of iron with cobalt, chromium, nickel, copper and zinc are also hot investigation topic in this field [42].

1.4 Superparamagnetic Iron Oxides Nanoparticles (SPIONs)

SPIONs are below 10 nm Fe_3O_4 (magnetite) or γ-Fe_2O_3 (maghemite) nanoparticles that have high magnetization values. Magnetite particles are very sensitive to the presence of oxygen and are rapidly oxidized to maghemite or magnetite-maghemite subtitutional series and this can be observed through the color change from black-brown to red-brown. SPIONs can be prepared by coprecipitation, microemulsions, high temperature decomposition of organometallic precursors, synthesis by aerosol/vapor methods and other wet chemical methods [43-48].

SPIONs have been used for years in drug delivery, magnetic resonance imaging or for various separation techniques [49, 50]. SPIONs are especially useful in biomedicine when they are dispersed in water to form ferrofluids. The stability of the particles can be sustained by balancing the attractive van der Waals forces with Columbic, steric and other repulsive interactions. A hydrophilic stabilizer dextran and polyvinylpyrrolidone (PVP) enhanced the blood circulation time and stabilized the solution whereas polyethylene glycol (PEG) and polyacrylic acid (PAA) increased the biocompatibility and colloidal stability [51-53]. The coating has been comprised by many other natural (gelatin, chitosan, pullulan)

and synthetic (poly(vinyl alcohol) (PVA), poly(ethylene-co-vinyl acetate), poly(lactic-co-glycolic acid) (PLGA)) polymeric materials [54-57].

The main focus of above mentioned studies is to improve the biocompatibility of the particles rather than improving the quality of the nanoparticles. The surface functionalization and its arrangement on the particle surface influence the hydrodynamic size and have a dramatic effect in the biokinetics and biodistribution of such particles within the body. Therefore, different types of FDA (Food and Drug Administration) approved biocompatible coating molecules were studied to increase the biocompatibility and colloidal stability.

1.5 A Hybrid Nanocomposite: Magnetic Fluorescent Nanoparticles

In the field of colloidal nanocrystals, quantum dots (QDs) and magnetic nanoparticles (MNs) have been predominantly investigated for several decades because of their unique optical, mechanical, electrical, magnetic or chemical properties distinguishing them from the bulk and due to the vast application areas from electronics to medicine. One way to combine the properties of QDs and MNPs is to form a nanocomposite. Such a nanocomposite will comprise both optical and magnetic properties. Dual functionality of nanocomposite increases the modes of detection or provides multiplicity. Besides both sensing and separation can be performed by a single entity. The detection and separation of the biomolecules, such as enzymes, proteins, and genes, has a significant importance for the early diagnosis of the diseases. Also the recognition of the tumor cells is crucial for the early diagnosis of the premature phase of cancer. Multifunctional magnetic fluorescent nanoparticles (MFNs) can be bound to a specific target cell and separated or dragged by applying magnetic field. In addition, the fluorescent domain can be associated to different target cells with different emission color to distinguish several targets in parallel. MFNs can also be used in controlled drug delivery applications where the carrier molecule can be released by applying an external field after the exact localization of the MFNs in the target region. The localization of the tumor cell can be obtained in the pre-operative phase in MRI

and by the aid of a fluorescent guidance; the tumor cell can be further detected during the surgery to minimize the collateral damages on healthy tissues. Another exciting application platform for MFNs is the integration of nanoparticles for lab-on a chip system.

MFNs can be synthesized by using different approaches that can be categorized into three groups (Figure 1.5). In the first method, preformed fluorescent and magnetic domains are encapsulated in a nano-shell. In this approach, the encapsulation shell has been chosen from either polymer or silica based materials. Silica coating is the predominantly used technique due to following reasons. First of all, the silica coating prevents the quenching of the fluorescent domain by magnetic cores where non-radiative couplings are reduced. Secondly, silica shell is an optically transparent material that does not interact with the emission of the QDs. Thirdly, silica shell surface can be functionalized by providing a chemical bonding with the domains. Finally, silica matrix is a non-toxic inert material that prevents the aggregation of hybrid particles and increases their solubility in the medium. In the literature, Lu et al. have reported the encapsulation of magnetic ferrofluids into silica shell where the outer shell moieties have been further modified by fluorescent organic dyes [58]. On the other hand, Kim et al. have prepared monodispersed oleic acid stabilized MFNs (Fe_3O_4-CdSe/ZnS) which were transferred into the mesoporous silica spheres with 150 nm average size [59]. In the polymer based encapsulation; polysaccharides, polypeptides, polyelectrolytes and styrene/acrylamide copolymers were used [43, 60, 61]. Kitagawa et al. have prepared MFNs by using cationic fluorescent polyelectrolyte (Poly(ethyleneimine)) which absorbs onto the anionic polymers (carboxylate functionalized) stabilizing the magnetic nanoparticles [62]. Rosenzweig and co-workers used DMSA (Dimercapto-succinimid acid) functionalized superparamagnetic Fe_2O_3 beads and hydrophobic TOPO capped CdSe/ZnS QDs in a mixture of chloroform/methanol/water solvent. The composite material had a 3-fold decrease in the luminescent quantum yield due to the quenching of the QDs by magnetic nanoparticles or between the closely packed QDs [63].

The second method is to link functionalized magnetic nanoparticles covalently to fluorescent nanoparticles. In this method, a spacer group has been used to prevent the

quenching of the luminescence. This cross-linker molecule mediates a space between the two entities. In the study of Corr et al., carboxylic acid porphyrin derivative was chosen to interact electrostaticly with the positively charged amino spacer attached to magnetic core.[64] You et al. on the other hand synthesized thioglycolic acid (TGA) stabilized MFNs at pH 3 through an electrostatic interaction [40]. A similar approach has been used by functionalizing the oleate bilipid layer coated magnetic nanoparticles with biotin in order to bind streptavidin coated fluorescent nanoparticles in the same assembly [65]. A similar approach was adopted in the stabilization of MFNs in a sandwich-type immunoassay by Zhang et al. [66].

In the third method, fluorescent nanoparticles are synthesized on the magnetic core like a shell through inorganic methods. In a study Gu et al., spherical domains of CdS was attached to the surface of FePt nanoparticles in a one pot reaction by a decomposition of the organometallic precursor in hot surfactants [67]. An increase in quantum yield from 2-3 % to 10-15 % has been reported for the deposition of heterogeneous semiconductor on magnetic nanoparticles (Fe_3O_4/CdSe/ZnS) at high-temperature by Du et al. [68].

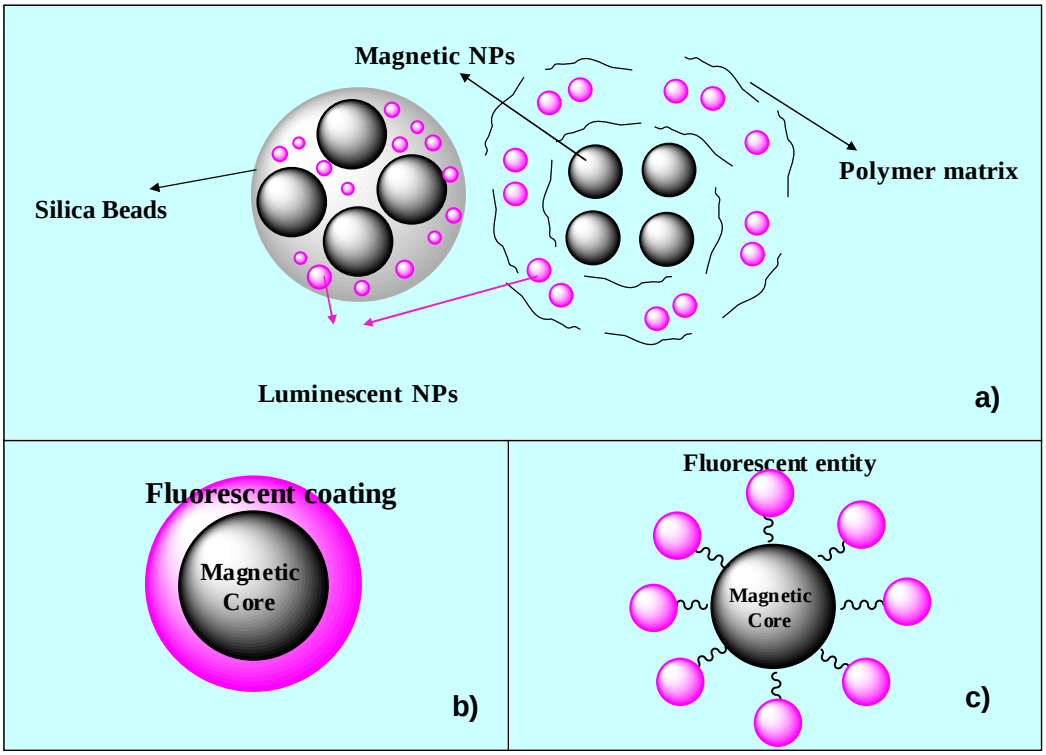

Figure 1. 5 a) The encapsulation of magnetic and fluorescent domains in nano shells b) core-shell structure c) the direct linkage between the fluorescent and magnetic domains by providing a cross linker [69].

1.6 The Goal of the Research and Objectives

For most applications, MFNs needs to be functionalized to be dispersed in water. Highly luminescent monodispersed quantum dots are generally capped with hydrophobic ligands which can be post-processed to be dispersed in water. However, they will suffer from the reduction of quantum yield with aggregation of the nanoparticles. Stabilizing both magnetic and fluorescent domains via single ligand through electrostatic or covalent binding have not been achieved in aqueous medium yet. An appropriate ligand choice plays an important role in the physical and chemical properties of the MFNs. As mentioned before, spacing the domains with a long polyelectrolyte polymer has been introduced in the literature but it is the first time a relatively short ligand has been used to stabilize MFNs [40]. A good candidate to stabilize a fluorescent domain should have a thiol group, whereas

the magnetic domains have already been well stabilized with carboxylate groups in the previous investigations by Acar et al. When both of these functional groups are used up for the binding of the domains, the solubility of the system can be enhanced by an additional hydrophilic functional. One of the objectives of the project is to use this multifunctional entity in biological applications which ought to be biocompatible as it is. Other than that narrow size distribution, high quantum yield, cost efficient fabrication through one-pot synthesis and total control on the surface chemistry are the desired properties of the MFNs. L-cysteine which is providing the as mentioned desired condition has been chosen for our studies. Our first approach is going to be the investigation of synthesizing highly luminescent water soluble L-cysteine capped CdS quantum dots. Finally, the obtained solution will be used to synthesize MFNs in a one-pot reaction.

Chapter 2

Development of Color Tunable Aqueous CdS-Cysteine Quantum Dots with Improved Efficiency and Investigation of Cytotoxicity

2.1 Introduction

In the last few decades, fluorescent semiconductor nanoparticles have attracted tremendous attention due to their size dependent optical and electronic properties [70-74]. Due to the quantum confinement effect, these novel materials exhibit unique physical and chemical properties that are exploited in several high-tech applications [75, 76]. High quality semiconductor nanocrystals have found use in a wide range of fields including the non-linear optical devices, solar cells, thin-film light-emitting devices, sensors and as fluorescent labels in biotechnology [72, 74, 77-79]. Lately, quantum dots (QDs) became quite popular for biolabeling and bioimaging [80, 81]. Therefore, there is an ever increasing need for the highly luminescent, stable and functional aqueous QDs. Considerable effort was devoted to the synthesis of aqueous dispersions of nanoparticles which possess high stability, high quantum yield and narrow FWHM (full width at half

maximum) in a simple and energy efficient way [82-84]. There are two approaches for the preparation of water-soluble nanoparticles. The first one involves ligand exchange on the hydrophobically modified QDs which are prepared at high temperatures from organometallic precursors with water-soluble thiols, phosphates or siloxanes [45, 84-89]. Usually, this method causes a dramatic loss in the luminescence, poor reproducibility and environmental problems due to the toxicity of the materials used [45, 86, 90]. The second approach involves direct synthesis of QDs in an aqueous environment. Aqueous synthesis is more favorable since it uses precursors with much lower toxicity, and is relatively inexpensive, reproducible and fast in producing aqueous particles [91].

A succession of exciting studies was done with thiol stabilized quantum dots (QDs) which were mainly concentrated on the group II-VI semiconductor nanoparticles [36, 92, 93]. Among those CdS is relatively easy to prepare but has complicated photochemical properties which usually result in low quantum yield [37].

We are interested in direct aqueous synthesis of cysteine capped QDs using relatively safer sources of cadmium (cadmium acetate) and sulfur (sodium sulfide). R(+)-cysteine is an excellent coating molecule for a QD, especially for biological applications: (1) It is non-immunogenic, (2) contains a thiol moiety which is known to bind cadmium effectively, which would provide a good surface passivization, (3) contains amine and carboxylic acid groups responsible from water dispersibility, aid the colloidal stabilization and provide functional surfaces for further functionalization such as PEGylation, or attachment of biologically significant molecules. Cysteine capped QDs have been reported to act as good selective ion probes, fluorophores in polymers and lately, renal clearance of

CdSe/ZnS/CdS/cysteine QDs have been reported encouraging the in vivo use of QDs [94-96]. There are also few reports on direct aqueous synthesis of cysteine coated quantum dots (CdS, CdTe or CdSe) [94, 97, 98]. Some of those require addition ligands or special reaction conditions or look into different sources of Te or Se [99]. Saha did a significant amount of work on CdS-cysteine nanoparticles [37, 38]. He achieved CdS-cysteine QDs in shorter reaction times than the initial reports in a method that uses rather dangerous H_2S gas at reflux conditions with 6-8% QY after size selective precipitation. None of these reports provided a detailed analysis of a complete set of reaction parameters on particle properties for the simple aqueous synthesis of CdS and usually posses low QYs and stability with no information on color tunability.

Our comprehensive study will be focused on the understanding of the influence of reaction variables, particularly reaction pH, temperature, Cd:S and ligand:Cd molar ratios, on the properties of R(+)-cysteine capped CdS nanoparticles. Development of CdS-Cysteine QDs luminescing in different colors with high colloidal and photostability and improved QYs in rather simpler techniques is highly desirable. We have seen that the storage conditions are influential on the optical properties as well, therefore the best storage pH for these QDs were also determined. Additionally, we have investigated the cell uptake and cell viability of these QDs as a function of dose and incubation time which is very important for the consideration of these nanoparticles for *in vitro* and/or *in vivo* use.

Cysteine QDs with 55% quantum yield and colloidal and optical stability up to nine months so far were achieved when we applied the optimum synthesis and storage

conditions. Best to our knowledge, this is the highest QY and best stability reported for CdS-cysteine QDs.

2.2 Experimental Section

2.2.1 Materials

All the chemicals used were of analytical grade or of the highest purity commercially available. Sodium sulfide trihydrate ($Na_2S{\cdot}3H_2O$), (R)-(+)-Cysteine, cadmium acetate dihydrate $(CH_3COO)_2Cd{\cdot}2H_2O$), rhodamine B and buffer solutions were purchased from Merck. Sodium hydroxide and acetic acid were purchased from Aldrich and LaCheMa, respectively. High purity water was used from Milli-Q water (Millipore) system. 3-(4,5-dimethylthiazol-2-yl)-2,5-diphenyl tetrazolium bromide (MTT) was purchased from Sigma. DMEM including 4.5g/L D-Glucose without L-Gutamine, Trypsin-EDTA solution C 0.05% Trypsin & EDTA (1:5000) in DPBS with phenol red, Pen-Strep solution with penicillin 10,000 units/mL & streptomycin 10 mg/mL, L-Glutamine solution 200mM and Foetal Bovine Serum 0.1µm membrane filtered mycoplasma tested & virus screened were purchased from Biological Industries.

2.2.2 Synthesis of (R)-(+)-Cysteine capped CdS QDs

(R)-(+)-Cysteine capped CdS QDs were prepared using a synthetic route reported earlier [100]. All the steps were performed under N_2. Briefly, 66.6mg of $Cd(Ac)_2{\cdot}2H_2O$ was dissolved in 50ml of water in a three-necked round bottomed flask under continuous agitation. An appropriate amount of cysteine was added to the cadmium containing

solution. Concurrently, the system was deoxygenated with constant nitrogen flow for twenty minutes after the adjustment of the reaction media to the desired pH conditions with 10M NaOH or concentrated acetic acid. The sulfide solution was prepared by dissolving 16.6 mg of $Na_2S{\cdot}3H_2O$ in 50 ml of water in an ultrasonication bath. The sulfide solution was deoxygenated and added to the cadmium-cysteine solution with a drop wise addition. Reactions were carried out for 40min at the desired temperature and then stored at 4°C.

Precipitation of the quantum dots were achieved briefly by the following procedure. A batch solution was lyophilized and dissolved in 3ml of water. The solution was well mixed with 5ml of isopropyl alcohol (IPA) and centrifuged for 15 minutes at 3900rpm. After discarding the non-luminescent solvent, the precipitate was further washed with the same method two more times. The final precipitate was dissolved in 5ml of water and lyophilized to produce clean CdS-Cystein QD in powder form.

The pH study was performed by dissolving an appropriate amount of the washed QD powder into 6mL of buffer solutions (borate buffer solutions). As a control same concentration of QD solution was prepared in water as well.

2.2.3 *In vitro* cell viability and uptake

MCF-7 and HeLa cells were cultured at a density of $5x10^4$ cell/well in 96-well plates for 24 hours in DMEM culture medium supplemented with 10% fetal bovine serum and 1% penicillin-streptomycine at 37^oC under 5% CO_2. Then the cells were incubated with QDs at doses between 0.05-0.15 mg QD/ml for 24 and 48h. Cytotoxicity was evaluated by MTT assay. Cells were cultured with MTT reagent for 4h, then lysed on the

plate with DMSO:EtOH and absorbance was measured on a ELx800 Biotek Elisa reader at 600 nm. In order to determine the QD uptake by cells, both MCF-7 and HeLa cells were incubated at 0.10 and 0.15mg QD/ml dose in 96-well plates as described above. At the end of 24 and 48h incubation times, medium was removed from the wells and fresh medium was added. Fluorescence from each well was measured on a Thermo Fluoroskan Ascent fluorescence plate reader ($\lambda_{excitation\ max}$=355nm, $\lambda_{emission\ max}$=460nm). QD uptake was quantified by a calibration curve prepared by the same QDs in the growth medium.

For the microscopy studies, cells were grown in 6-well plates as described above and incubated with 0.10mg/mL QD for 24h. Microscopy images were taken after the removal of the medium and fixation of cells by 2% formaldehyde at 4°C 30 min. Morphological changes and uptake of ODs were visualized by phase contrast and fluorescence microscopy (Zeiss LSM 510 with Axiovert 200M inverted microscope).

2.3 Characterization Techniques

The absorption spectra of the particles were recorded with Schimadzu UV-Vis-NIR spectrophotometer model 3101 PC. Dilution of the samples was adjusted to a maximum absorption of 15% at the excitation wavelength of 355nm. The particle size was determined from the absorption onset wavelength of the samples using the Brus equation [10]. Photoluminesence (PL) spectra were recorded at room temperature with a Horiba Jobin-Yvon FluoroMax-3 Spectrofluorimeter at an excitation wavelength of 355nm. The data were collected in the range of 365nm to 850nm at a 0.5nm interval with a 370nm emission

filter. All measurements were done in triplicates. PL spectra were calibrated with respect to their absorptions at the excitation wavelength. PL quantum yield (QY) of each sample was estimated from the integrated emission area of the samples using Rhodamine B as a reference (31% QY in water at 515nm)[101] as described before [100]. Transmission electron microscopy (TEM) images were recorded on FEI Tecnai F20 operated at an acceleration voltage of 200kV by applying an aqueous solution on a carbon coated copper grid at Max-Planck Institute in Mainz. Powder X-ray diffraction analysis (XRD) was recorded by using HUEBER G670 diffractometer with a germanium monochromator and Cu-Kα radiation at 1.54056Å in 2θ range from 5° to 100° with 0.005° interval. FT-IR spectra were recorded from KBr pallets of washed samples using JASCO FT-IR-600PLUS spectrometer. Raman spectra were obtained from BRUKER FT-Raman RFS100 spectrometer with a Nd:YAG laser source and Ge diode detector up to 4000cm^{-1}. Brookhaven Instruments Corporation Zeta Potential Analyzer was used with a Zeta Phase Analysis Light Scattering method to determine the surface charge of the nanoparticles. Malvern Instruments ZetaSizer Nanoseries Nano-S was used to determine the hydrodynamic size of the CdS-cysteine nanoparticles.

2.4 Results and Discussions

2.4.1 Characterization of CdS quantum dots

Cysteine coated CdS nanoparticles were synthesized in a simple aqueous method. Structure of the washed nanoparticles was determined by XRD (Figure 2.1) and TEM (Figure 2.2). XRD peaks at 28.2° and 47.1° correspond to the (1 1 1) and (2 2 0) planes of

cubic zinc blende structure of CdS. The lattice distance calculated from the fast Fourier Transform (FFT) image by using the ring pattern were measured as 3.36Å and 2.06Å for the (1 1 1) and (2 2 0) planes, respectively. The approximated particle size was calculated as 2.8nm by Debye-Scherrer equation. The average particle size obtained from XRD was comparable to the sizes calculated from the UV-Vis spectra (Table 1). In the investigation of ultra small nanoparticles, the approximated Bragg peaks are different than that of the micron size particles and broadening malfunctions the calculations [102]. Therefore, a slight difference in size calculated by different methods and from XRD may exist. DLS measurement of the same sample indicates 3.3nm which is reasonable considering the existence of a hydrated cysteine shell.

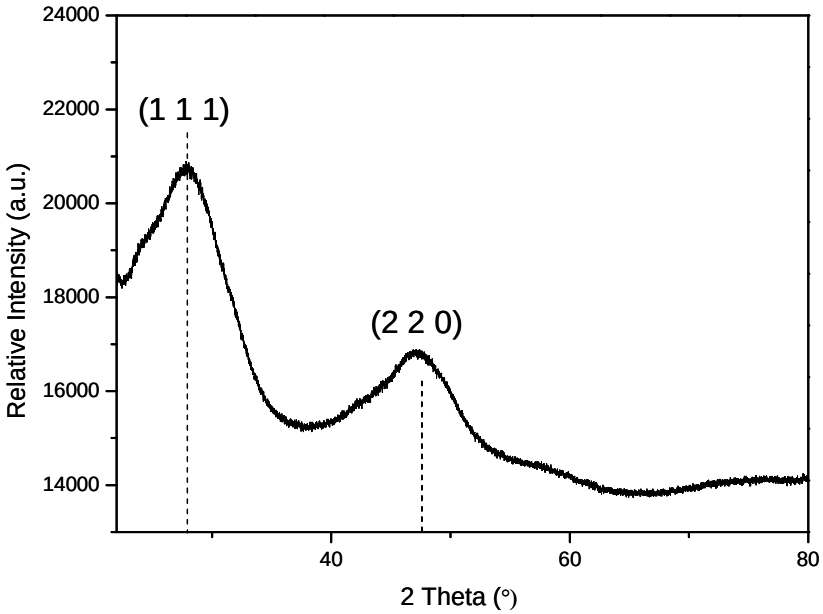

Figure 2.1 XRD pattern of CdS-cysteine nanoparticles.

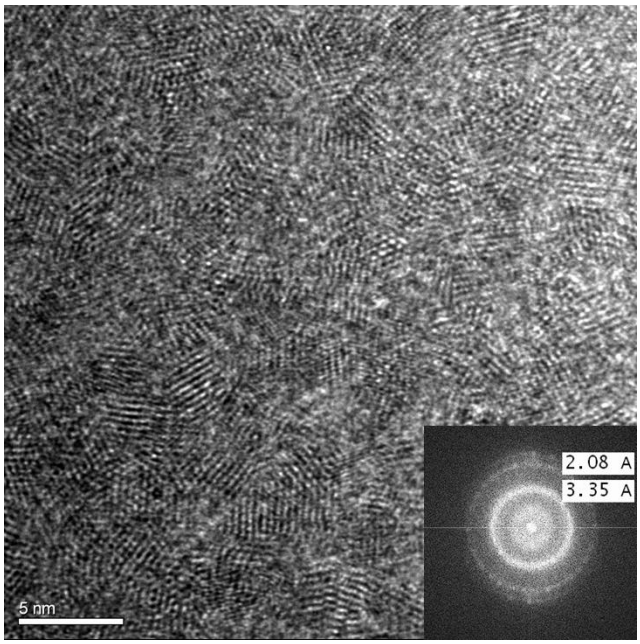

Figure 2.2 TEM image of CdS-Cysteine QDs. Inset: High Resolution FFT image.

FT-IR (Figure 2.3) and Raman (Figure 2.4) spectra of the washed nanoparticles provided information about the cysteine coating. Binding from the thiol was confirmed by the disappearance of the thiol peak at around 2550 cm^{-1} in both spectra. Broad peak between 3000-3500 cm^{-1} in FTIR and 3260 cm^{-1} in Raman are for the N-H stretching. Broadening can be attributed to the possible hydrogen bonding. Carbonyl stretching peak of cysteine visible at 1690 cm^{-1} was replaced with two peaks at 1569 cm^{-1} and 1402 cm^{-1} in CdS-Cysteine QDs corresponding to the asymmetric and symmetric stretching modes of carboxylate.

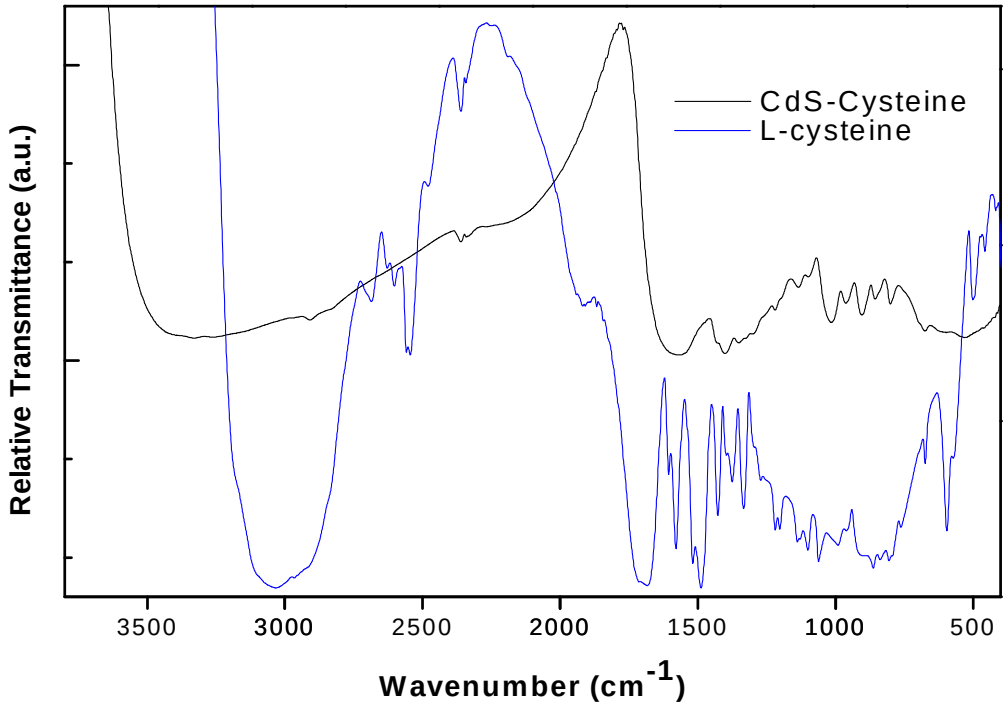

Figure 2.3 FT-IR spectra of washed CdS-Cysteine QDs and L-cysteine**.**

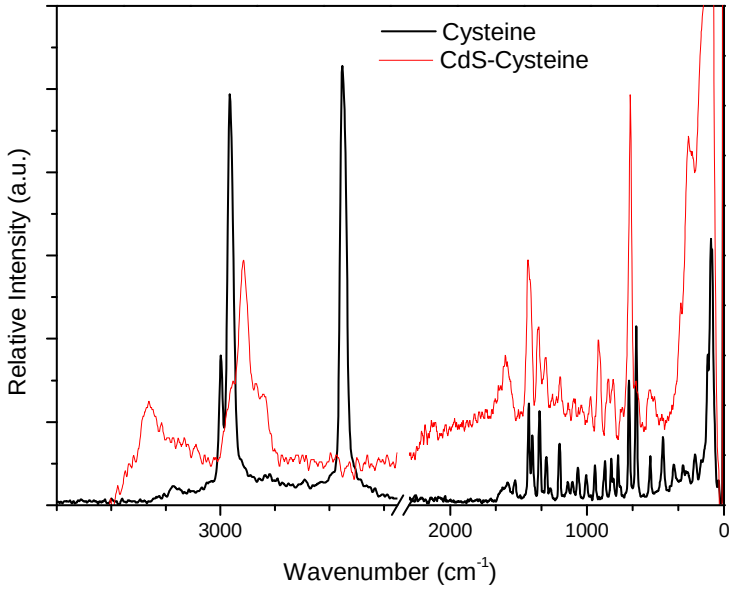

Figure 2.4 Raman spectra of washed CdS-Cysteine QDs and L-cysteine**.**

All CdS nanoparticles luminesce under 366nm excitation. A clear blue shift of the absorption onset of the samples with respect to bulk CdS (515nm) in the UV-Vis absorption spectra is a result of quantum confinement (Figure 2.5). The existence of the first excitonic peak absorption suggests that a relatively low particle size distribution in confined structures were achieve [103].

2.4.2 Effects of Cysteine:Cd ratio on the particle size and optical properties

Influence of the cysteine amount on the particle size and luminescent properties were investigated at a fixed Cd^{2+}:S^{2-} ratio of 2.5 and reaction pH around 7.8 before sulfide addition (Figure 2.5 and

Table 2.1).

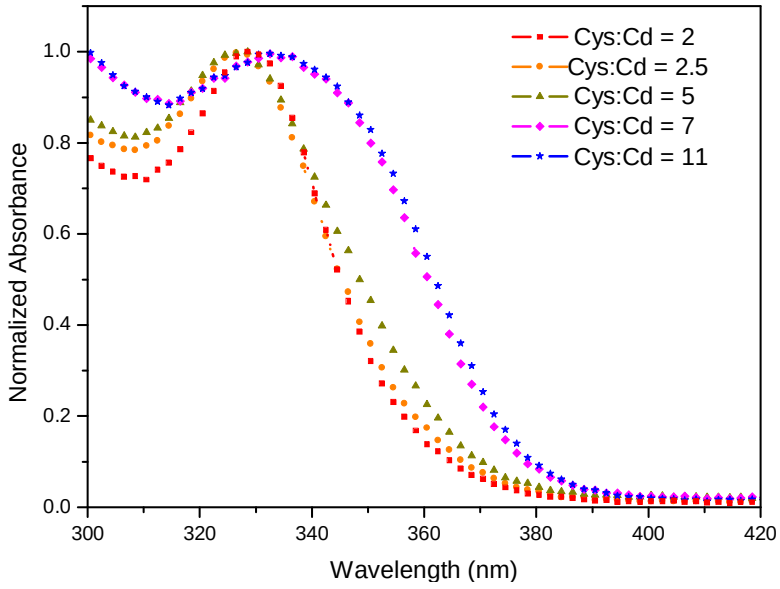

Figure 2.5 Room temperature UV-Vis absorption spectra of CdS nanoparticles with varying cysteine:Cd^{2+} ratio.

Table 2.1 Properties of QDs prepared at different ratios of Cysteine:Cd^{2+} at fixed Cd^{2+}:S^{2-} ratio of 2.5.

Cysteine/Cd^{2+}	QY (%)	FWHM (nm)	PL Max (nm)	Abs. Edge (nm)	Particle Size (nm)	Final pH	Initial pH
1.5	13	122.0	466.3	375	2.3	9.55	7.8
2.0	19	118.7	462.5	370	2.3	8.95	7.8
2.5	14	123.4	460.6	371	2.3	8.70	8.0
5.0	11	121.5	462.2	372	2.3	8.30	7.8
7.0	10	130.0	465.8	382	2.4	8.14	7.7
11.0	10	134.9	472.0	383	2.4	7.90	7.9

Initial pH: pH before Na_2S addition; Final pH: pH after Na_2S addition

As the cysteine:Cd^{2+} ratio increased from 1.5 to 11, crystals got slightly larger above the ratio of 7. This is accompanied with a slight red shift in the absorption onset and emission maximum. However, all of these QDs emit in the green region indicating similar and quite small crystal sizes (2.3 and 2.4 nm) and renders such difference in emission wavelength insignificant. Size of the CdS prepared under reflux conditions using H_2S at pH 11 are usually larger and was reported to increase with the increasing cysteine:Cd^{2+} ratio (4nm at a ratio of 1.5 versus 5 nm at a ratio of 5) [104]. Such difference may originate from the difference in source of the sulfide, pH and/or more importantly the reaction temperature. At room temperature not only the reaction kinetics slow down but also the binding of cysteine to surface is more stable. Cysteine also forms complexes with Cd^{2+} prior to addition of S^{2-} and these complexes are quite important for the nucleation and

growth. As the cysteine amount increases less cadium is left free in the solution, allowing more homogenous nucleation and growth. Cysteine is also influential in limiting the growth through thiol binding competing with S^{2-}. However, once a critical size of a crystal is achieved with sufficient amount of coating, existence of excess may not cause a significant change in size.

On the other hand, cysteine:Cd^{2+} ratio had a dramatic effect on the QY of the particles. Highest QY of 19% was achieved at the cysteine:Cd^{2+} ratio of 2 and a two fold decrease in QY was observed as the ratio increased to 11. Based on the size and QY results, optimum cysteine:Cd^{2+} ratio determined as 2. QY is a complex thing that depends on many factors such as crystallinity, size, size distribution, effectiveness of the capping and surface quality. The surface charge of the particles at the reaction medium is negative which creates electrostatic repulsion between the neighboring cysteine, therefore increase the surface energy of the particle inhibiting optimum growth condition and surface passivization. As the number of the defects within the structure and surface increases during the growth, the non-radiative defects and surface traps lower the QY [105]. Another thing that one has to consider tough is the decreasing pH of the reaction medium with the increasing cysteine amount which might impact the observed optical properties.

At the optimum ratio the full-width at half-maximum (FWHM) reaches its minimum value which increases with the increasing cysteine:Cd^{2+} ratio. This also indicates a more controlled growth at the ratio of 2. Cysteine:Cd^{2+} is also important for the stability. Nanoparticles with cysteine:Cd^{2+} ratio greater than 7 precipitated in one week, but those

prepared at the optimum ratio of 2 preserved both the colloidal stability and the QY after nine months, so far.

2.4.3 Effects of pH on the particle size and optical properties

At fixed cysteine:Cd^{2+}:S^{2-} ratio of 2.5:1.0:0.5, pH of the reaction (initial pH before sulfide addition) was set to a value between 7 and 11. In this study, we have shown that initial pH of the solution before the nucleation had a drastic effect on the quantum yield (Table 2.2).

Table 2.2 Properties of QDs prepared at different initial pH values at fixed Cysteine:Cd^{2+}:S^{2-} ratio of 2.5:1.0:0.5.

Initial pH	Final pH	QY (%)	FWHM (nm)	PL Max (nm)	Abs. Edge (nm)	Particle Size (nm)
7.00	8.80	9	122	462.3	372	2.3
7.80	9.55	13	119	466.3	375	2.3
9.45	10.20	27*	129	470.6	390	2.5
11.07	10.70	21	130	481.3	387	2.4

Initial pH: pH before Na_2S addition; Final pH: pH after Na_2S addition
*QY estimated for the same sample after 9 months was also 27% without any precipitation.

When the initial reaction pH was set to 7, only 9% QY was obtained. Increasing pH resulted in an increase in the QY and a slightly larger crystal sizes. Best initial pH based on the QY (27%) estimations is determined as pH 9.45. Actually, addition of Na_2S increases the pH of the reaction solution (final pH) and QY above 20% is obtained only after final pH of 10. Several factors can be considered to explain this behavior. One of them is the

formation of cadmium complexes with cysteine before the nucleation has started. Complexation of Cd^{2+} increases with the pH, reaching a maximum around pH 10. When pH increases the concentration of the thiolate group increases ($RSH \rightarrow SH^- + H^+$) since the pKa value of the sulfhydryl group of cysteine is 8.3. Therefore, at high pH values the number of free cadmium ion decreases which enables more controlled growth and decreases the possibility of uncoordinated surface cadmiums. On the other hand, type of the complexes formed is considered critical for the nucleation and crystal growth but also structure of the complex does depend on the pH [70]. Extensive investigation has been performed to explain the types of cadmium complexes formed at different pH with other thiols.[106] The complex formation process was previously studied for the RSH molecules that lead to a cluster formation with Cd^{2+} [107]. At the high pH values, Cd^{2+} complexes have a higher coordination number which decreases the cadmium concentration and hardens the penetration of the S^{2-} in the nucleation state, imposing a greater control in growth, limiting defects both in the crystal and surface. Another point to be considered is the significantly lower solubility of CdS at higher pH values (http://www.hoffland.net/src/ks/3.xml). About two fold decrease occurs in going from pH 7 to 9. Such behavior may cause better crystallization of the CdS at basic pH which enhances the luminescent properties tremendously [108]. Deprotonation of carboxylic acid at basic pH is probably another factor enhancing QY at higher pH values. Carboxylates may also contribute to the coordination of surface cadmiums through backbiting forming a six-member ring (Scheme 2.1) [109]. Overall, various surface features can be seen in the scheme 1. Increase in the luminescence efficiency in alkaline medium can be attributed to

the formation of hydroxides that reduces the surface defect sites, as well [93]. Yet, the surface hydroxylation could not dominate the surface structure since the known K_{sp} value of CdS ($\approx 10^{-27}$) is much lower than K_{sp} of $Cd(OH)_2$ ($\approx 10^{-14}$). Overall, this reaction pH study indicates that in order to maximize the QY, reaction should be started around pH 9.5 which usually ends around pH 10. This pH range should be optimum for the complexation of the cadmium before the nucleation, for the controlled growth, crystallization and for the most effective surface passivization (Table 2.2).

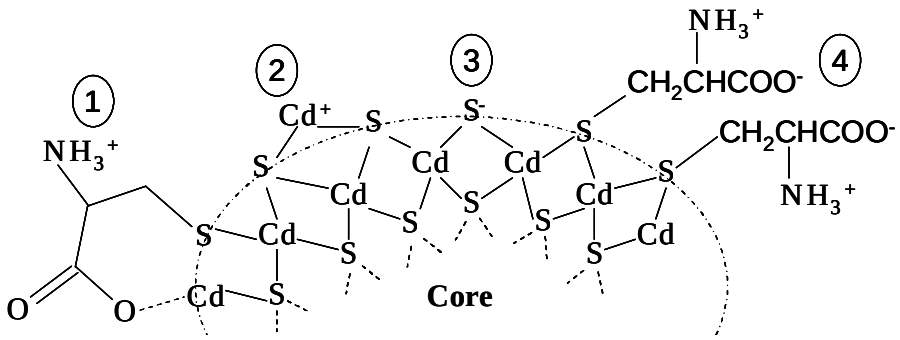

Scheme 2.1 The surface structure of L-cysteine capped CdS quantum dots.

Although color of luminescence is same for the particles prepared at different pH values, with increasing pH there is a slight increase in the absorbance onset in general (Table 2.2). Apart from the discussions provided above, formation of HS^- which is suggested to mediate the crystal formation might be considered as well. As the pH increases concentration of the HS^- would decrease (pK_a of Na_2S is 6.90) enhancing growth through S^{2-} addition on the surface.

QDs find a variety of use which may also involve applications at different pH values. Therefore, optical properties of the ready-for-use QDs were investigated in fixed

pH solutions. For this purpose, CdS-Cysteine QDs (QY of 23%.) were washed by isopropyl alcohol and dried to eliminate the possible effects of excess coating material and ions in the solution. Then they were dissolved in different buffer solutions. Absorption calibrated PL graphs are shown in Figure 2.6.

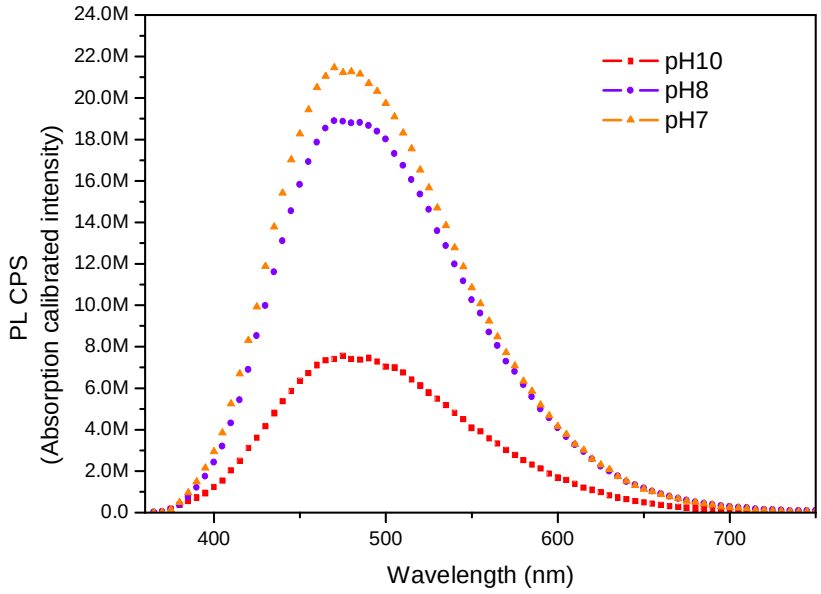

Figure 2.6 Absorption calibrated PL spectra of washed samples in different pH buffer solutions.

A significant increase in the PL intensity with decreasing pH was observed with no change in the particle size. Therefore, etching on the crystal surface can not be considered as a function of pH [95]. In pH 7 buffer solution, the QY of the particles increased to 38%. A similar pH study was repeated with the same washed and dried samples by dissolving QDs in water and adjusting the pH with 0.1M NaOH and 0.1M acetic acid. Same trend of increasing QY with decreasing pH was observed. The QY of the particles at pH 10, pH 8 and pH 7 were obtained as 28%, 46% and 55%, respectively, without giving any significant

change in PLmax or in particle size. The difference in QY values between the buffer solutions and aqueous solution with adjusted pH values might originate from the ions existing in the buffer. This is quite exciting since pH 7 is the biologically significant pH. Therefore, we believe that under these conditions, CdS-cysteine QDs that we have developed are good candidates with improved luminescence for in vitro and in vivo fluorescent imaging/labeling applications.

Cysteine is a multifunctional material and therefore surface charge of the CdS-Cysteine nanoparticles should be affected by the pH which in return may influence the properties. Zeta potential measurements revealed a surface potential of -20mV and -4mV for particles dissolved in pH 10 and 7 buffers, respectively. At higher pH close to the deprotonation of the NH_3^+ the particles have high negative surface charge that prevents the agglomeration of the particles due to charge repulsion. On the other hand, at pH 7, the zwitterionic cysteine molecule looses the benefit of strong repulsive forces. Yet, strong carboxylate stabilization might be influential in improving the luminescence of the particles. The luminescence of the particles decreases tremendously below pH 7 and vanishes at pH 6. At the acidic pH partial protonation of the thiol may cause desorption of the cysteine from the surface creating surface defects known to cause non-radiative events. Actually, such behavior can be exploited for pH sensitive probes or even in the cancer cell detection via luminescence, at relatively acidic pH of tumor cells the luminescence will drop dramatically [110].

2.4.4 Effects of reaction temperature on the particle size and optical properties

Reaction temperature has a dramatic influence on particle growth and emerged as a powerful tool to tune the color of emission. Green, yellow and red luminescent quantum dots were obtained by adjusting the reaction temperature at fixed reaction time (40 min), initial pH (9.5) and cysteine:Cd^{2+}:S^{2-} ratio of 2.5:1:0.5 (Figure 2.7). Increasing temperature leads into an increase in the reaction kinetics followed by an Ostwald ripening and in turn causes larger particles with relatively larger size distributions [111]. The particle growth was observed through the red shift of the absorption wavelength of the particles. On the other hand, increasing reaction temperature above the room temperature resulted in a loss of luminescent properties (Table 2.3). QYs estimated for QDs prepared at 30°C, 60°C and 100°C was 27%, 19% and 1%, respectively. Possible reasons of the inferior luminescence at higher reaction temperatures might be as fallows: Growth is faster at the higher temperatures and this may cause crystal defects that could act as deep traps. Besides, as the crystal size increases with the reaction temperature, ability to correct these defects by the coating molecule becomes unlikely. Also, at higher temperatures adsorption-desorption equilibria of the coating molecule speeds up leading to a less effective surface coverage leaving uncoordinated surface sites that would contribute to the non-radiative events as well.

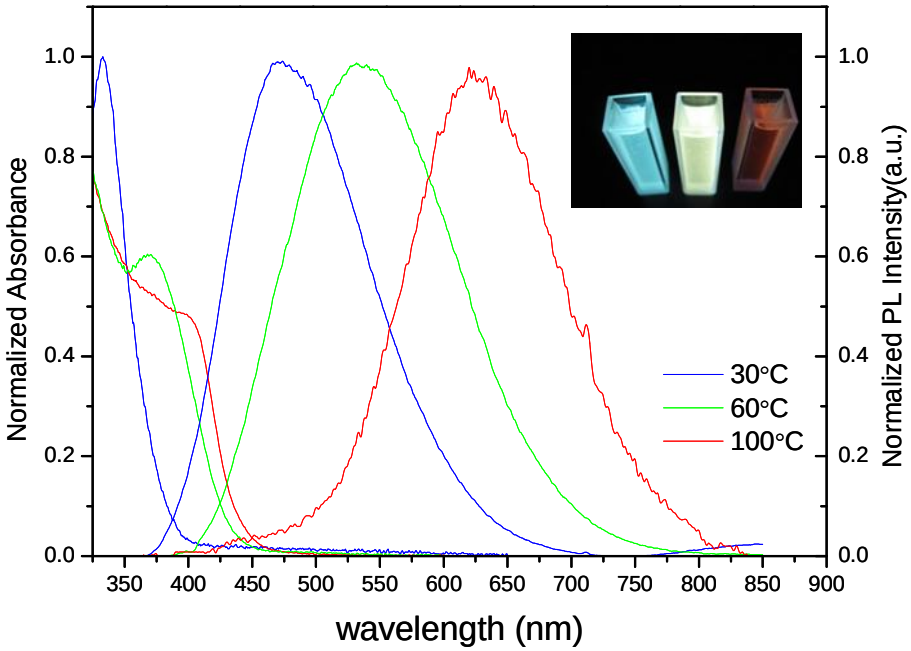

Figure 2.7 Different color emitting particles synthesized at 30, 60 and 90°.

Table 2.3 Properties of QDs prepared at different temperatures with fixed Cysteine:Cd^{2+}:S^{2-} ratio of 2.5:1.0:0.5.

Temp. (°C)	QY (%)	FWHM (nm)	PL Max (nm)	Abs. Edge (nm)	Particle Size (nm)
0-4	19	133	495.0	372	2.3
30	27	129	470.6	361	2.5
60	19	157	466.3	533	3.0
100	1	133	470.6	624	3.2

2.4.5 Cell viability and uptake

The *in vivo* use of quantum dots is limited due to the important concern of toxicity. Although there are few reports claiming no adverse effect or renal clearance, exposure to heavy metal ions raises a great suspicion about the realistic application of QDs *in vivo* [95]. Cadmium toxicity is well established [112]. Toxicity of cadmium containing QDs are mostly attributed to bleaching of Cd^{2+} ions as a result of degradation and oxidation of QDs and to the formation of reactive oxygen species [113]. Coating QDs help to protect the semiconductor core by preventing the oxygen diffusion, preventing particle degradation and aggregation. Colloidal instability is also claimed to attribute to the cytotoxicity of QDs, therefore improvement of colloidal stability is also essential [114]. It is quite difficult to compare the toxicity of new QDs with the existing ones since tests were generally performed with different cells and in different dosing methods. Nonetheless, it is crucial to investigate the cytotoxicity of these QDs *in vitro*.

L-Cysteine is an advantageous coating since it is not toxic itself. CdS-Cysteine QDs developed here demonstrated extended colloidal stability compared to other reported values of the similar QDs. Cytotoxicity of CdS-Cysteine QDs was evaluated *in vitro* at doses covering a broad range from 0.05-1.15 mg QD/ml at two incubation times of 24 and 48 hours to HeLa and MCF-7 cells. As a control, 0.05 mg/ml Cd^{2+} was also studied representing the Cd^{2+} amount present in the maximum dose of applied CdS-cysteine. Morphological changes of cells incorporating QDs were followed by phase contrast microscopy. Cell uptake and cell viability were determined by fluorescence measurements

and MTT assay measuring the mitochondrial activity. Figure 2.8 shows the cell viability data.

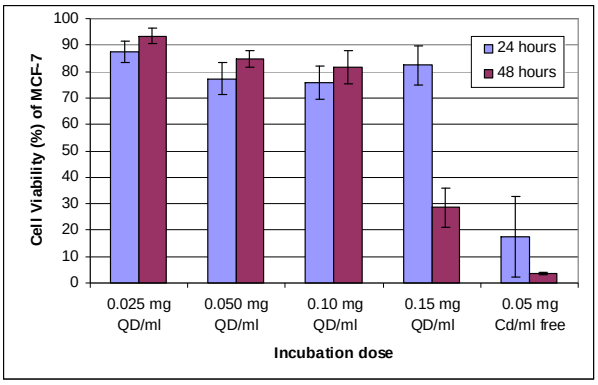

(A)

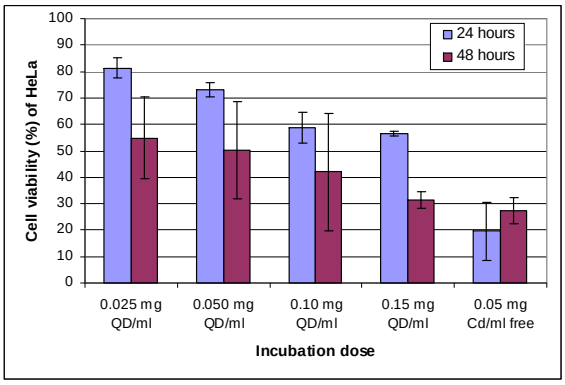

(B)

Figure 2.8 Cell viability of MCF-7 (A) and HeLa (B) cells in the presence of CdS-Cysteine QDs as a function of QD concentration at 24 and 48h incubation times. Last column in each plot represents the cell viability in the presence of free cadium acetate as a reference.

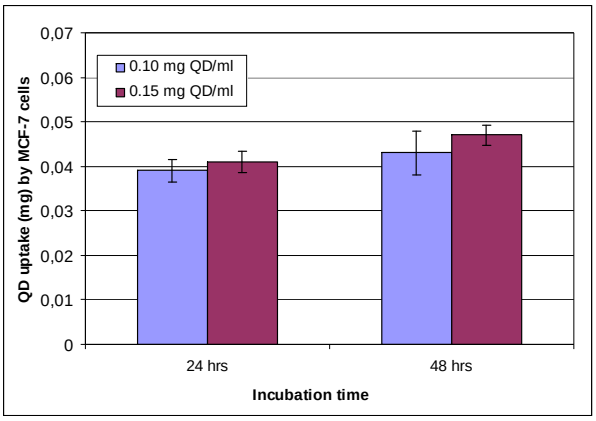

(A)

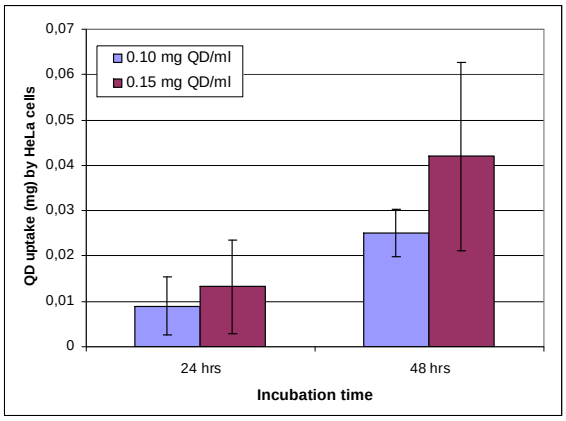

(B)

Figure 2.9 QD uptake of (A) MCF-7 and (B) HeLa cells treated with CdS-Cysteine at high dosages (0.10-0.15 mg/ml QD) after 24 and 48 hours of incubation.

Regardless of the cell line, cysteine coating improved the biocompatibility of the CdS QDs dramatically as cells are much more viable with CdS-Cysteine than pure cysteine

ion. Viability of MCF-7 cells is around 75-90% within the full range of QD doses at both incubation times, except at 48h with 0.15mg/ml dose. In case of HeLa cells, a dose and time depended toxicity was observed. In general, CdS-Cysteine QDs are more toxic to HeLa cells. Viability around 80% decreases below 60% at the highest dose in 24h, from over 50% to 30% in 48h. In the evaluation of toxicity, cell uptake of QDs should be considered as well (Figure 2.9). We have quantified the amount of QDs internalized by the cells at the two high doses (0.10 and 0.15 mg/mL QD) by the fluorescence intensity of the cells. Firstly, it should be stated that MCF-7 cells uptake significantly more QD than HeLa yet, they are more viable. So, there is a natural selection of cells which might be advantages for biotechnology and medical applications. Uptake of QDs by MCF-7 cells does not increase significantly after 24h or by increasing the amount of QD in feed, which would explain the relative insensitivity of viability to incubation time and dose for this cell line. On the other hand, HeLa cells internalize more particles at higher doses of QDs and a four-fold increase in uptake was seen at 48h. Cytotoxicity correlates with the intracellular level of the CdS-cysteine for the HeLa cell line. Increasing dose and time of exposure to QDs decreases the viability as the amount of QDs in the HeLa cells increases. Figure 2.10-A and 10-B shows the phase contrast and fluorescence microscopy images of the MCF-7 cells with no QD. Healthy cells with no luminescence were observed. Figure 2.10-C shows the MCF-7 cells with CdS-Cysteine QDs having normal morphology and epifluorescence image in Figure 2.10-D shows luminescence inside the cells confirming internalization. Such effective luminescence from the cells demonstrates the great potential of these QDs for imaging. Microscopy images of HeLa cells that internalized QDs at these high dose

and long incubation times were not shown since the viability is quite low under such conditions.

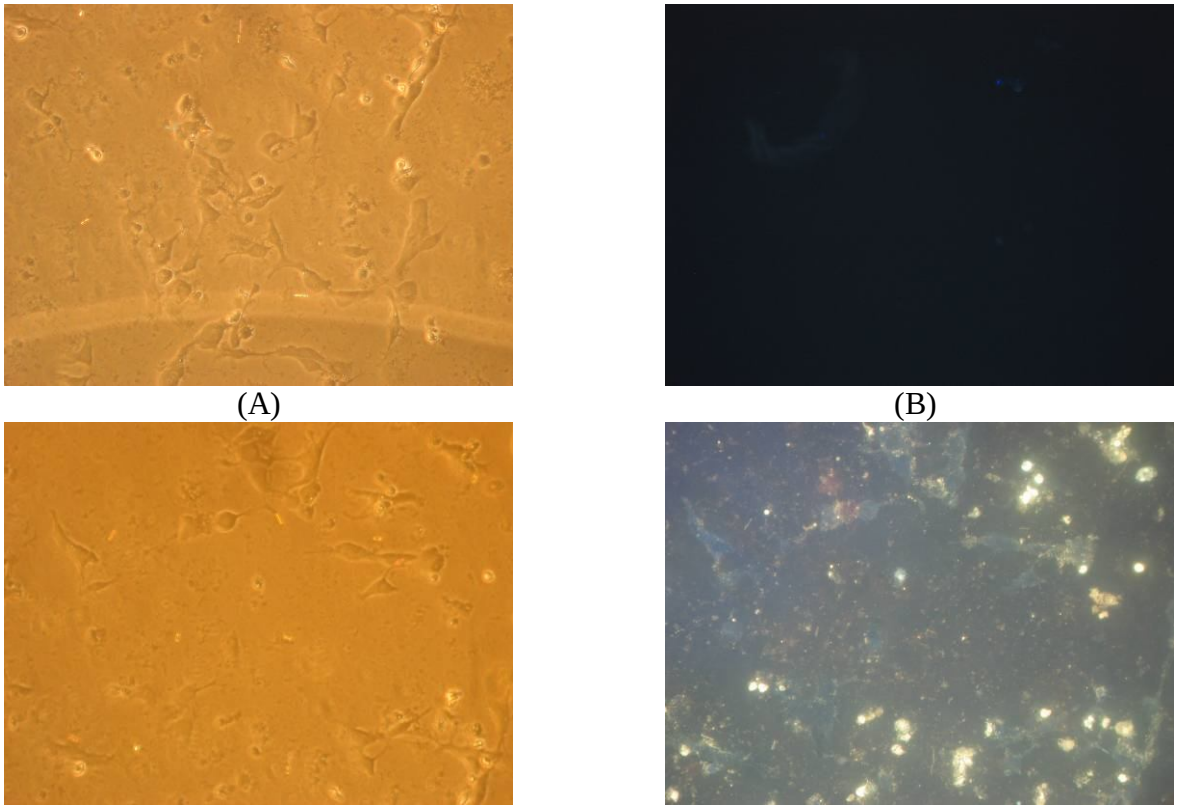

(A) (B)

(C) (D)

Figure 2.10 Phase contrast and fluorescent microscopy images of untreated (A and B) and treated (0.10 mg/ml CdS-Cysteine after 24h incubation) (C and D) MCF-7 cells. All transmitted light images were taken with phase contrast objectives/condenser. All epifluorescence images were taken with Zeiss Fset01 filter cube (DAPI filter). Yellow luminescence in D is an indicative of QD internalization by the cells**.**

2.5 Conclusions

Aqueous CdS-cysteine QDs with improved stability and luminescence were prepared in a simple, safe and non-expansive one-pot reaction method in short times and low temperatures. The crystal growth, quantum efficiency and stability were investigated as

a function of cysteine:Cd^{2+} mole ratio, pH and reaction temperature. Interestingly cysteine:Cd^{2+} ratio did not provided enough control to tune the particle size but the ratio was influential in the luminesence. pH of the medium emerged as an important factor not for the crystal size that much but for the luminescence intensity of the QDs, as well. Results revealed an optimum cysteine:Cd^{2+} ratio of 2 and a reaction pH of 9.5 for the best luminescing QDs. At the optimum conditions QYs as high as 19% was achieved at room temperature. Particles are colloidally stable and maintain the original luminescence even after 9 months so far. QY of the particles improved up to 55% when washed and redispersed in pH 7 medium. Best reported QY was 13% so far [104].

Aqueous CdS-cysteine QDs luminescing in different colors are first reported here to the best of our knowledge. As the temperature of the reaction increases, particle size increases causing a red shift in the luminescence but with a drop in the QY. This also suggest that the improved properties and smaller size of the QDs prepared here at 30°C may also depend on the reaction temperature compared to prior ones mentioned above. Besides, lower reaction temperature adopted here allowed color tuning by adjustment of the reaction temperature which was not possible for the previous higher temperature processes. Availability of few different emission colors with the same QD chemistry is advantages in many applications especially in imaging, barcoding and multiplexing.

In vitro cell studies of these QDs in a broad range of doses indicated an interesting preferential uptake and difference in the toxicity for different cell lines. MCF-7 cells have a significantly higher uptake of the particles but yet are more viable than HeLa. QD

internalization and effective luminescence from the cells confirm the utility of CdS-cysteine for in vitro and in vivo imaging.

Cysteine coated quantum dots with such improved properties and simple preparation method emerges as a valuable candidate for bio-applications requiring aqueous QDs. These particles can replace the commercial aqueous QDs which are usually less luminescent [115]. Although CdS is used here, the method can be successfully applied to other cores such as CdTe or core shell structures such as CdSe/ZnS. For all the particles described here, luminescence can be improved further by capping CdS core with a wider band-gap material such as ZnS. Other methods such as size selective precipitation and metal cation addition can further enhance the luminescence. Functional groups of cysteine residing on the particle surface can be utilized to attach biologically significant molecules such as drugs, targeting ligands, polyethylene glycol chains, proteins, etc. Currently, we are improving the system and utilizing such particles for the development of hybrid systems exploiting the improved luminescence and surface functionality.

Chapter 3

ONE-POT AQUEOUS SYNTHESIS OF MAGNETIC LUMINESCENT CdS-Fe_3O_4 NANOPARTICLES

3.1 Introduction

Nanoparticles are important in the biological area with their abrupt transition in the last few decades. Significant amount of investment was done on quantum dots and superparamagnetic iron oxide nanoparticles which found potential applications in biotechnology and healthcare [116]. Quantum dots with unique optical and electronic properties offers enormous benefits in optical imaging, immunoassays, sensors and fluorescent labeling [86, 117]. On the other hand, magnetic nanoparticles have been used in medical imaging and therapy as contrast agents in magnetic resonance imaging or for drug delivery and magnetofection. For many applications of QDs and MNPs, surface functionality is the key factor to control the interaction of nanoparticles with biological species, self-assembly, dispersion and particle size. As explained previously in Chapter 1, many methods have been urged to provide a hybrid system with the optical properties of

luminescent quantum dots and magnetic properties of iron oxides. Development of such a multi-functional single entity will potentially provide delivery through magnetic field and detection mode both optically and magnetically. Therefore, individually prepared quantum dots and magnetic nanoparticles in appropriate organic synthetic routes were traditionally unified through silica matrix. The drawback of such organic route is the urgent need to transfer such systems into aqueous phase for biological applications. The consequences of such a process are the broadening in size distribution, imperfections on the surface leading to agglomerations and unpredictable optical and magnetic properties. Our approach in the production of composite structure is a greener route using a biologically safe coating and a one pot synthesis method. Specifically, biocompatible L-cysteine capped aqueous CdS QDs will be used in the stabilization of iron oxide nanoparticles in an aqueous environment. Hereby, L-cysteine with functional units of carboxylate and amine groups will provide the water solubility and stabilization of iron oxide nanoparticles.

The knowledge that is gained from the previous studies will be helpful to optimize the reaction parameters like; reaction temperature, reaction concentration, surfactant to cation ratios and significantly the number of quantum dots per each iron oxide nanoparticles. Usually, aqueous synthesis of the QDs luminesces less than the organically prepared QDs. Therefore, our approach in the design of the composite structure first involves the synthesis of QDs individually in the best conditions such as; narrow size distribution, high quantum efficiency, colloidal stability and biocompatibility. Then, these highly luminescent QDs are used as a coating material in the aqueous synthesis of magnetic iron oxide nanoparticles. An important challenge in the project is the design of multi-color

magnetic luminescent nanoparticles. Our studies with L-cysteine revealed that the size and the emission color of QDs can be altered by reaction temperature which would provide an opportunity towards the achievement of such a goal.

Magnetic fluorescent nanoparticles have a great potential in biomedical applications especially in imaging, sensing and separation by combining two entities. Also, the one-pot synthesis of composite structures will provide ease in the production and characterization of the magnetic fluorescent nanoparticles and will be the first one-pot synthesis in the literature.

3.2 Experimental Section

3.2.1 Materials

All the chemicals used were of analytical grade or of the highest purity commercially available. Sodium sulfide trihydrate ($Na_2S{\cdot}3H_2O$), (R)-(+)-Cysteine, cadmium acetate dihydrate $(CH_3COO)_2Cd{\cdot}2H_2O$), iron(III) chloride hexahydrate ($FeCl_3{\cdot}6H_2O$), iron(II) chloride tetrahydrate ($FeCl_2{\cdot}4H_2O$) and rhodamine B were purchased from Merck. Sodium hydroxide and acetic acid were purchased from Aldrich and LaCheMa, respectively. High purity water was used from Milli-Q water (Millipore) system.

3.2.2 Synthesis of (R)-(+)-Cysteine capped CdS QDs

(R)-(+)-Cysteine capped CdS QDs were prepared using a synthetic route reported earlier.[100] Briefly, 66.6mg of $Cd(Ac)_2{\cdot}2H_2O$ was dissolved in 50ml of water where the

three-necked round bottom flask was constantly stirred with 400 rpm through out the reaction. An appropriate amount of L-cysteine was dissolved in the above solution. Concurrently, the system was deoxygenated with constant nitrogen flow for twenty minutes after the adjustment of the reaction media to the desired pH conditions with 10M NaOH or concentrated HAc. The sulfide solution was prepared by dissolving 16.6 mg of $Na_2S{\cdot}3H_2O$ in 50 ml of water with ultrasonic agitation. The sulfide solution was deoxygenated and added to the cadmium solution through an addition funnel with a drop wise addition. Reactions were stirred under N_2 for 30 minutes and then stored in refrigerator.

Precipitation of the quantum dots were achieved by the following procedure. A batch solution was lyophilized and dissolved in 3ml of water. The solution was well mixed with 5ml of isopropyl alcohol (IPA) and centrifuged for 15 minutes at 3900rpm. After discarding the non-luminescent solvent, the resulted precipitate was treated in the same way three more times. The final precipitate was dissolved in 5ml of water and lyophilized to remove IPA and water from the system.

The pH study was performed by dissolving an appropriate amount of the previously obtained precipitate into 6mL of buffer solutions (Merck borate buffer solutions). In order to have a comparable data, a sample was dissolved in 6ml of double distilled water, as well.

3.2.3 Synthesis of Cysteine-CdS-γ-Fe_3O_4 Hybrid nanoparticles

Quantum dot solutions were used for the synthesis of the hybrid nanoparticles without any treatment. After the deoxygenatation of the solution for 15 minutes, Fe^{3+} and Fe^{2+} salts were added at a 2:1 ratio. The hypothetical ratio of γ-Fe_3O_4/CdS was ranging

from 2.4 to 30. The concentration of CdS was kept fixed at 1mM and only the total iron concentration in the solution was varied from 2.4 mM to 30 mM). The amount of the base was calculated by considering the amount of the carboxylic acid and chosen as [Base] = [carboxylic acid] + 2.5×[iron]. Approximately 360-1100µL of NH_4OH (%25, Merck) was added directly to the solution when the system was equilibrated at 85°C for 15 minutes. The color of the solution turned to black from an orange color with the addition of the base. Reaction usually stirred at this temperature under nitrogen for 45 min, then cooled to room temperature.

The excess amount of quantum dots were washed off by distilled water from a 30K molecular weight cut-off ultracentrifuge device until no more quantum dots were detected in the filtered solution. Horiba Jobin-Yvon Fluoromax-3 Spectrofluorometer was used to check the PL intensity of the filtrate. The concentrated supernatant was lyophilized for further characterizations.

3.3 Results and discussion

In the synthesis of magnetic fluorescent quantum dots, nanoparticles do not form a direct linkage but a spacer molecule is introduced to stabilize both entities simultaneously. The quenching of the fluorophores is partially prevented by providing a sufficient distance between the two particles to hinder the interference of the magnetic core. L-cysteine is a relatively small molecule with three functional groups when compared with the previous studies using spacer groups such as carboxylic acid modified porphyrin,

poly(ethyleneimine) or oleate bilipid layer in the synthesis of fluorescent magnets [64, 65, 118].

L-cysteine is a trifunctional molecule with carboxylic acid, amine and thiol groups, and as explained in Chapter 2 successfully coats CdS nanoparticles through sulfur binding leaving the amine and the carboxylic acid moieties free. The simultaneous passivization of the magnetic nanoparticles is achieved by the carboxylate units of the system. Simply, L-cysteine coated CdS acts as a coating for the magnetic nanoparticles (Scheme 3. 1).

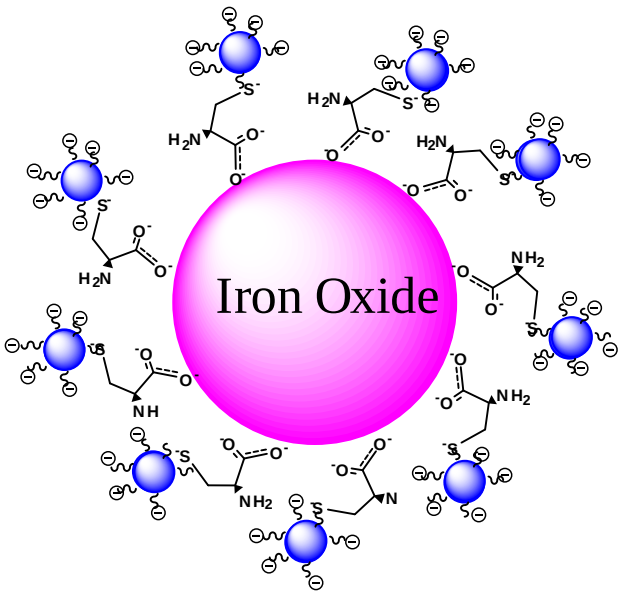

Scheme 3. 1 The representation of hybrid system CdS/L-cysteine/**γ-**Fe_2O_3.

In our experiments, hybrid magnetic fluorescent nanoparticles were obtained by varying the Fe/Cd ratio, pH and reaction time. The stabilization of the iron oxide particles were done by using the L-cysteine capped fluorescent particles as stabilizer for the magnetic core. Therefore, the most important parameter was the ratio of the luminescent particles for each iron oxide particle. The number ratio of the fluorescent nanoparticles to

magnetic particles is more important than the concentration ratio. The following equation can be used to calculate the number of luminescent particles needed to cap the core of a certain size magnetic nanoparticle [63].

$$N_{QD} = \frac{2\pi(R_{Fe_3O_4}{}^2 + R_{QD}{}^2)}{\sqrt{3}R_{QD}^2} \qquad (3.1)$$

N_{QD}, R_{QD} and R_{Fe3O4} are the number of QDs, radius of the iron oxide and QD, respectively. Stable colloidal solutions of magnetic fluorescent nanoparticles were synthesized by taking the radius of quantum dot and the radius of iron oxide as 2-8 (SS13GFe8) and 3-15 nm (SS13GFe6). When the radiuses of the particles were taken as 3 and 15 nm, N_{QD} was calculated as 96. Such a calculation considers the formation of gaps between the QDs in the first layer coating and neglects the formation of clusters around the magnetic core. When the radius of QD was taken as 3nm and the radius of magnetic core was taken as 50nm, N_{QD} was calculated more than 1000 QDs. As the N_{QD} increases, the calculated concentration of iron oxide increases. Trials for the hybrid nanoparticles synthesis were summarized in Table 3. 1.

Table 3. 1 Hybrid nanocomposite trials at different iron and base concentration. Best working conditions are highlighted.

Sample name	Cd concentration [mM]	Fe concentration [mM]	(NH_4OH) [mL]	Luminescent / Magnetic
SS13GFe1	1	6.3	6.00	N/Yppt
SS13GFe2	1	5.5	1.00	N/Yppt
SS13GFe3	1	5.5	0.30	Y/Yppt
SS13GFe4	1	30.0	1.10	N/Yppt
SS13GFe5	1	30.0	1.10	N/Yppt
SS13GFe6	**1**	**3.0**	**0.36**	**Y/Y**
SS13GFe7	1	10.0	0.93	Ysol/Yppt
SS13GFe8	**1**	**2.4**	**0.10**	**Y/Y**
SS13GFe9*	**1**	**3.4**	**0.36**	**Y/Y**
SS13GFe10	1	11.0	0.36	Ysol/Yppt

*Synthesized with method 2.
Ysol : Luminescence from solution.
Yppt : Magnetic precipitation.
N : No ; Y : Yes

When the concentration of iron increased above 3.5 mM, hybrid particles were precipitated out of the solution but they were all magnetic. In these cases the capping could not prevent the agglomeration of the magnetic particles. As the concentration of the iron oxide increases, the size of the magnetic core and possibility of cluster formation increases and the stabilizer can not passivate the surface effectively. Another important parameter in the synthesis is the amount of NH_4OH that is used to adjust the pH value. The aqueous syntheses of paramagnetic iron oxides are done around 85°C with rapid injection of NH_4OH. When the iron salts are introduced into the colloidal luminescent QD solution, the

pH drops from 10 to 3.5. At this pH value, no luminescence is observed from the solution. When the ammonia source is injected at 85°C, the color of the solutions turns to dark brown from orange. The final pH of the solution is adjusted to 10 with the appropriate amount of NH_4OH solution that is calculated by considering the amount of carboxylic acid to be neutralized and the amount needed to form Fe_3O_4. In the reactions, the calculation that is used to obtain the amount of base needed was done by 2.5 times the iron concentration with additional base for each carboxylate unit in the system. As obtained base concentration was too much to raise the pH of the reaction to 10 and therefore the amount is lessen in such to keep the final pH around 10. The last important variable in the synthesis is the reaction time. As the reaction time increases more than two hours, the fluorescence disappears. The optimum reaction time for the production of stable colloidal composite was not more than one hour. Particle size of QDs increase with extended reaction times causing a decrease in the luminescence with red shift in PL maximum. In addition to that, the magnetic particles tend to agglomerate with longer reaction time (data not presented). Hereby, we have only demonstrated yellow luminescent hybrid nanocomposite prepared with the QD having initially a bluish luminescence.

A novel method was tried to prevent the aggregation and the drop in luminescence. The pH of the QD solution drops down to acidic range, when Fe^{3+} salt was introduced into the quantum dot solution which can be explained by the hard-soft acid base theory. Then, the surface modification annihilated by the hydronium ion at acidic pH but the luminescence is recovered when pH is adjusted over 6 with some loss in the PL intensity (data not presented). On the other hand, the addition of Fe^{2+} into the basic quantum dot

solution first will result into the rapid formation of iron oxide and iron hydroxide molecule at this high pH due to the soft character of Fe^{2+}. A better method (method 2) is to add the previously dissolved iron salts into basic quantum dot solution. In here, NH_4OH was added to the quantum dot solution simultaneously which did not dramatically change the pH of the solution or the PL intensity. Then the QD solution temperature was adjusted to 85°C and the iron solution was added gradually. Such a reaction method when compared with the traditional method resulted in higher concentration of iron oxide formation. This has been confirmed through the color of the solution and the absorption spectra (Figure 3. 1).

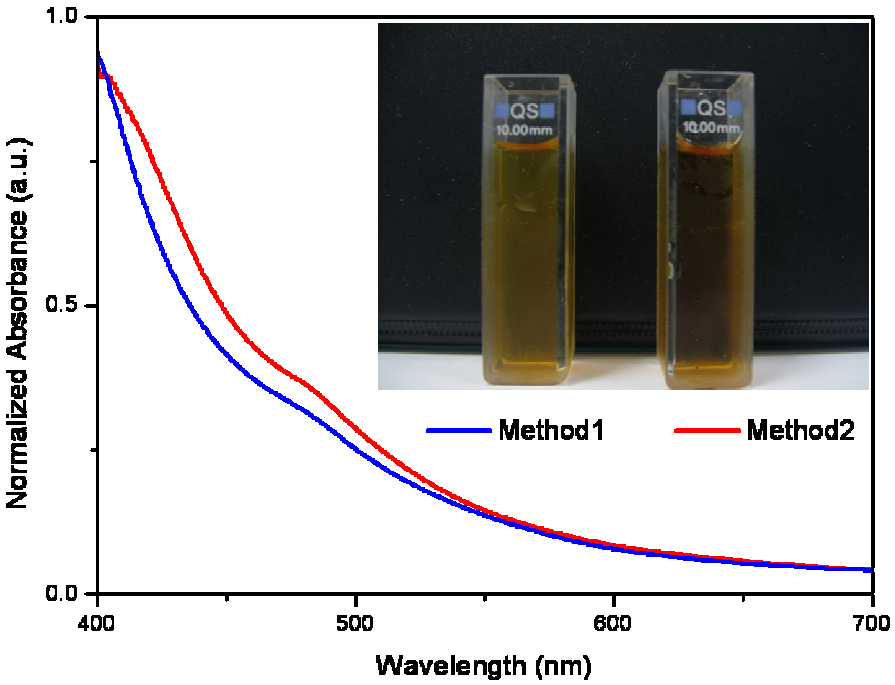

Figure 3. 1 Normalized absorption spectra of hybrid nanocomposites synthesized with different approaches. Inset picture, the left one is the traditional (method 1) and right one is the new method (method 2).

The color of the colloidal hybrid solution at the end of the reaction is dark brown, which is a typical color for iron oxide solutions, where as QD solutions were colorless.

When the concentration of the iron oxide increases, the color becomes more intense. On the other hand, no matter how concentrated the solution is, there is always luminescence on the surface of the solution when excited at 355nm UV lamp (Figure 3. 2). When the solutions were washed through 5K ultrafiltration devices and lyophilized, the dried powders respond to external magnet demonstrating the magnetic nature of the hybrid nanoparticles (Figure 3. 3).

Figure 3. 2. The left cuvette in both pictures is L-cysteine/CdS/γ–Fe_2O_3 hybrid system and right cuvette belongs to L-cysteine/CdS QDs. Picture in the left taken under daylight and the right with UV radiation at 355nm excitation.

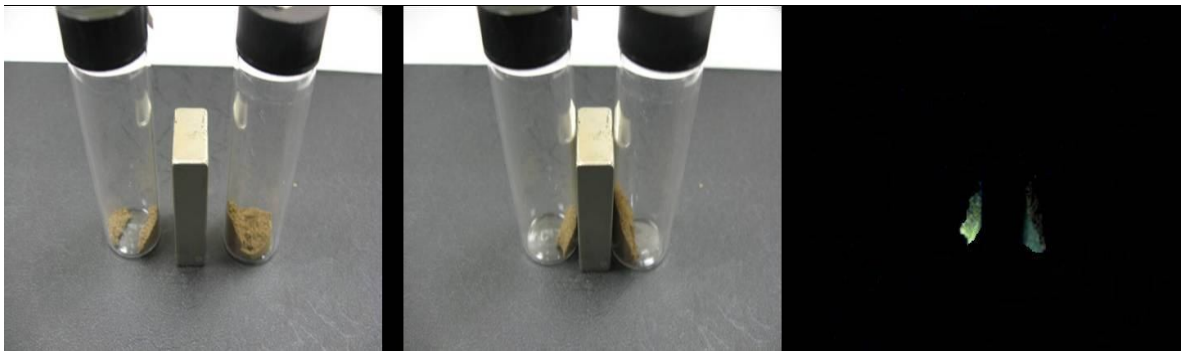

Figure 3. 3 Response of the hybrid nanocomposites to the external magnetic field under day light (left and middle) and under 355nm excitation (right). In each picture on the left side is SS13GFe8 and on the right side is SS13GFe6.

The absorption and photoluminescence spectra of the QD and the hybrid nanostructure were shown in Figure 3. 4. The hybrid system absorption spectra did not reveal any peak maxima as was observed for the CdS QD at 368nm. The hybrid absorption started around 700 nm and covered the whole absorbance region of CdS. A typical absorbance spectrum of iron oxide was also demonstrated in the Figure 3. 5.

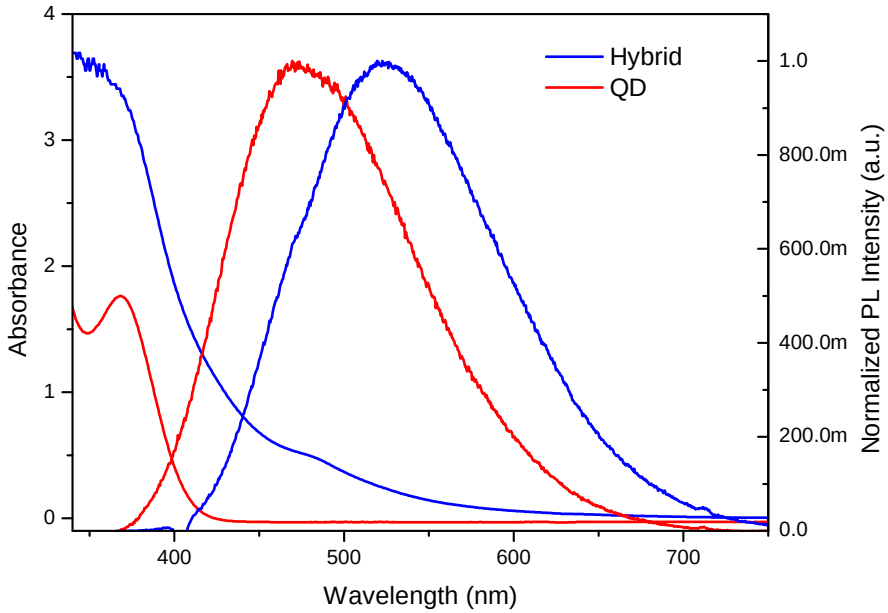

Figure 3. 4 The absorption and normalized PL spectra of L-cysteine/CdS/γ–Fe_2O_3 (blue) and L-cysteine/CdS QDs (red).

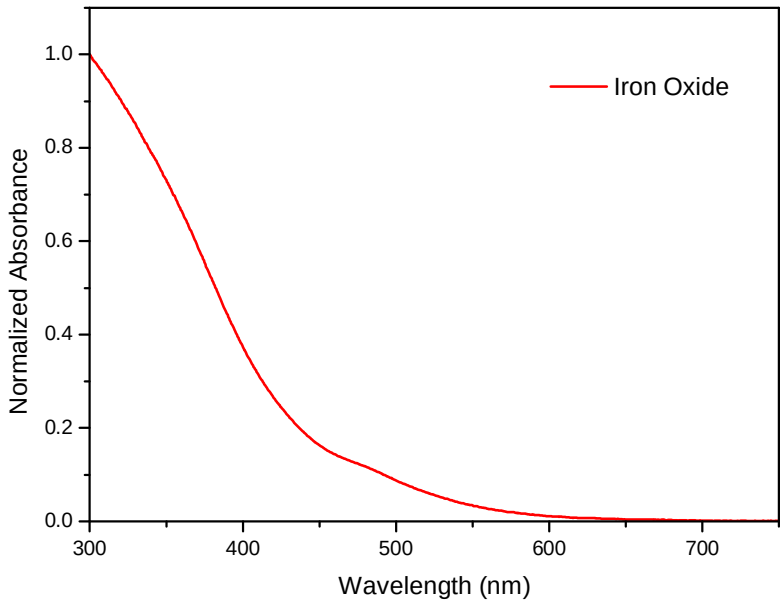

Figure 3. 5 UV/VIS spectrum of superparamagnetic iron oxide synthesized through aqueous route.

When we compare the emission spectra, the emission peak for the hybrid system shift to a longer wavelength approximately 50 nm, possibly indicating the formation of larger QDs. In order to explain such a crystal growth during the hybrid synthesis, sample synthesized at 30°C was heated up to hybrid reaction temperature of 85°C. The sample was then refluxed at 85°C for one hour which is the shortest reaction time used for the hybrid synthesis. The change in absorption and PL spectra was shown in Figure 3. 6. There is a significant red shift in both absorbance and PL spectra of the samples. The absorption edge of the particle shifted from 396 nm to 437 nm which corresponds to the particle size of 2.5 nm and 3.1nm, respectively (calculated from Brus equation). The particle size increase complements the shift in PL intensity from 499 nm to 519 nm. Hereby, 20 nm shifts in PL intensity was observed by keeping the reaction parameters constant other than the reaction temperature. A further red shift in PL can be partially explained by the reaction temperature effect on particle size but also the change in reaction pH initially with the addition of iron salts and finally with NH_4OH should also be considered.

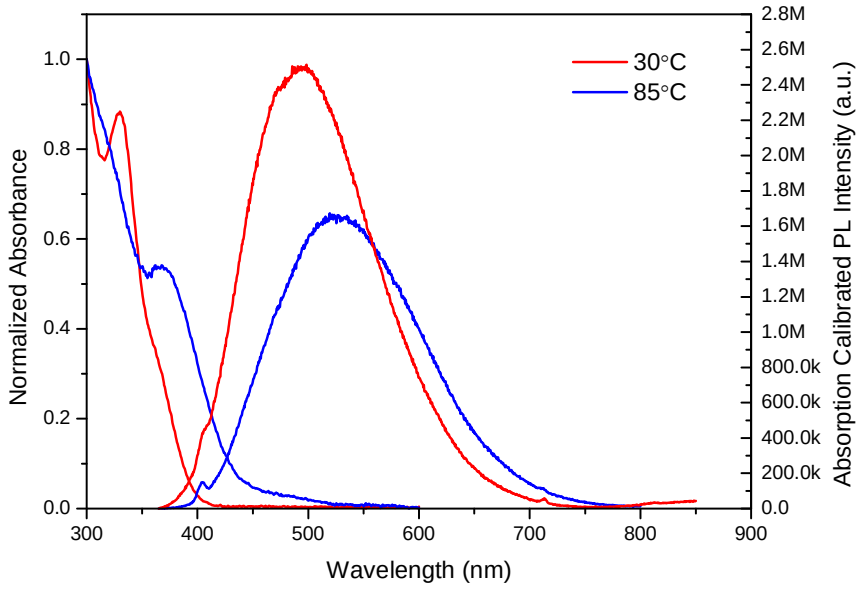

Figure 3. 6. The change in absorption calibrated PL intensity and normalized absorbance of L-cysteine/CdS QD synthesized at 30°C and refluxed at 85°C.

A similar study was repeated to understand the growth of luminescent nanoparticles during the hybrid synthesis, L-cysteine/CdS QD was placed in a UV-spectrophotometer and temperature was ramped to 70°C (maximum possible temperature for the instrument). Then the UV absorbance spectra were recorded at different time intervals. In Figure 3. 7, a red shift in the absorption edge of the particles with time is visible. Also, absorbance at 420 nm showed a linear increase with time (Figure 3. 8). Therefore, 50nm red shift in the emission spectra of the hybrid nanoparticles at least partially can be attributed to the further crystal growth of the CdS. Actually this is in agreement with the observed color changes of the luminescence between the QDs and the hybrid structures from bluish to yellow luminescences.

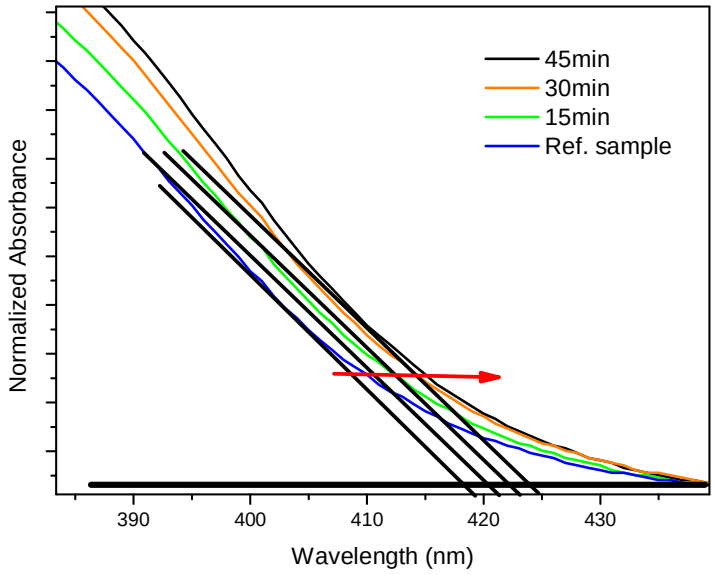

Figure 3. 7 The red shift observed for the absorption of L-cysteine/CdS QDs in 15 minutes intervals at 70°C.

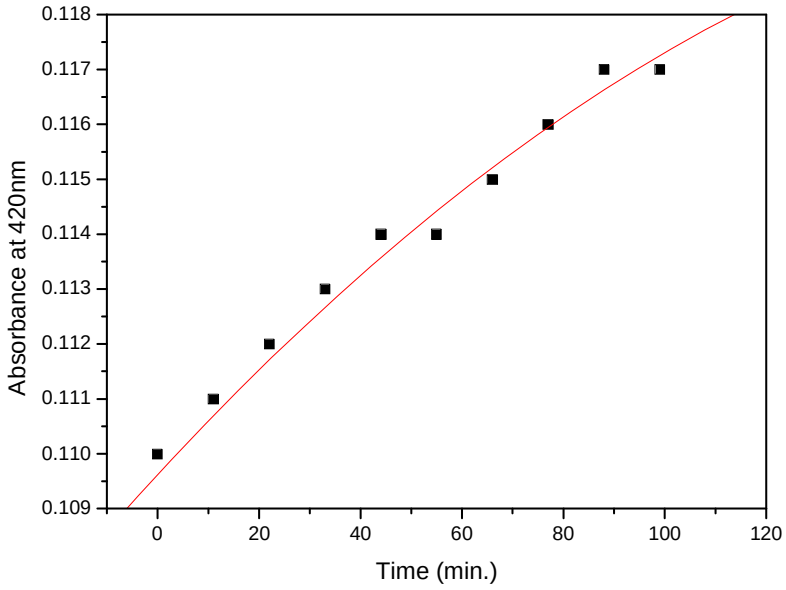

Figure 3. 8 The intensity change for the L-cysteine/CdS QDs at 420 nm absorption plotted against increasing reaction time.

As can be seen in Figure 3. 2, luminescence of the hybrid nanoparticles are not as good as the parent QDs. The photon emission from luminescent nanoparticles is absorbed

by the magnetic iron oxide particles. As can be seen in Figure 3. 5 iron oxides have strong absorbance in the region where QDs emits. Therefore, any QY calculation in such systems will be difficult when the system is calibrated with the absorption values. The other reason attributed to the decrease in QY can be explained by the growth kinetics. The particle reaction temperature around 80-90 °C initiates the Ostwald ripening that results into larger luminescent particles. Thus, the increase in the amount of surface defect sites increases the non-radiative recombination that consecutively decreases the QY. The QY was calculated below 1% for CdS QDs synthesized at 90°C due to the above mentioned problem; and the highest QY for hybrid nanoparticles was calculated as 0.3% (Sample SS13GFe6). The QY can be increased by providing a controlled close packed structure that decreases the lattice mismatch in the structure, or by controlling the magnetic nanoparticles/QD ratio.

The samples were washed from 5K filter in order to avoid the unbounded fluorescent QDs and excess residuals. All FT-IR, TEM, p-XRD and VSM measurements were performed on washed samples. FT-IR spectrum of the L-cysteine, L-cysteine capped CdS and L-cysteine stabilized CdS-Fe_2O_3 hybrid were shown in Figure 3. 9. The carboxylate formation was also observed for the hybrid system like QDs where the characteristic peaks showed up at 1407 and 1600 cm^{-1}. The absorption of Fe-O stretching vibration was observed with a sharp peak at 541 cm^{-1} with broad peaks at 675, 614, 584 and 461 cm^{-1} [119, 120].

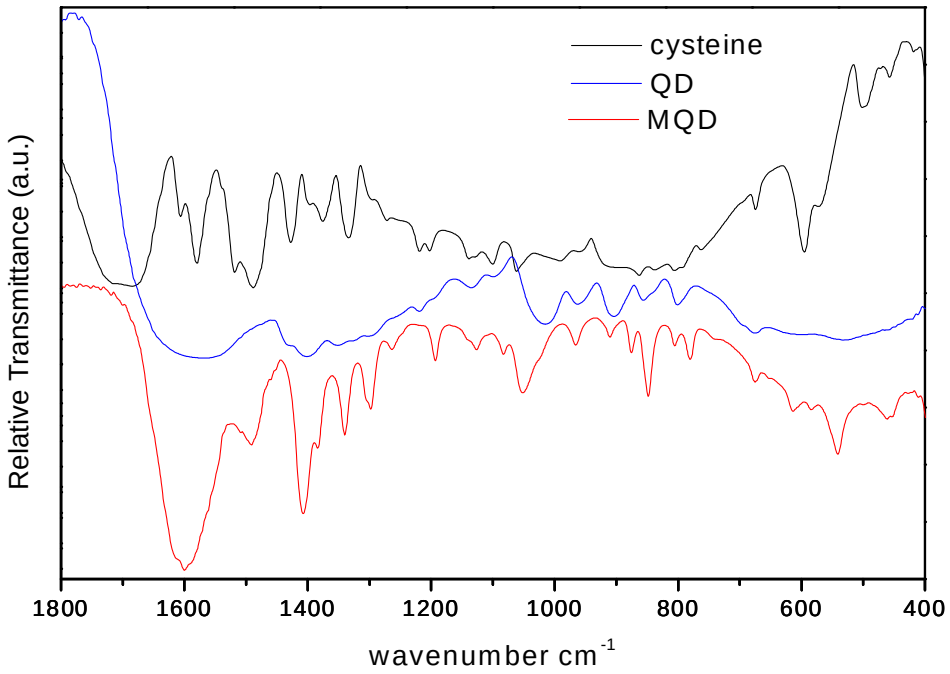

Figure 3. 9 FT-IR spectra of L-cysteine, L-cysteine/CdS QD and L-cysteine/CdS/γ–Fe_2O_3

The magnetic luminescent nanostructure sustained colloidal stability in water for more than seven months. The surface charge of the hybrid particles were measured as -50mV. This indicates that most of the carboxylate units on the CdS surface are still free after some have been used for the stabilization of the iron oxide nanoparticles. Negatively charged surfaces create repulsive forces that prevent agglomeration and enhance the water solubility. pH has a tremendous effect on the stability of the colloidal solution. This effect was inspected by dissolving the nanoparticles in different pH buffer solution. The zeta potential in the pH range of 6 to 10 was negative where the potential value was tend to decrease going from 7 to 6 which could cause loss of stability at pH values below 7 (Figure 3. 10).

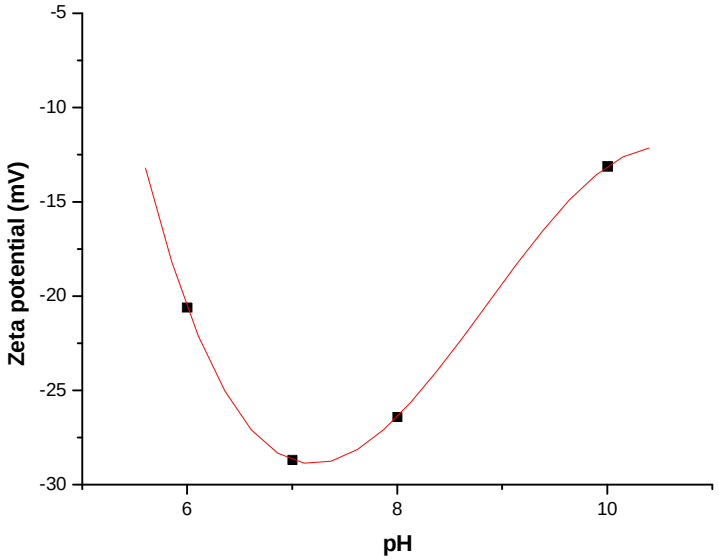

Figure 3. 10 Surface charge measured by ζ-potential at varying pH for washed L-cysteine/CdS/γ–Fe_2O_3 solution.

Such behavior was supported by the hydrodynamic size measurements as well. Colloidal solutions of the hybrid nanoparticles show a single size distribution around 108 nm. When the particles are washed and dissolved in buffer 6, the hydrodynamic size increases up to 300 nm (Figure 3. 11).

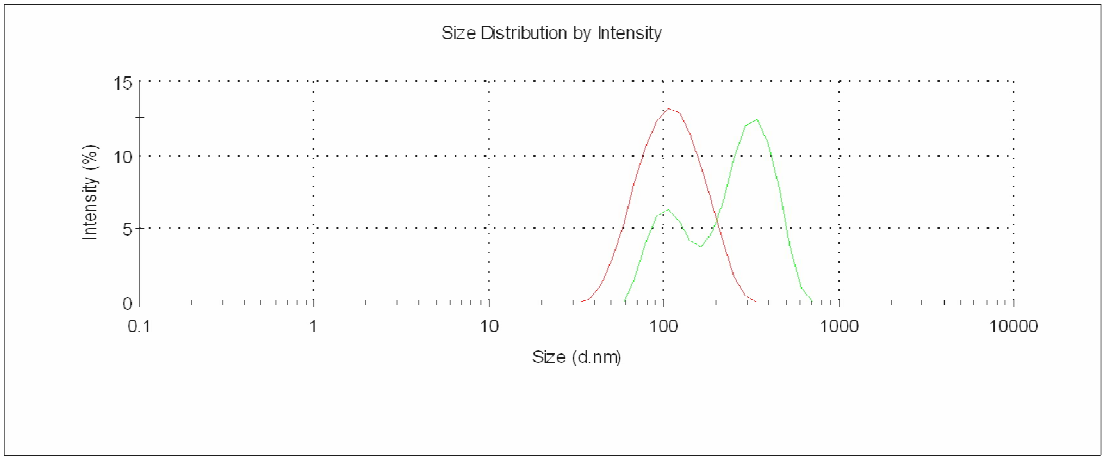

Figure 3. 11 Hydrodynamic size distribution of hybrid nanoparticles at final pH around 10 (in red) and dissolution of washed sample in buffer 6 solution (in green).

In the characterization of the hybrid nanoparticles with hydrodynamic measurements, the particle size increase was observed. The bare CdS QD solution gave a Gaussian sharp curve which indicates the narrow size distribution of the nanoparticles. The number and intensity distributions were almost exact match which is common for monodisperse size distributions. When the hybrid samples are measured, the peak position has shifted to larger particle sizes. There was no indication for the unbounded luminescent nanoparticles existence in the system since no peak showed up around 3nm (Figure 3. 12). Therefore, iron oxide nanoparticles were stabilized by the QD nanoparticles as coordinating group. Overall, the hydrodynamic size of the nanoparticle increased from 3.3nm to 106nm.

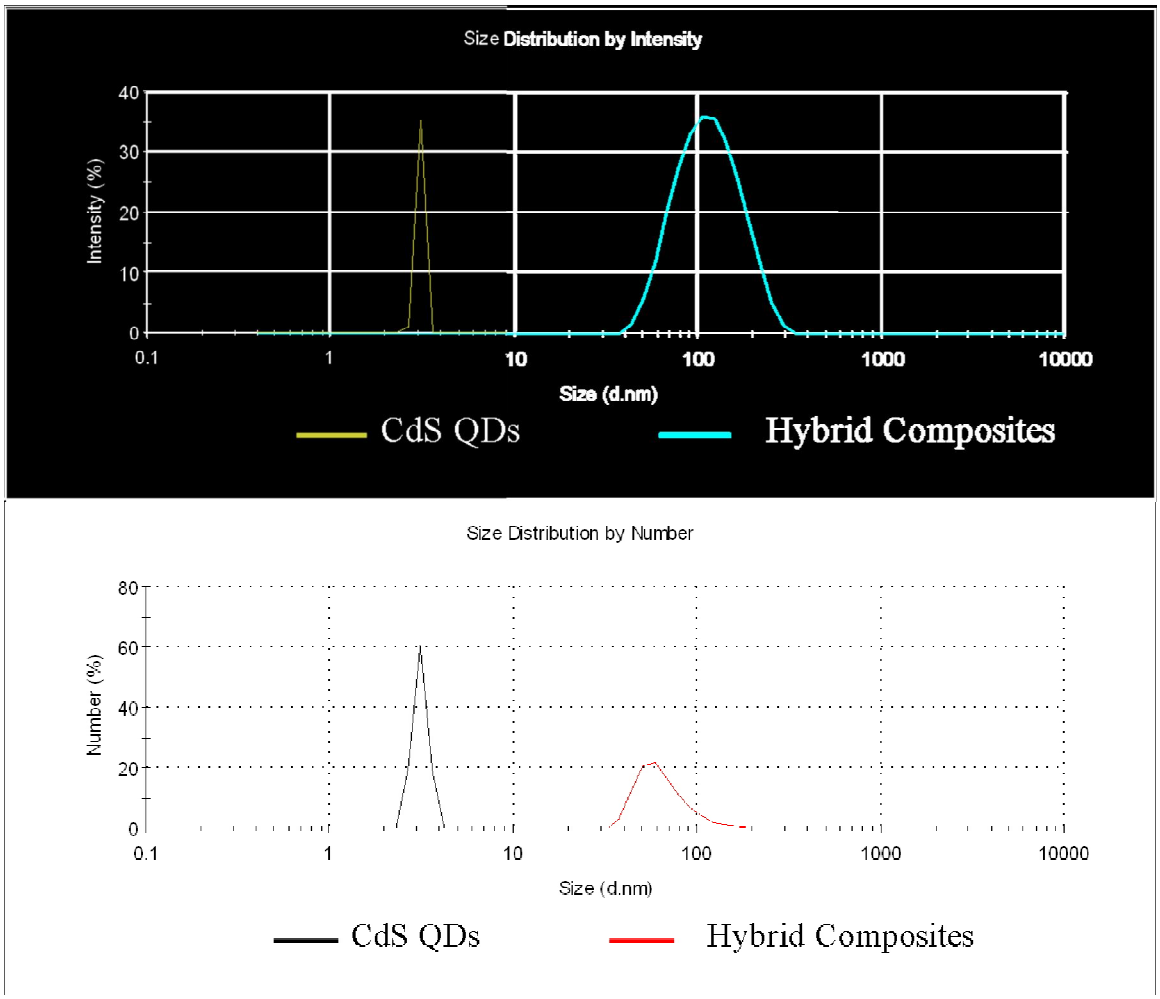

Figure 3. 12. Size distribution by intensity (top) and number (bottom) of L-cysteine/CdS QDs and L-cysteine/CdS/γ–Fe_2O_3.

The particle size determination was also done by TEM to the washed samples. The method that is used in taking the images of the samples causes our particles to coagulate. When a dilute sample is deposited on the grid, the specimen let to be dried on the grid through evaporation. The image taken from a coagulated region can be seen in Figure 14. A representation of the coagulation unit was also imaged where the particle size of single unit was no larger than 20 nm.

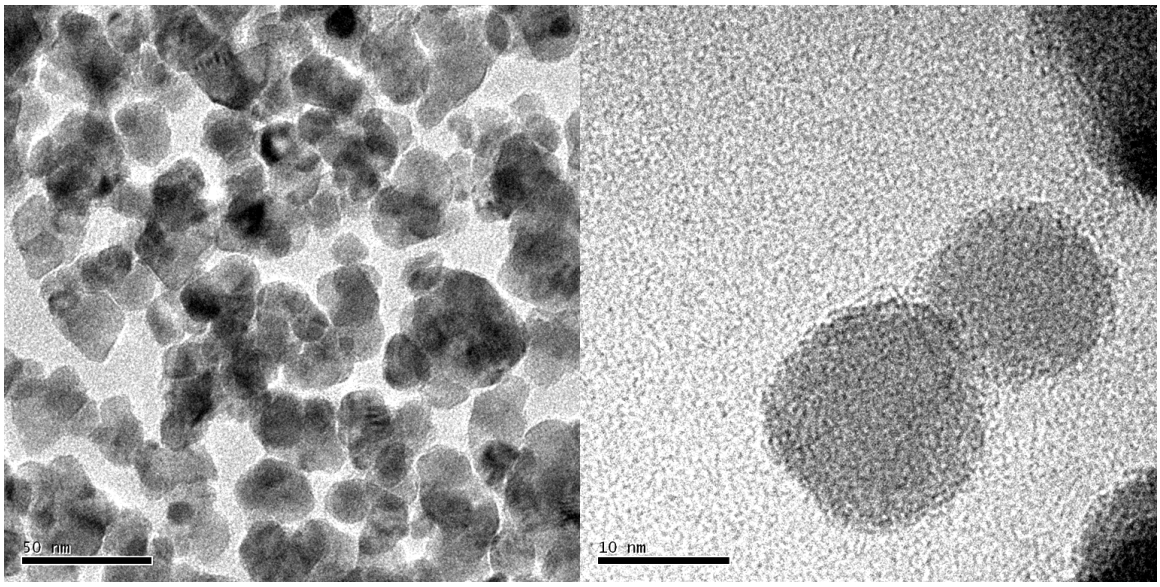

Figure 3. 13 TEM image of L-cysteine/CdS/γ–Fe_2O_3 (left) and representation of the coagulation (right).

In order to investigate the existence of the both species in the hybrid structure, samples for p-XRD measurement were prepared. The diffraction pattern of the composite has broad peaks due to averaging of reflections coming from different directions which are very common for small crystals. The powder XRD pattern of the hybrid particles was well matched with the theoretical peak positions of the γ-Fe_3O_4 (Maghemite) and cubic CdS peaks were diminished within the iron diffraction peaks and also less intensified (Figure 3. 14). The average particle size of γ-Fe_3O_4 was calculated as 6 nm by Scherrer equation.

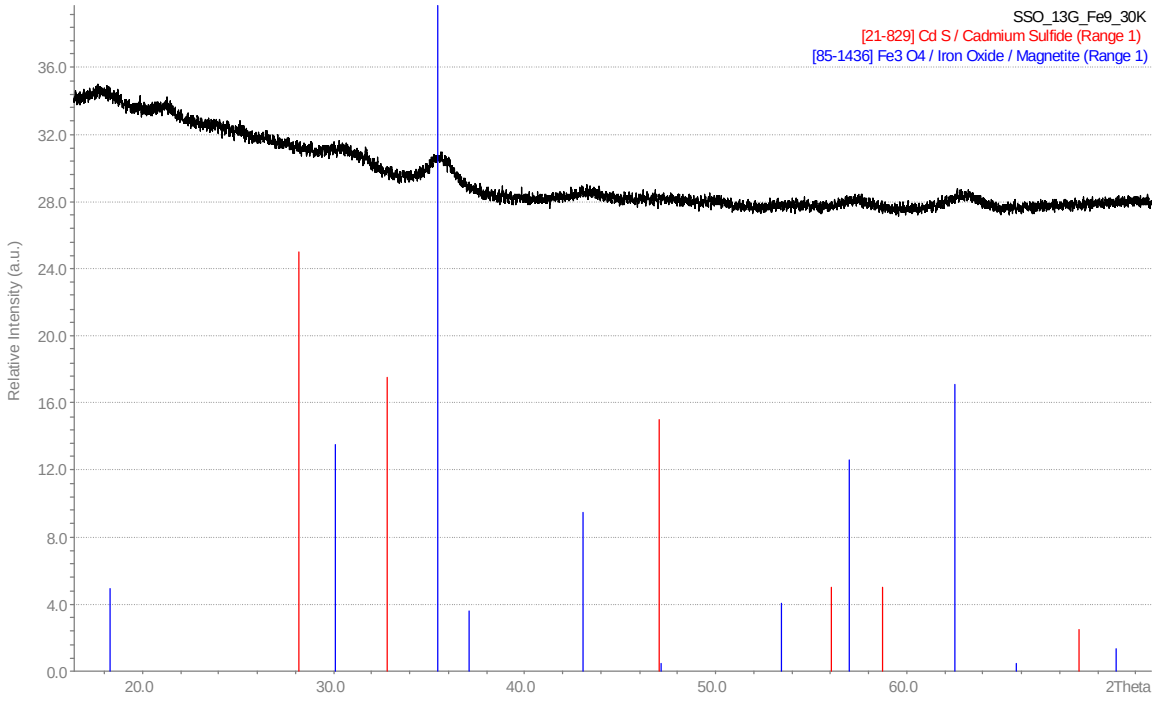

Figure 3. 14 p-XRD diagram of L-cysteine/CdS/γ–Fe_2O_3 plotted with the theoretical peaks of CdS and γ–Fe_2O_3.

The magnetic property of the particles was analyzed with VSM. According to the Neel's superparamagnetic model, the value of magnetization is low at low temperatures where the spins of the clusters are blocked and frozen at random orientations. The magnetization value is also low at high temperatures because of the thermal fluctuations where the spin alignments are destroyed. This is known as magneto crystalline anisotropy that the magnetic properties are different along different crystal domain directions [121]. In VSM analysis the saturation magnetization was measured around 9.5 emu/g sample at 300 K (Figure 3. 15). For ZFC measurement, the particles were cooled down to 5K before applying a 50 Oe magnetic field. The field remained constant up to 300K and for FC

measurement, the magnetic field was held constant as the temperature decreases (Figure 3. 16). The blocking temperature where the particle starts to behave as superparamagnetic behavior was determined around 44K through ZFC/FC measurements which indicate the absence of large aggregates [122]. This can be attributed to the separation of the interparticular domains by the coating which decreases the magnetic dipole-dipole interactions at low blocking temperature. On the other hand, relatively sharp peak of ZFC curve indicates homogenous size distribution of magnetic nanoparticles with homogenous blocking temperature [123].

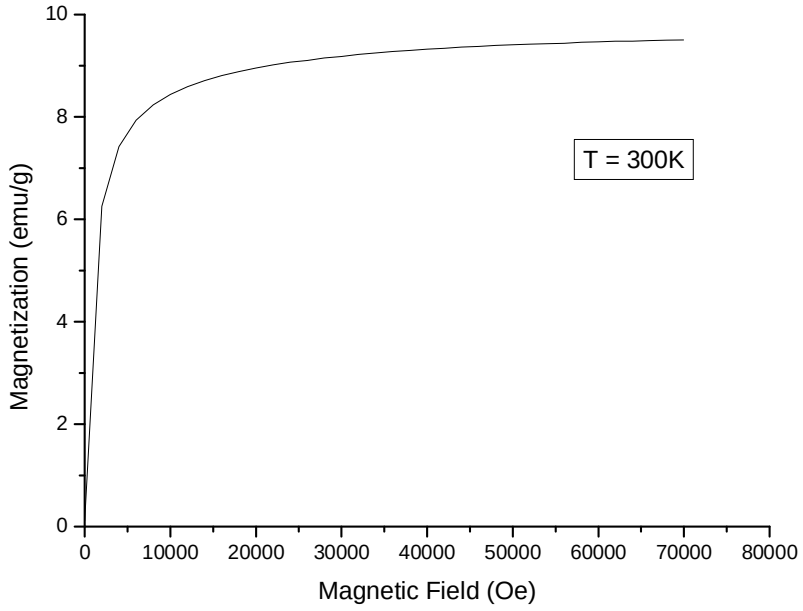

Figure 3. 15 The saturation magnetization of L-cysteine/CdS/γ–Fe_2O_3 measured at constant T = 300K.

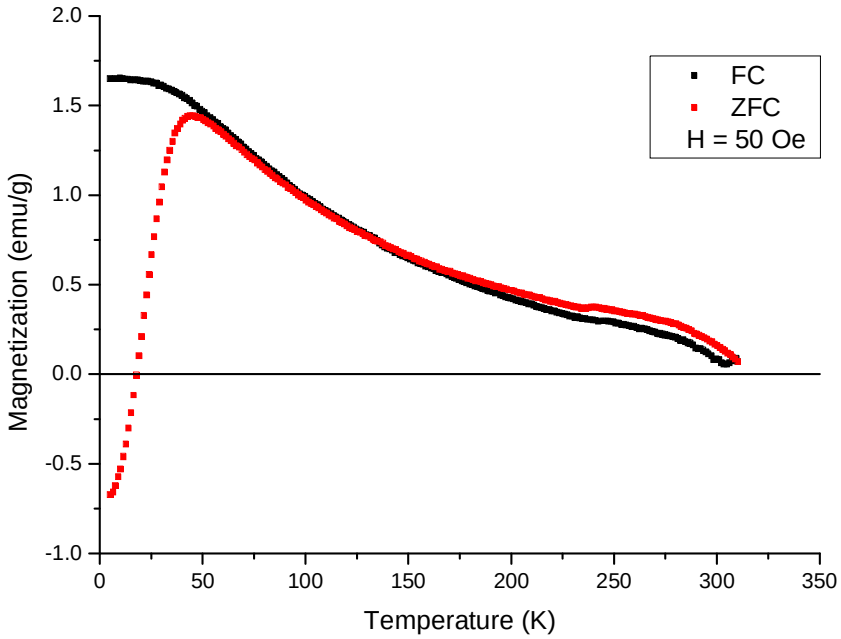

Figure 3. 16 ZFC/FC measurements of L-cysteine/CdS/γ–Fe_2O_3 at net magnetic field of 50Oe.

When the external magnetic field is applied to the washed samples, the particles were agglomerated at the bottom of the flask. In the absence of magnetic field, the agglomerated particles were easily redispersed with a gentle shaking.

XPS analysis of magnetic fluorescent nanoparticles confirmed the existence of Cd, S, C, N, O and Fe elements in the hybrid nanocomposite. The spectrum is initially standardized by the reference C 1s peak at 284.6eV (Figure 3. 17). The existence of γ-Fe_3O_4 was concluded from the absorption peak at 711eV appeared with the satellite peak of $Fe2p_{3/2}$ at 718eV and also $Fe2p_{1/2}$ peak at 723eV which are characteristic peaks of Fe^{3+} ion (Figure 3. 18). Another confirmation for the existence of γ-Fe_3O_4 is the peak showed up at 530eV corresponds to O1s (Figure 3. 19) [124]. The peaks observed at 405.6eV and 412.3eV with 6.7eV spin-orbit separation are well matched with the positions of Cd $3d_{5/2}$

and Cd $3d_{3/2}$ binding energies (Figure 3. 20) [125]. S^{2-} characteristic peak for the reported CdS molecule was observed at 161.9eV correspond to S $2p_{3/2}$ binding energy (Figure 3. 21) [126].

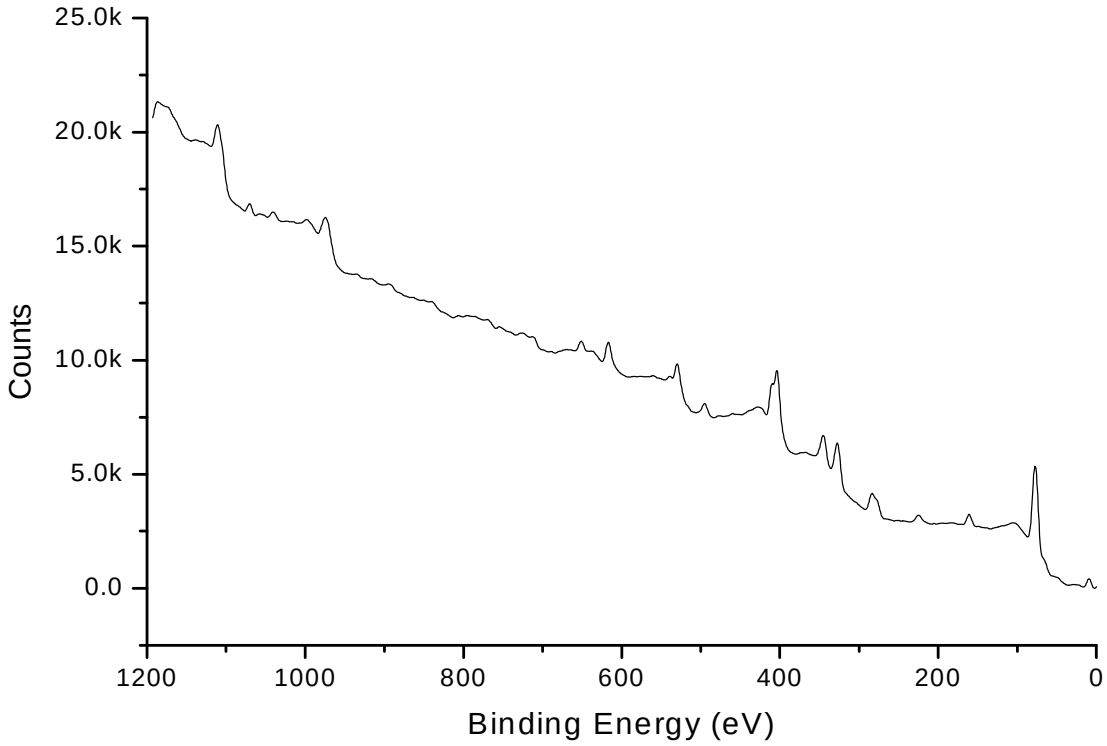

Figure 3. 17 The wide and extended XPS spectra of L-cysteine/CdS/γ–Fe_2O_3.

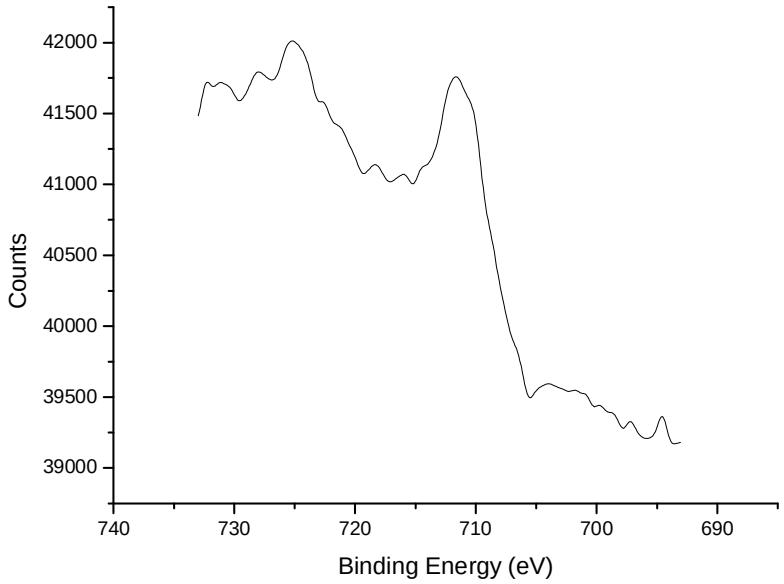

Figure 3. 18 The XPS spectra focused on iron content at 711eV.

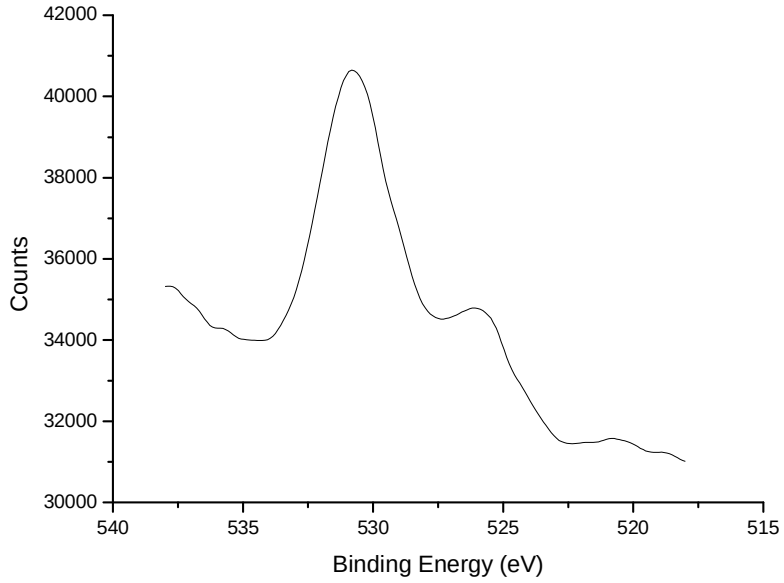

Figure 3. 19 The XPS spectra focused on oxygen content at 530eV.

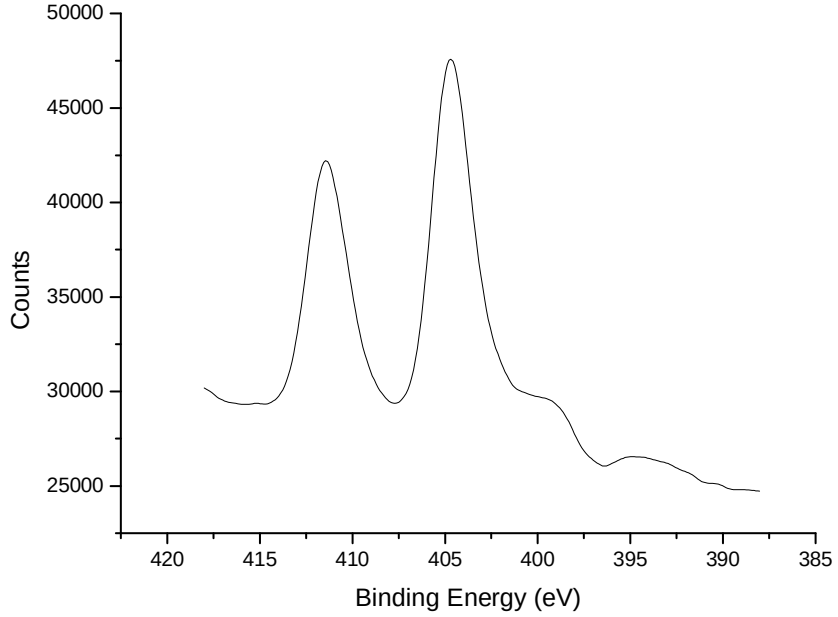

Figure 3. 20 The XPS spectra focused on cadmium content at 405.6eV.

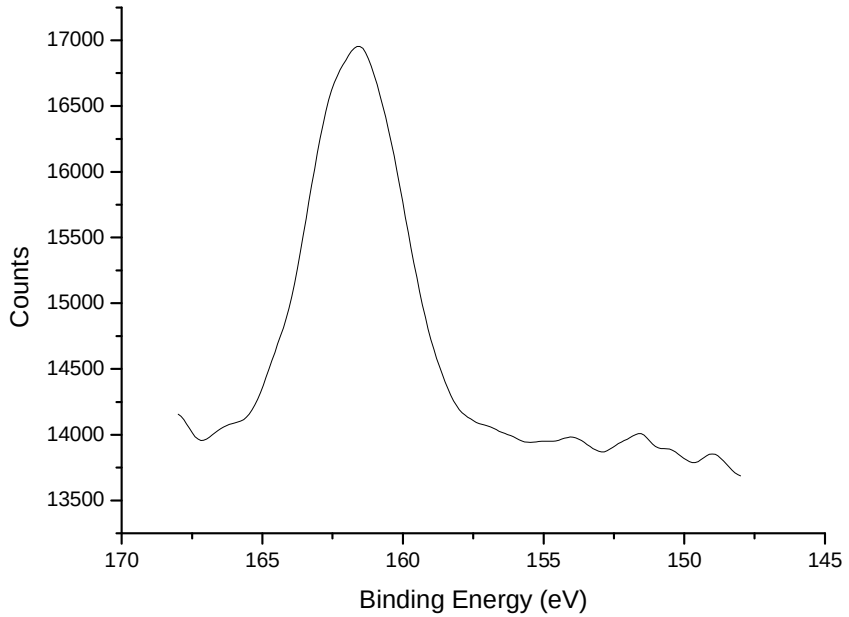

Figure 3. 21 The XPS spectra focused on sulfur content at 161.9eV.

The hybrid samples with varying iron concentrations were measured by inductively coupled plasma (ICP). Cadmium and iron concentrations were measured for 2 different samples (SS13GFe6 and SS13GFe8). When the concentration of iron to cadmium is 3 (SS13GFe6), the concentration of cadmium was measured as 0.3038 mg/mL of solution whereas the concentration of iron was 0.1451 mg/mL of solution. On the other hand, for the solution prepared by choosing the ratio as 2.4 (SS13GFe8), the concentration of cadmium was measured as 0.2348 mg/mL of solution and iron concentration as 0.1111 mg/mL of solution. The ratio of Cd/Fe for the SS13GFe6 is 2.09 and 2.11 for SS13GFe8. This behavior can be explained by the concentration of iron in the solutions. In SS13GFe6 the concentration of iron is 3mM and the concentration of iron is lower in SS13GFe8 which is 2.4mM. An additional confirmation was also observed through absorption spectra of the samples. The concentration plays an important role in the absorption spectra of the samples. When the absorption of the samples without any dilution is measured, SS13GFe6 absorbed more when compared to SS13GFe8 (Figure 23). Since the absorption of SS13GFe6 sample is higher than SS13GFe8 sample, the uncalibrated PL intensity of SS13GFe6 sample measured lower than SS13GFe8 sample (Figure 24). So the more QD exists in the hybrid solution, the more luminescent are the hybrid particles.

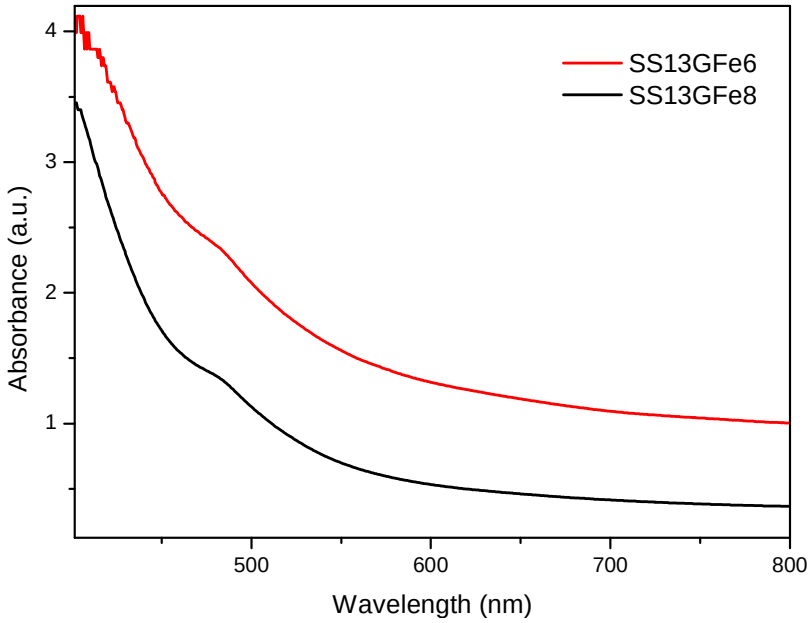

Figure 3. 22 The absorption spectra difference of two different concentration of L-cysteine/CdS/γ–Fe_2O_3.

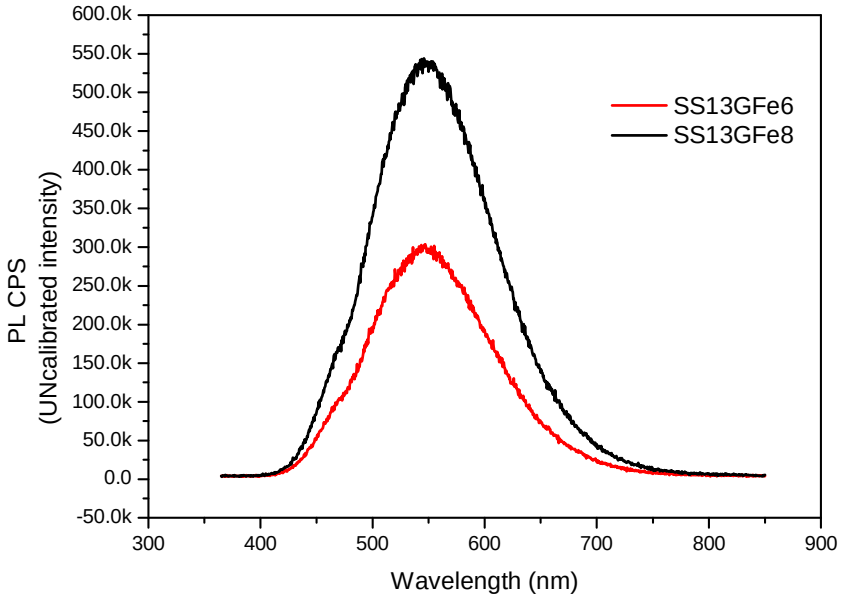

Figure 3. 23 The uncalibrated PL spectra difference of two different concentration of L-cysteine/CdS/γ–Fe_2O_3.

When the hydrodynamic size of the particles that was measured in ICP is compared, SS13GFe6 has smaller size than SS13GFe8. SS13GFe8 has larger hydrodynamic size confirmed through intensity and number average size distribution (Figure 3. 24).

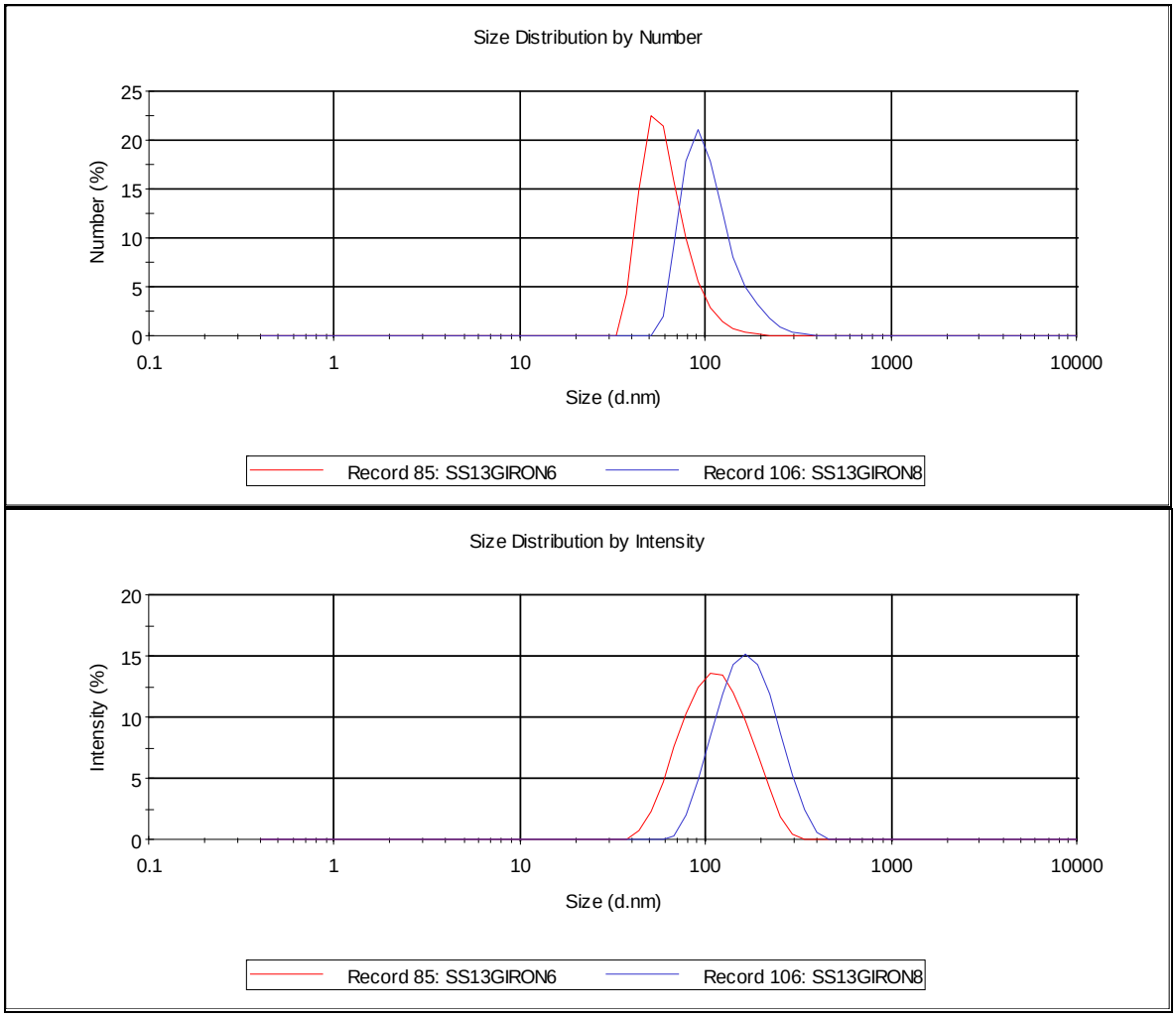

Figure 3. 24 DLS measurements of SS13GFe6 and SS13GFe8. Size distribution by intensity (top) and number (bottom).

Another important aspect of the hybrid systems is to synthesize multi-color fluorescence samples for the detection of different biomolecules. The limitation that prevents the multi-color fluorescence is the reduction in luminescence when the

nanoparticle size increases. There is an exponential decrease in the QY when the emission wavelength shifts to higher values (refer to Chapter 2). In addition to that, iron absorption considerably continues at the emission region of red luminescence nanoparticles which as a result decreases the QY further. A better approach to obtain multi color magnetic luminescent nanoparticles is to synthesize fluorescent nanoparticles with high intensity emission at longer wavelengths since the absorption of magnetic nanoparticles is relatively lower at higher wavelengths. Such an approach can be better satisfied by CdTe nanoparticles that has higher luminescence at longer emission wavelengths. An example of such a hybrid nanocomposite will be presented in chapter 4.

3.4 Conclusion

Aqueous synthesis of L-cysteine stabilized magnetic fluorescent nanoparticles was achieved through one-pot all-aqueous reaction which is time efficient and non-labor intensive method. Overall, small multifunctional molecule, L-cysteine, was capable of stabilizing both particles simultaneously, and attained good colloidal stability over time. Here, it is important to state that QD solutions were used as is without purification. It may come to minds that excess L-cysteine may stabilize the iron oxide and then instead of having hybrid nanoparticles, reaction may produce co-existing MNPs. But, our efforts to synthesize MNPs with L-cysteine fail due to the cystine formation and/or FeS formation. Therefore, we have strong believe that when MNPs are produced and stabilized in the aqueous QD solution with QD coating on the MNPs through free carboxylates.

In order to achieve a colloidal stability with high quantum efficiency, we focused on the number of CdS-QDs per iron oxide, pH of the medium, and the reaction method. The ratio of Cd/Fe played a crucial role in the luminescence of the composite and colloidal stability. The increasing amount of iron concentration in the system decreased the luminescence of the composite. Since the photons emitted by the QDs are absorbed by the iron oxide nanoparticles, the number of photons emitted decreased and lowered the quantum efficiency, so the luminescence intensity. Iron oxide absorbs in the full spectra of visible region which is correlated with the concentration of the iron oxide. Therefore, the best quantum efficiency achieved was no higher than 0.3%.

One-pot synthesis of composite structure can be used to obtain different color luminescing magnetic nanoparticles. L-cysteine coated CdS molecule can be synthesized at different particle size and color emission which can be directly used for the stability of iron oxide nanoparticles. The main drawback in this approach is the significant luminescence drop with increasing surface defect sites causing non-radiative recombinations.

A better approach to achieve multi color magnetic luminescent nanoparticles might be the use of better luminescing CdTe as a QD. It is well documented in the literature that, multi color emission of CdTe can be achieved. A red luminescing CdTe with around 700nm emission wavelength will suffer less from the iron oxide photon absorption. The synthesis of multi color emitting L-cysteine capped CdTe will be discussed in the next chapter.

As-prepared magnetic luminescent nanoparticles with good stability and compatibility exhibit good magnetic respond to the magnetic field and efficient

characteristic emission peak which can be easily detectable under UV radiation are good candidates to be used in biological applications. The composite particles with dual functionality can detect cell, pathogen or receptors through optical or magnetic imaging/sensing and can be separated magnetically for detoxification or targeting.

Chapter 4

AQUEOUS SYNTHESIS OF CdTe QUANTUM DOTS AND ONE-POT SYNTHESIS OF BIOCOMPATIBLE CdTe-Fe_3O_4 HYBRID NANOPARTICLES

4.1 Introduction

Quantum dots (QDs) play an important role in biological applications as biosensors and luminescent labels. The unique quantum confinement effect which is related to the change of band gap energy by tuning the size makes QDs advantageous over fluorescent dyes. When compared with the organic dyes, QDs are more stable to photo-bleaching and they have a narrow, Gaussian type emission curve with strong intensity that can be excited over a broad absorption wavelength. In II-VI type semiconductors; CdS, CdSe and CdTe are the most studied ones due to tunable color emission in the visible range.

Thiol stabilization of CdTe luminescent nanoparticles provides good stability, solubility and better surface passivization for the dangling bonds with controlled growth kinetics [127]. Although, the traditional aqueous methods used in thiol stabilization of CdTe resulted in low QYs, typically around 1-10% [36, 128], post-synthetic treatments

such as photochemical etching [36], size selective precipitation [129] and long-term UV-illuminations [130] improved the QYs dramatically . Hereby, I will be presenting a new approach for the synthesis of L-cysteine stabilized CdTe quantum dots in an aqueous environment. The fundamental difference in the synthesis is the source of tellurium instead of highly air sensitive and toxic NaHTe and H_2Te compounds [131, 132].

4.2 Experimental Section

4.2.1 Synthesis of Na_2Te

The synthesis of Na_2Te has been done in liquid NH_3 with precautions to exclude humidity and oxygen. The synthesis has been done as previously reported [133]. The manipulation of the synthesis was initially done under inert atmosphere in glove box (O_2 and H_2O below 1 ppm). The stoichiometric amount of elemental Na and Te were weighed in a silica schlenk tube.

$$2\ Na + Te \rightarrow Na_2Te \qquad (4.1)$$

The reaction tube is then transferred into the vacuum line where the sample was vacuumed down to 10^{-3} mbar pressure (Figure 4. 1a). The reaction tube is placed into liquid nitrogen bath under vacuum to reach higher vacuum conditions (Figure 4. 1b). The exothermic reaction was controlled by a slow reaction kinetic at low temperatures. Then, the vacuum line and reaction tube were purged with constant ammonia flow. The ammonia flow is condensed at cold temperature trap where liquid ammonia was formed. The formation of dark blue color was observed at -196°C where the coolant was liquid N_2 (Figure 4. 1c). After the liquefaction of the ammonia in ca. -40°C liquid glycerol bath, the

tube was connected to the Hg manometer that acts as a pressure relief for NH_3 gas (Figure 4. 1d).

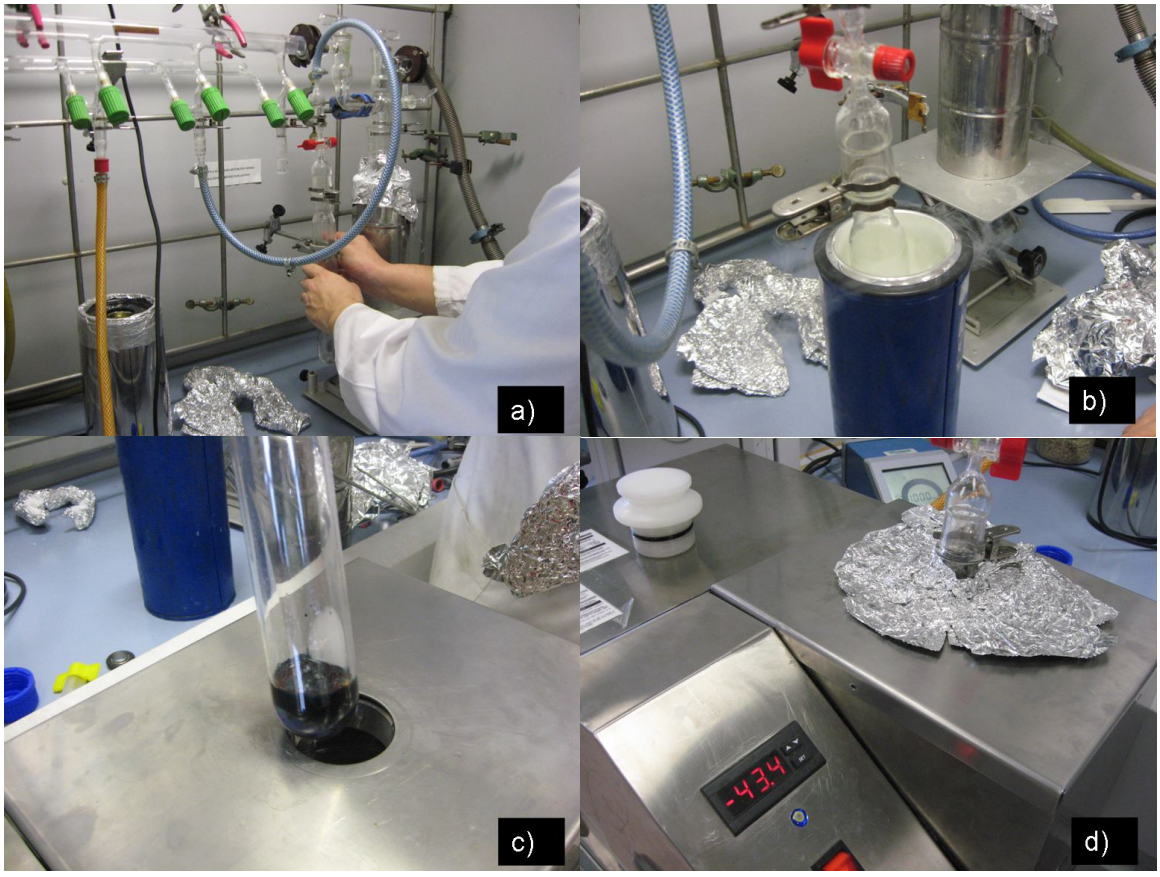

Figure 4. 1 a) Vacuum line to prevent the oxidation, b) Liquid nitrogen to cool the exothermic reaction, c) Blue color of NH_3 solvent, d) Glycerol bath around 40°C.

Hereby, the evaporation of NH_3 gas has been sustained very slowly which lasted for 36 hours. The completion of the reaction was controlled by the color change. The dark blue color of liquid NH_3 disappeared and white Na_2Te powder was formed on the walls of the tube. The product was mechanically scratched from the wall and taken into a sealed ampoule in a glow box.

In order to investigate the formation of any residual product in the system, a sample for p-XRD measurement was prepared. Theoretical peaks of Na_2Te were well matched with the sample's (Figure 4. 2). Residual elemental sodium or tellurium was not observed in the product.

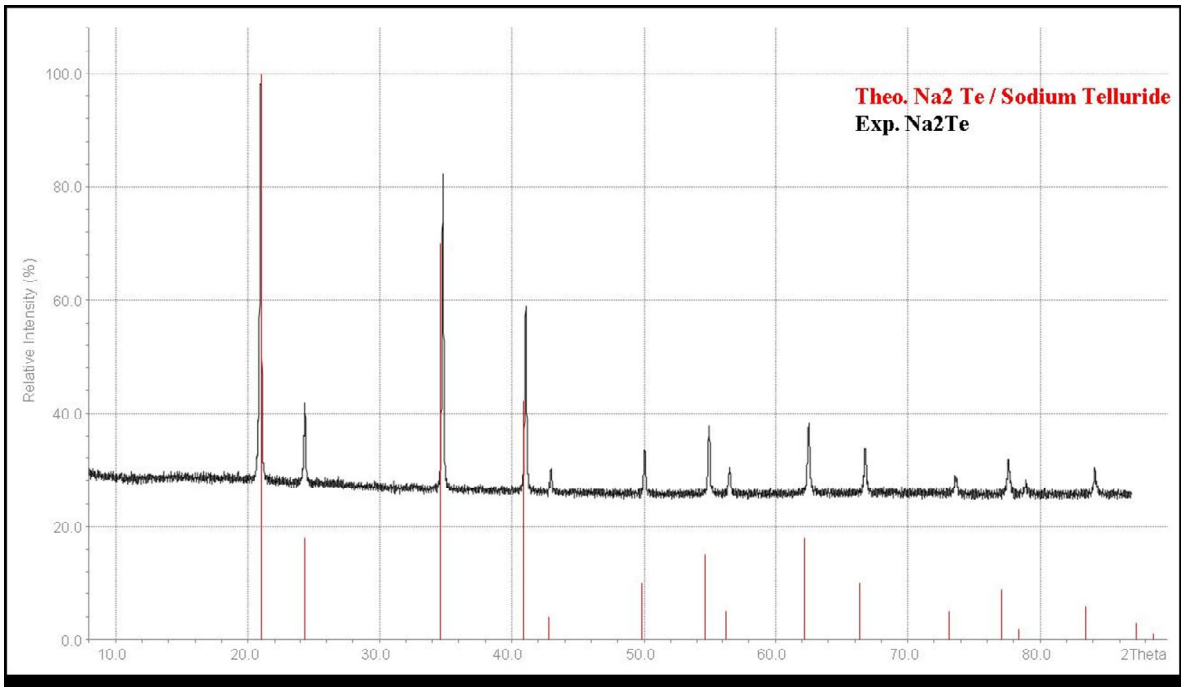

Figure 4. 2 XRD pattern of experimentally obtained Na_2Te (black) and theoretical data fit (red).

4.2.2 Synthesis of L-cysteine capped CdTe QDs

For the synthesis of CdTe in an aqueous environment three different approaches were studied. Each approach provides the source of Te in different ways. The important issue is to prevent the oxidation of the Te source. An uncontrollable oxidation reduces the amount of Te in the system which limits a systematic alteration of Cd^{2+} to Te^{2-} ratio in a controlled way which plays an important role in the quantum efficiency. *The first*

approach is based on the production of H_2Te gas which is actually highly toxic and flammable. The generation of H_2Te was done by the reaction of Al_2Te_3 with 0.5M H_2SO_4. An example for the sample preparation is shown in Figure 3. Al_2Te_3 was deoxygenized in a round bottom flask and with the rapid injection of H_2SO_4, H_2Te gas was generated (Figure 4. 3a). The cold trap is used to prevent the penetration of solidified Te powder with the N_2 flow (Figure 4. 3b). As obtained H_2Te gas can be directly transferred into the solution of Cd precursor for the generation of CdTe nanoparticles but the ratio of Cd/Te would be ambiguous since the transferred gas can not be measured quantitatively. A better way, *the second approach*, to control the Cd/Te ratio is to pass H_2Te gas into a known concentration of NaOH (Figure 4. 3c). In this way, the concentration of the product NaHTe can be controlled and transferred into the solution of Cd precursor. Here, the excess amount of H_2Te gas is used to saturate the NaOH solution. The product NaHTe is highly unstable and readily oxidizes in the trace amount of oxygen, so that NaHTe has to be freshly prepared and can not be stored for other reactions.

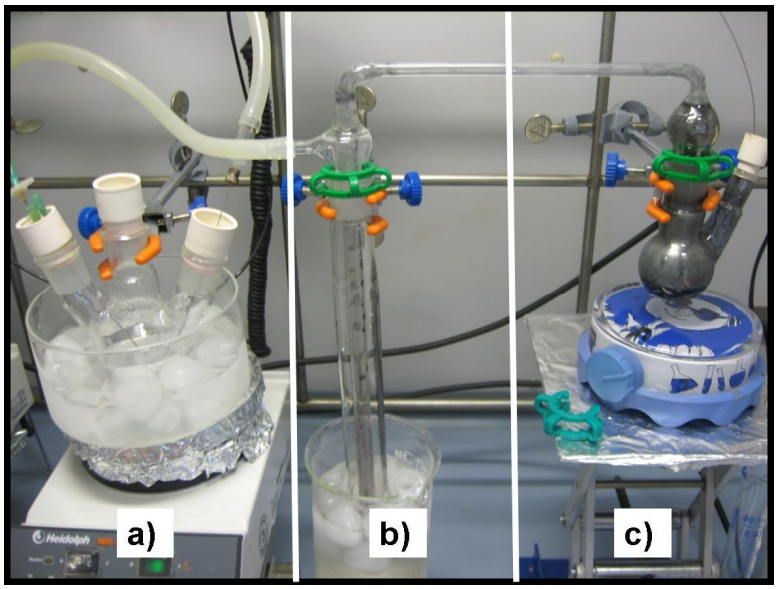

Figure 4. 3 a) Generation of H_2Te from Al_2Te_3 b) Cold trap to prevent elemental Telluride c) The reaction of H_2Te with NaOH to form NaHTe.

The last approach involves the reducing of TeO_3^{2-} to Te^{2-} with sodium borohydride ($NaBH_4$) under nitrogen flow.

$$NaBH_4 + Na_2TeO_3 \rightarrow Te^{2-} + BO_2^- + H_2O \quad (4.2)$$

In this approach freshly prepared Te^{2-} from sodium tellurite is reacted with the cadmium precursor to obtain CdTe nanoparticles. The final reaction color turns to purple and white sodium borate precipitates at the bottom of the flask and the solution is decanted from the precipitation.

All of the tellurium sources are added to the cadmium precursors which has been prepared in four necked round bottom flask. Briefly, 66 mg of $Cd(Ac)_2 \cdot 2H_2O$ was dissolved in the flask with 50 mL water at constant stirring of 400 rpm. An appropriate amount of L-cysteine was added and the reaction pH was adjusted with 10M NaOH or concentrated HAc. The reaction medium was deoxygenized for 15 minutes and the reaction temperature was set to 60°C. Reaction temperatures higher than 60°C produced an

insoluble cadmium complex which is undesirable. 18mg of Na_2Te was dissolved in 50 mL of water and added to the reaction flask at 60°C drop wise. Finally, the reaction temperature was set to 110°C and the solution is refluxed for the desired duration.

4.3 Results and Discussion

CdTe QD solutions have significantly different color than CdS QD solutions. The typical color for bulk CdTe is dark brown whereas yellow for CdS [134]. Also, the bulk band gap of CdTe is 818 nm which corresponds to 1.52eV and for CdS the band gap energy is 2.4eV. Therefore, capping of the CdTe core with a larger band gap material like CdS increases the QY [135]. A further increase can be achieved by implementing a composite structure with a much larger band gap material like ZnS with 3.68eV (Figure 4. 4).

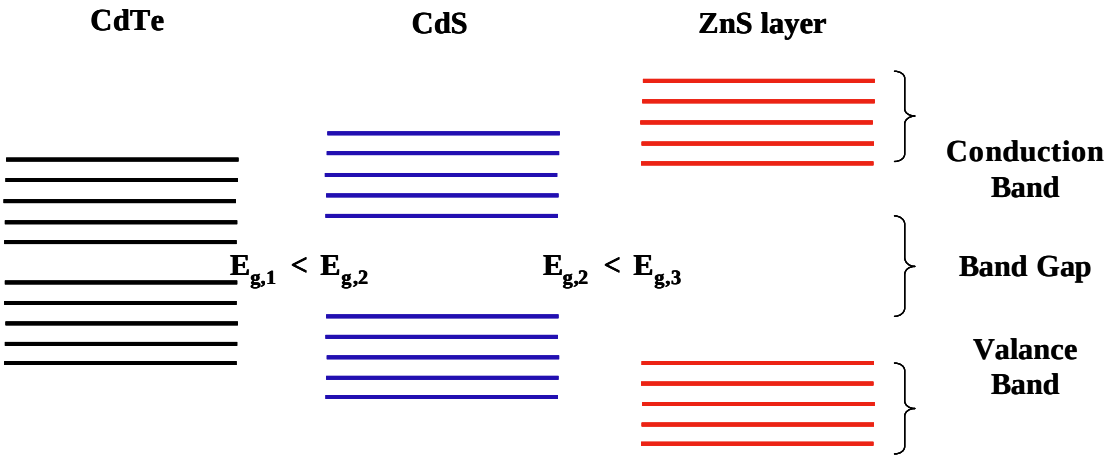

Figure 4. 4 Band gap configuration of CdTe, CdS and ZnS

In a typical reaction, extreme precautions are taken to prevent oxygen leakage to the reaction medium. The color of Na_2Te is white and turns rapidly into black when exposed to oxygen and the reaction would not proceed further. Previously deoxygenized distilled water is used to dissolve Na_2Te. The color turns to purple which indicates the formation of

NaHTe (Figure 4. 5 a) [136]. Even though the tellurium precursor is deoxygenized by nitrogen flow, the trace amount of oxygen is sufficient to turn the color from purple to black. The color of the reaction changes to light brown with the very first addition of tellurium to the cadmium precursor (Figure 4. 5 b). The color darkens as the addition of tellurium continues. The color of the solution turns to black when the solution is transferred to a capped bottle; it takes less than 30 minutes to turn the solution color to black (Figure 4. 5 c and 5d).

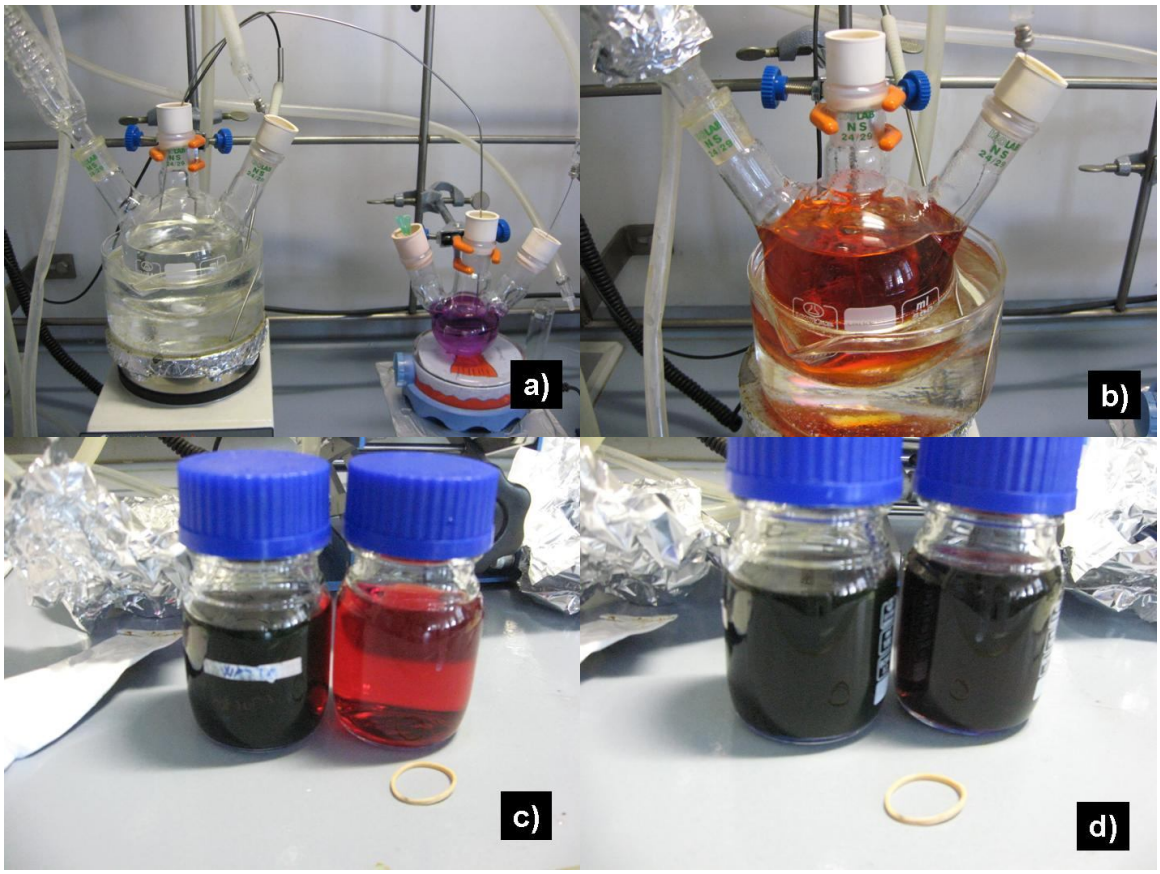

Figure 4. 5 a) Purple color solution contains NaHTe, b) Initial formation of dark red-brown CdTe with the addition of tellurium source, c) Before the oxidation, dark red color of CdTe solution on the right, d) Red color solution turns to black within 30 minutes.

4.3.1 Growth kinetics of CdTe

The growth mechanism of L-cysteine capped CdTe was monitored by absorption and fluorescence spectroscopy. Samples were taken from the reaction mixture at different time intervals during the reflux. The absorption spectra revealed that as the time of reflux increases, there is a gradual increase in the absorption onset of the particles. This red shift to a higher wavelength corresponds to an increase in particle size throughout the reflux in the first hour (Figure 4. 6a). The particle size growth was still observed when samples were taken after 8 hours of reflux time (Figure 4. 6b).

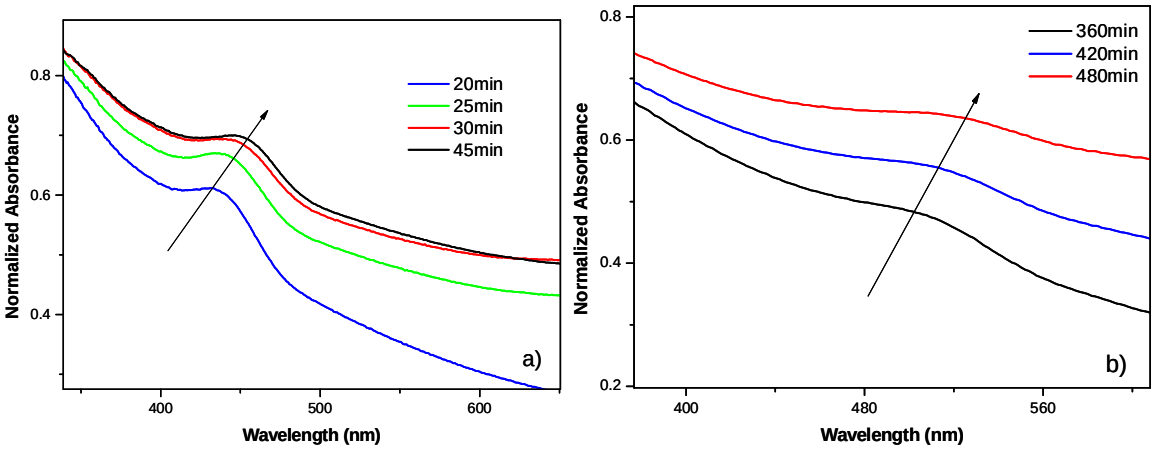

Figure 4. 6 a) The absorption onset change within first hour b) absorption change after 6-8 hours.

The reaction kinetics of the sample can be investigated in terms of nucleation and growth. According to Peng et al. [137], the reaction kinetic is difficult to study but an explanation to the nucleation of the reaction can be obtained when the concentration of the nanoparticles are known [93]. The particle concentrations were calculated from the molar extinction coefficient correlation that changes by the particle size and absorbance of that

sample [138]. The particle size increases exponentially with reflux time and reaches to the plateau after 160 minutes of reflux time. On the other hand, the concentration of nanoparticles decreases exponentially with reflux time. Hereby, the particle size keeps growing whereas the concentration of the monomer decreases (Figure 4. 7). Therefore, Ostwald ripening dominates the growth and smaller particles dissolve to form larger particles. The growth rate is faster initially but gradually slows as the particle size increases. Initially, a higher concentration of nucleation centers form. As the particle size grows, the number of monomer decreases with reflux time. The growth rate can be monitored better by plotting the growth rate (dr/dt) against inverse average particle diameter (1/r) (Figure 4. 8).

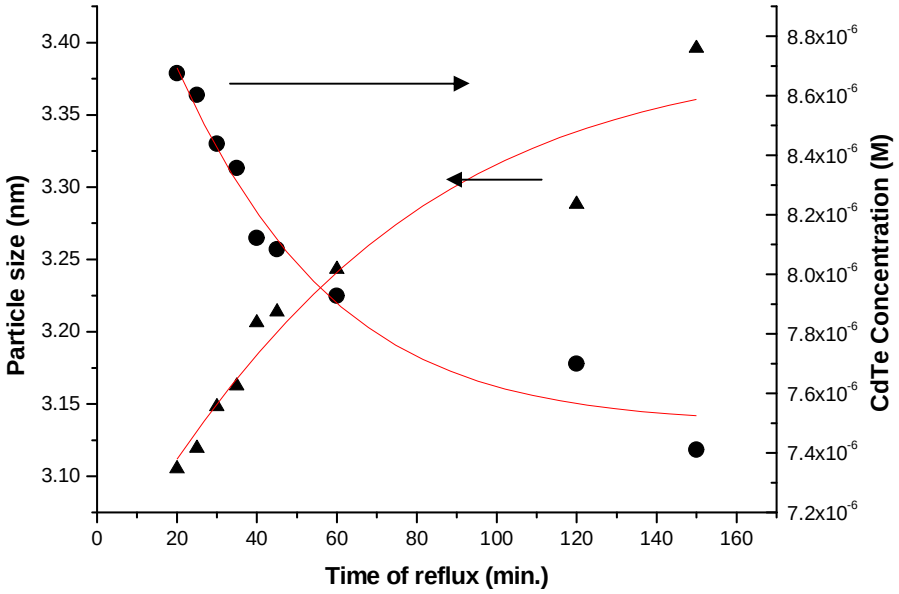

Figure 4. 7 The change in the particle size (●) and CdTe concentration (▲) with varying reflux time.

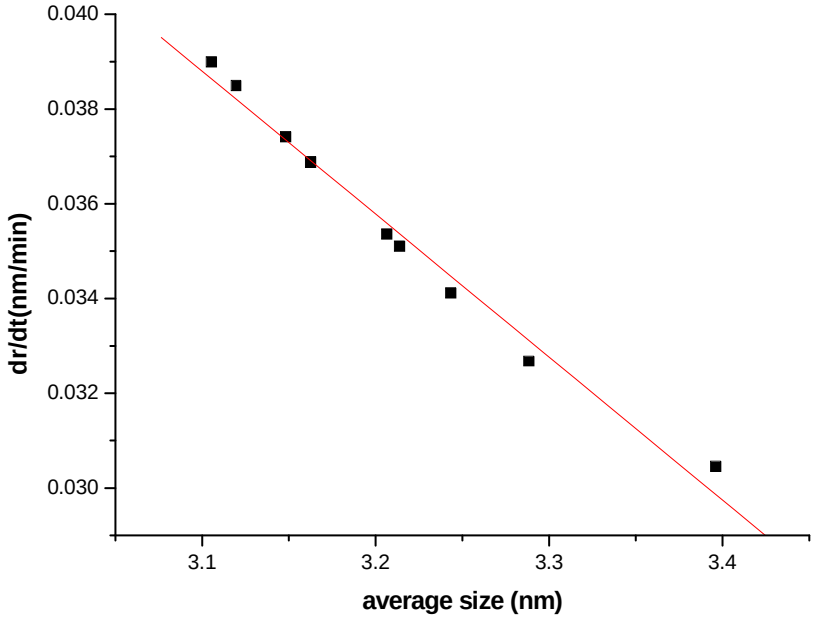

Figure 4. 8 The change in average particle size with growing rate dr/dt.

As the particle grows, there is a linear decline in the growth rate which also well fits to the modified equation of Sugimoto et al. by Talapin et al. [139]:

$$\frac{dr}{dt} = DV_m C^0_{flat} \left\{ \frac{\left([M]_{bulk} / C^0_{flat} \right) - \exp\left[2\gamma V_m / rRT \right]}{r + \left(D / k_g^{flat} \right) \exp\left[\alpha \left(2\gamma V_m / rRT \right) \right]} \right\} \qquad (4.3)$$

Here, V_m is the molar volume of solid, D the diffusion coefficient of the monomer, $[M]_{bulk}$ the monomer concentration in the bulk of solution, C^0_{flat} the solubility of the bulk material, γ the specific surface energy of the particles, k_g^{flat} the rate constant for the growth of a flat surface ($r=\infty$).

The empirically fitted function can be simplified with correlation coefficient of 0.9951 to the following equation:

$$\frac{dr}{dt} = -0.06377 + 0.31837 * \frac{1}{r} \tag{4.4}$$

The evolution of photoluminescence spectra for the growing particles was also recorded at different reflux times. As the reflux time increases and the particles grow, the number of defects in the lattice and therefore the number of non-radiative recombinations decrease which results in a higher PL intensity (Figure 4. 9).

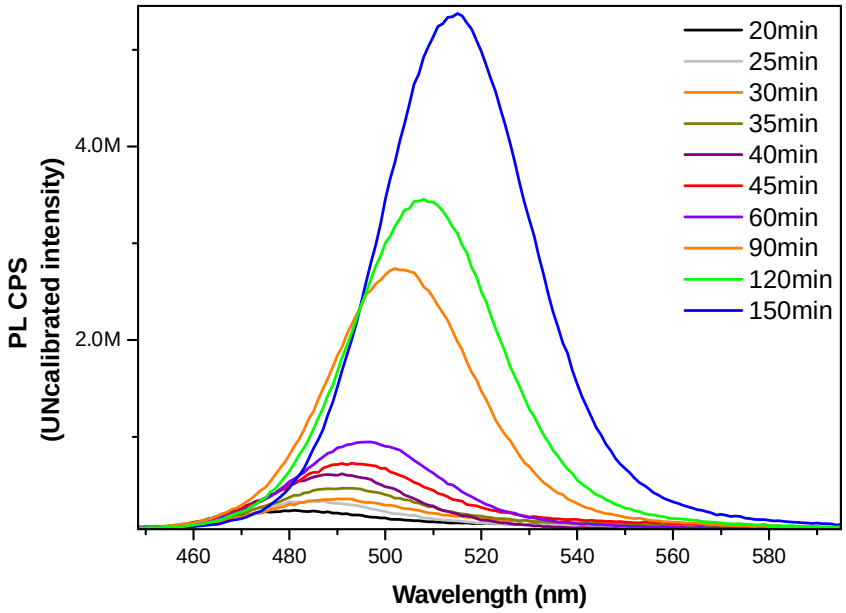

Figure 4. 9 PL intensity change with the reflux time.

As the order in the crystalline lattice increases with controlled growth, the particle size distribution decrease and FWHM decreases for particles up to 2 hours of reflux time. FWHM value at 2 hours is 35nm. FWHM value increases and reaches to a value of 54 nm after 8 hours of reflux time. Hereby, PL maximum shifts to longer wavelengths with

prolonged reflux time (Figure 4. 10). The crystal growth can also be verified by the shift in the position of PL maximum from 481 nm to 700 nm. When the PL maximum reaches to 700 nm after 9 hours reflux, the luminescence was almost ceased. As the emission maximum shifts to the longer wavelength of the spectrum, the emission color changed from green to red.

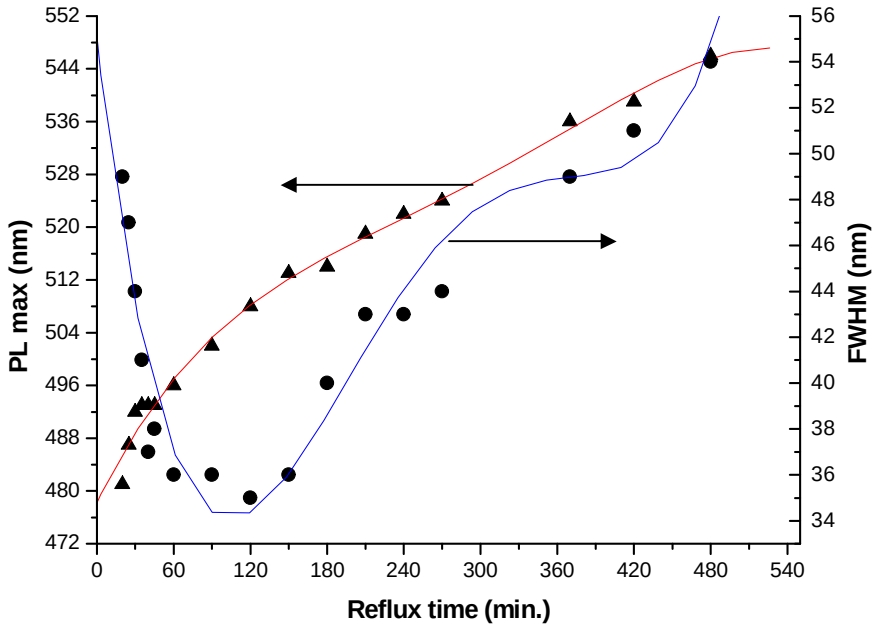

Figure 4. 10 The change in PL max (▲) and FWHM (●) with reflux time.

The particle size of the QDs can be calculated by the effective mass approximation which is being established by Brus in 1984. The equation derives the particle size by using an effective mass approximation based on quantum well approximation and columbic interactions between the atoms. Below is the final modified equation to calculate the band gap difference of the nanoparticles from its bulk:

$$E_{(R)} = E_g + \frac{h^2}{8R^2}\left[\frac{1}{m_e} + \frac{1}{m_h}\right] - 1.786\frac{e^2}{\varepsilon R} - 0.248E^*_{Ry} \tag{4.5}$$

In here the band gap difference can be calculated as follows:

$$\Delta E = E_{(R)} - E_g \tag{4.6}$$

When we substitute the Planck equation for the calculation of band gap energy of a nanoparticle and the known bulk bad gap of CdTe as E_g = 1.5 [eV] into the equation, the term can be represented as follows:

$$\Delta E = \frac{h \cdot c}{\lambda_R} - E_g = \frac{\hbar \cdot 2\pi \cdot c}{\lambda_R} - E_g \tag{4.7}$$

$$\Delta E = \frac{6.58\times10^{-16}\left[eV\cdot s\right]\times 2\times 3.14\times 3\times10^{8}\left[m/s\right]\times10^{9}\left[nm/m\right]}{\lambda_R} - 1.5\left[eV\right]$$

$$\Delta E = \frac{1240.7\left[eV\right]}{\lambda_R} - 1.5\left[eV\right]$$

In the equation λ_R refers to the absorption edge of the particle which can be calculated from the UV spectrum of the sample. The absorption edge is the corresponding intersection wavelength that the linear lines that is being plotted from two regions. First line is plotted from the region where the curve gets steeper and the second line is plotted parallel to the baseline.

In the equation the term represents the quantum well approximation is calculated by using the known constants of CdTe like:

$$m_e = 0.14\times m_0\,,\ m_h = 0.37\times m_0, \varepsilon_{CdTe} = 10.2$$

$$\varepsilon_0 = 8.854\times10^{-12}\left[F/m\right], m_0 = 9.109\times10^{-31}\left[kg\right]$$

$$\frac{h^2}{8R^2}\times\left[\frac{1}{m_e}+\frac{1}{m_h}\right] \tag{4.8}$$
$$=\frac{\left(6.582\times10^{-16}\left[eV\cdot s\right]\right)^2}{8\times R^2}\times\left[\frac{1}{0.14\times9.109\times10^{-31}\left[kg\right]}+\frac{1}{0.37\times9.109\times10^{-31}\left[kg\right]}\right]$$
$$=\frac{5.415\times10^{-32}\left[eV\cdot s\right]^2}{R^2}\times\left[\frac{1}{12.278\times10^{-31}\left[kg\right]}\right]$$
$$=\frac{0.0441}{R^2}\times\frac{\left[eV\cdot s\right]^2}{kg}\times\frac{1.60\times10^{-19}\left[kg\times m^2/s^2\right]}{1\times eV}$$
$$=\frac{0.0706\times10^{-19}}{R^2}\left[eV\right]$$
$$=\frac{7.06\times10^{-3}}{\left(R_{nm}\right)^2}\left[eV\right]$$

The other term in the equation is the columbic interactions between the cadmium and tellurium atoms:

$$1.786\times\frac{e^2}{\varepsilon R}=1.786\times\frac{e^2}{\varepsilon_{CdTe}\times4\times\pi\times\varepsilon_0\times R} \tag{4.9}$$
$$=\frac{\left[eV\right]^2}{10.2\times4\times\pi\times8.854\times10^{-12}\left[F/m\right]\times R}$$
$$=\frac{\left[eV\right]^2}{1134.304\times10^{-12}\left[CV/m\right]\times R}\times\frac{CV}{j}\times\frac{1.6\times10^{-19}\left[j\right]}{eV}$$
$$=\frac{0.1399\times10^{-6}\left[eV\right]}{R}$$
$$=\frac{139.9}{R}\left[eV\right]$$

The last term in the equation is negligible and its contributions will be neglected. The final version of the equation can be represented for any CdTe atoms with radius R in nanometers and absorption edge value as λ_R.

$$\frac{1240.7[eV]}{\lambda_R} - 1.5[eV] = \frac{7.06\times10^{-3}}{(R_{nm})^2}[eV] - \frac{139.9}{R_{nm}}[eV] \quad (4.10)$$

Below is the Matlab code to calculate the size of the nanoparticles in the absorption edge limit of 400 to 700 nm. The particle size calculation gives the diameter of the nanocrystals specifically applicable to CdTe nanoparticles. Table 1 summarizes the representation of the data output.

```
% This program calculates the particle size of CdTe nanoparticles
% with band gap energy values.

clear all, close all

% electron effective mass me=0.14mo
% hole effective mass mh=0.37mo
% dielectric constant for CdTe e=10.2
% Band gap of the bulk CdTe nanoparticles Eg=1.5[eV]
CdTecoeff=[0.14 0.37 10.2 1.5];

% mo is the mass of electron [kg]
m0=9.1095*10^-31;
% planck constant in [Js]
h=6.63*10^-34;
% permittivity of vacuum in [F/m] or in terms of [C*V/m]
e0=8.854*10^-12;
% conversion 1 ev = 1.6*10^-19 [C]
c=3.0*10^8;

% number of iterations in the range of 400-700nm
N1=301;

range=linspace(400e-9,700e-9,N1);
wavelengths=range*10^9;

for i=1:N1
bandgap(i)=h*c/(range(i)*1.602*10^-19);
dband(i)=bandgap(i)-CdTecoeff(4);
```

```
z=dband(i);
emass=1/(1/(CdTecoeff(1)*m0)+1/(CdTecoeff(2)*m0));
A=h^2/(8*emass*10^-18*1.602*10^-19);
B=1.8*(1.602*10^-19)/(4*pi*CdTecoeff(3)*e0*10^-9);
p=[z 0 -A];
r=roots(p);
if r(1)>r(2)
a=r(1);
else
a=r(2);
end
p1=[z B -A];
r1=roots(p1);
if r1(1)>r1(2)
a1=r1(1);
else
a1=r1(2);
end
diameter(i)=a;
diameter2(i)=a*2;
diametera1(i)=a1;
diameter2a1(i)=a1*2;
end
diameter_r=diameter2';
wavelength_range=wavelengths';
bandgap_range=bandgap';
diameter_ra1=diameter2a1';
```

Table 4. 1 An output sample for the corresponding particle size and Band gap energy calculated from absorption edge of nanoparticles.

Absorption edge [nm]	Band Gap energy [eV]	Particle Size [nm]
451	2.7529	3.2433
452	2.7468	3.2508
453	2.7408	3.2582
454	2.7347	3.2657
455	2.7287	3.2732
456	2.7227	3.2807
457	2.7168	3.2883
458	2.7109	3.2958
459	2.705	3.3034
460	2.6991	3.311
461	2.6932	3.3187
462	2.6874	3.3263
463	2.6816	3.334
464	2.6758	3.3417
465	2.67	3.3494
466	2.6643	3.3571
467	2.6586	3.3648
468	2.6529	3.3726
469	2.6473	3.3804

4.3.2 The quantum yield calculations for CdTe quantum dots

In the quantum yield calculation of quantum dots, the zero dimensional nanoparticles are simulated as semiconductors. When a semiconductor material is excited at a specific wavelength corresponding to its band gap energy, the electrons in the valance band jumps to higher energy state known as conduction band with many vibrational states. The amount of energy can be determined by absorption spectra of the sample. When an electron initially jumps to a higher vibrational state, it loses its energy by non-radiative

recombinations down to lowest energetic vibrational state found in the first excited state. Then the electron falls back to the ground state with radiative combination known as luminescence. Overall, the energy absorbed by the electron is lost within the transitions of the vibrational state or through energy trap sites throughout the combination Figure 4. 11.

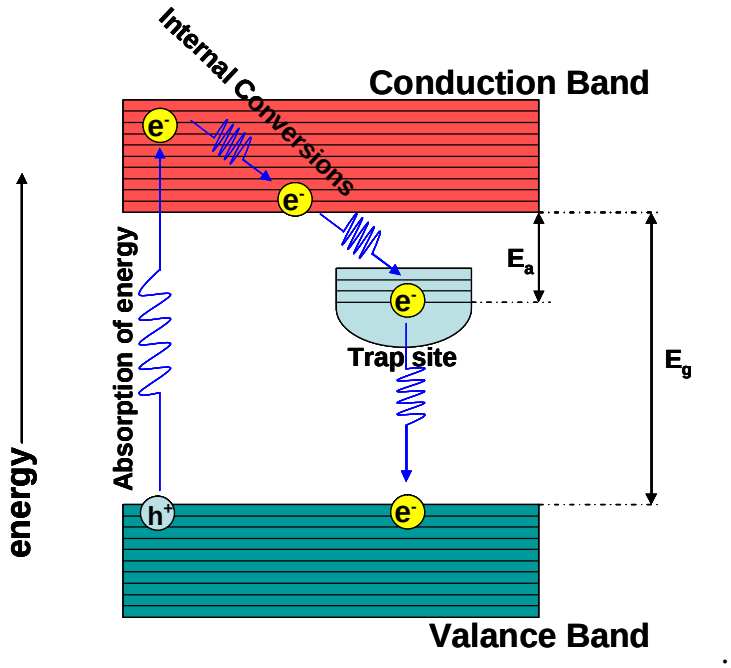

Figure 4. 11 The representation for the loss of absorbed energy in vibrational state and trap site.

QY is the relation between the number of fluorescence photons emitted per number of incident photons absorbed. As the definition implies, to achieve high quantum yields, the number of emitted photons should be as much as the number of photons absorbed. In theory, the absorbed energy is lost by internal conversions or trap sites and to achieve 100% QY is not possible. In the QY calculations, the comparison is done with respect to organic fluorophores. In the determination of QY for CdTe samples, Rhodamine 6G

dissolved in ethanol was used as the reference (96% QY in ethanol at 445nm).[140] The QY calculation was performed by PL measurement of three dilutions of the QD solution and the reference with absorbance values below 0.2 at the excitation wavelength. The QY calculation was done according to the below equation:

$$\frac{QY(A)}{QY(B)} = \frac{iei(A)/Abs(A)}{iei(B)/Abs(B)} \times \frac{n^2(A)}{n^2(B)} \qquad (4.11)$$

Where QY is the quantum yield, iei is the integrated emission intensity, Abs is the absorbance at the excitation wavelength, and n is the refractive indices of samples.

Since many of our syntheses are done in aqueous environment, the QY of Rhodamine 6G in water can be calculated from the known reference Rhodamine 6G in ethanol (%96 QY) by using the refractive indices as 1.359 and 1.33 for ethanol and water, respectively. The calculated QY of Rhodamine 6G in water is 71% at 445nm excitation. From now on, the QY of CdTe will be calculated by the taking Rhodamine 6G in water as reference. When the integrated emission intensity is plotted against absorbance values at 445nm (the excitation wavelength), the slope of samples can be used in the determination of QY for unknown sample with refractive indices (Figure 4. 12).

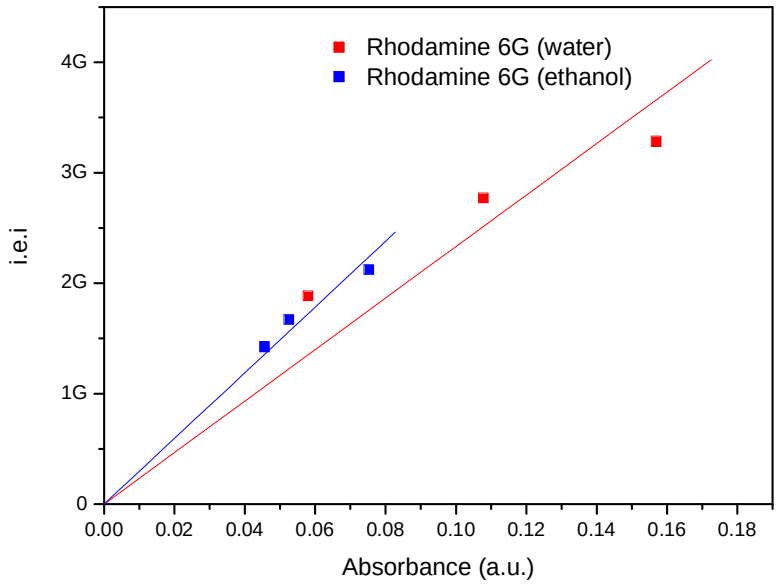

Figure 4. 12 The integrated emission intensity of Rhodamine 6G in ethanol and in water are plotted against absorbance at 445nm. The gradient of the lines are used to calculate the QY of Rhodamine in water.

4.3.3 Characterization of L-cysteine coated CdTe nanoparticles

L-cysteine coated CdTe nanoparticles are synthesized in a simple aqueous method as mentioned before. The synthesis was performed with the optimized ratio that was used in chapter 2. The L-cysteine:Cd ratio was chosen as 2.5 and Cd:Te ratio as 2. The reaction pH was adjusted to 10.5 prior to the addition of telluride source. The telluride solution was added at 80°C to the cadmium precursor. The system was refluxed for 24 hours by taking samples at different time intervals as 30 minutes (SS17F1), 90 minutes (SS17F2), 300 minutes (SS17F3) and 22 hours (SS17F4). The sample absorption spectrum was monitored as the particle size increases (Figure 4. 13). The luminescence of the samples shifted from

green to red through 22 hours of reflux time. Figure 4. 14 demonstrates the red shift in the emission profile of the samples.

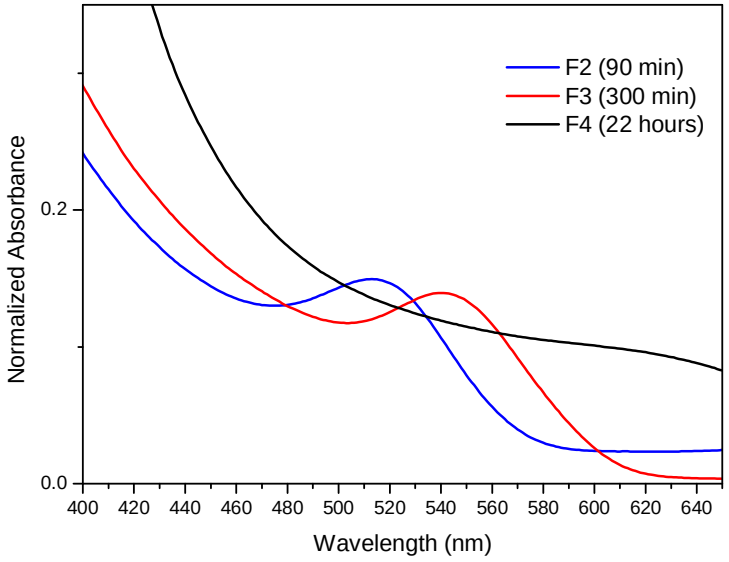

Figure 4. 13 The normalized absorbance of CdTe sample at different reflux time.

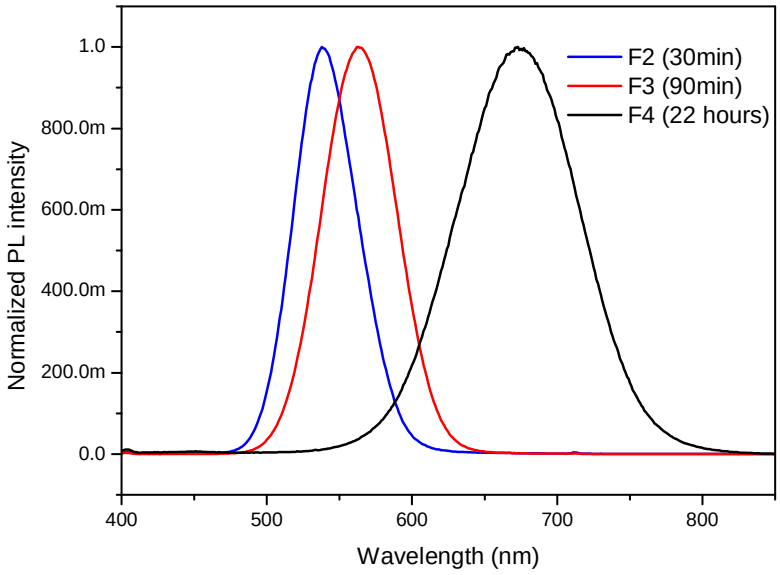

Figure 4. 14 Normalized PL intensity of CdTe solution taken at different time intervals.

All samples were stored in the refrigerator around 4°C. The storing temperature and place play an important role in the crystal growth. The particle size tends to grow if samples are stored under day light at room temperature. The crystal structure of the samples was determined by p-XRD. Characteristic XRD peaks of CdTe crystallized in cubic phase showed up at 24.0°, 39.7°and 47° with the corresponding (111) (220) and (311) planes (Figure 4. 15).

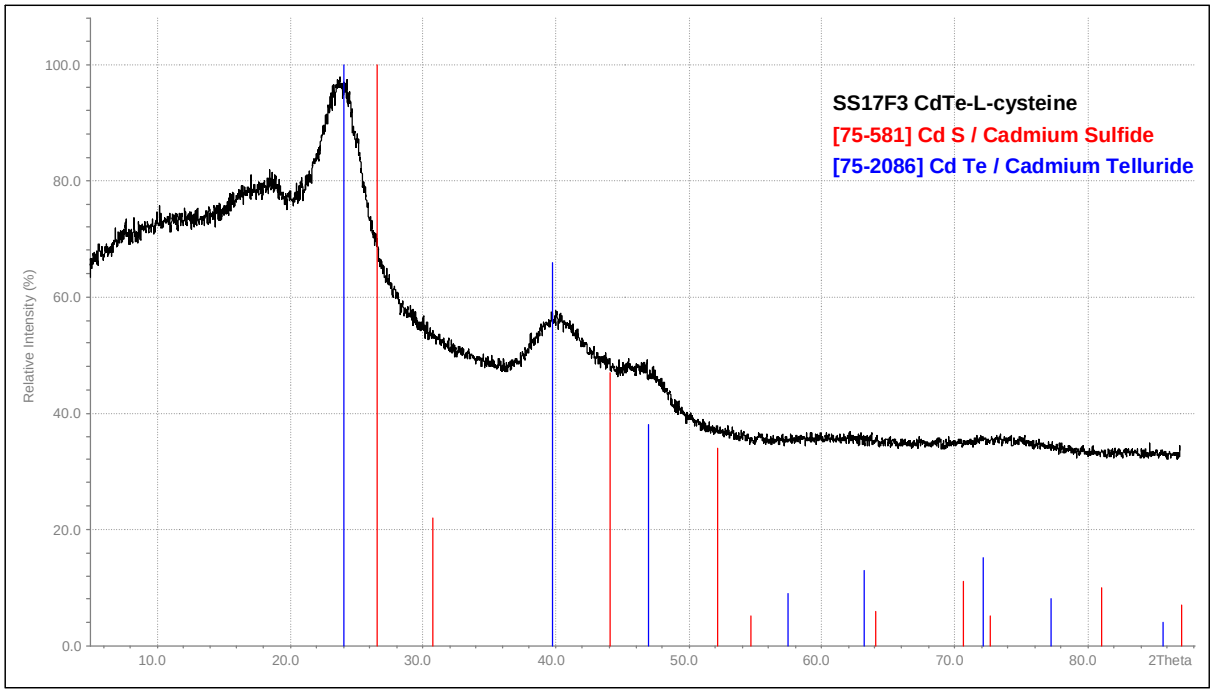

Figure 4. 15 X-ray diffraction of L-cysteine coated CdTe (SS17F3) with theoretical peak positions of CdTe and CdS.

In the literature, usually a thin CdS shell formation on CdTe core was reported when thiol ligands were used [141-143]. This was attributed to the partial decomposition of thiol at high reflux temperatures. Here, from the XRD pattern, it is difficult to judge the existence of such CdS shell. The theoretical patterns of CdTe and CdS are close to each

other and hard to differentiate when the peaks are broad but at least we can state that there is no significant CdS formation at the L-cysteine amount that we have used. The approximated average particle size from Debye-Scherrer equation was calculated as 3.5nm.

In order to investigate the coating of CdTe nanoparticles, FT-IR spectrum of the washed samples was taken (Figure 4. 16). The thiol (-SH) peak at 2544 cm^{-1} disappeared which confirms the thiol binding to the CdTe surface. The stretching vibration band of N-H had broadening between 3000cm^{-1} and 3600cm^{-1} which can be attributed to the hydrogen bond formation in the structure. Carbonyl stretching peak of L-cysteine at 1690cm^{-1} was replaced by carboxylate peaks at 1577cm^{-1} and 1398cm^{-1} which corresponds to the asymmetric and symmetric stretching modes, respectively.

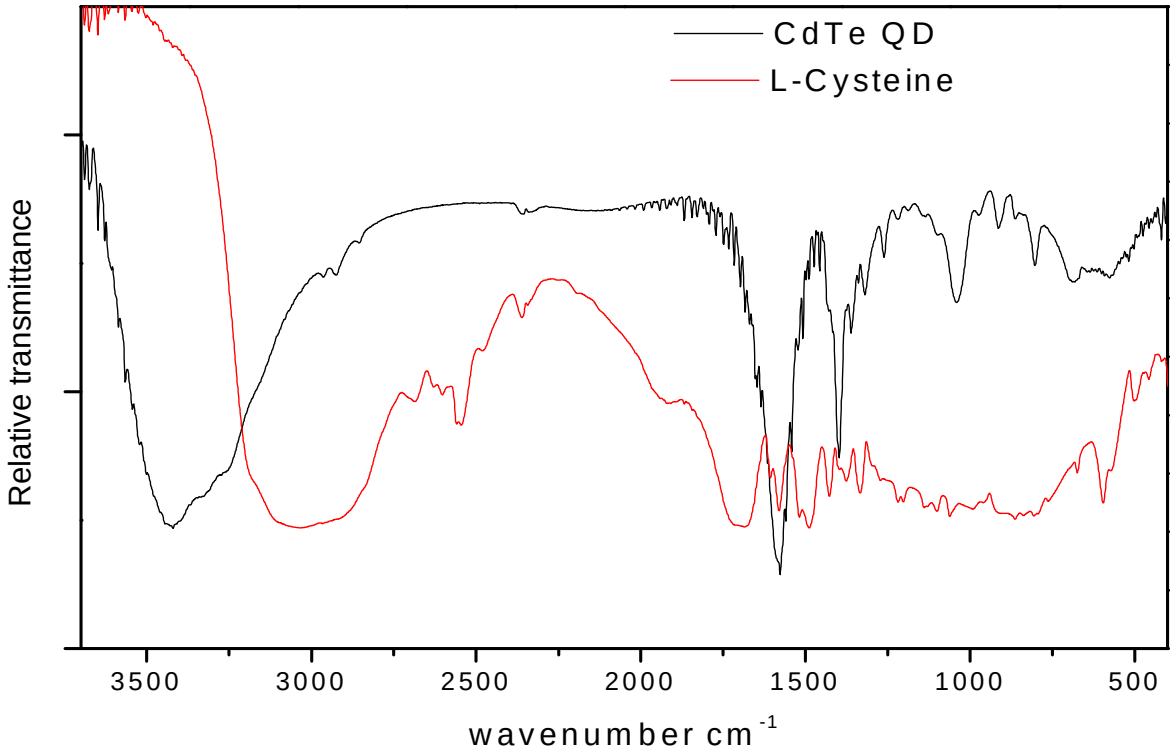

Figure 4. 16 FT-IR spectra of washed L-cysteine coated CdTe and L-cysteine.

4.3.4 CdTe/Iron oxide hybrid nanoparticles

The luminescent nanoparticles synthesized through cost efficient one-pot synthesis were used to conjugate paramagnetic iron oxide NPs. CdTe nanoparticles are advantageous when compared with CdS. CdTe synthesis is performed at high reaction temperatures like iron oxides which does not defoliates the luminescence of the particles. On the other hand, CdS nanoparticles lose its luminescing with increasing temperature as explained in chapter 2. The decomposition of thiol groups in L-cysteine at high reaction temperatures forms or may form a larger band gap material CdS which is appreciated in this type of reactions. The emission wavelength of CdTe is on the longer wavelengths of the spectrum where the absorption of iron oxide is low. On the other hand, CdS emission wavelength is absorbed by iron oxide molecules significantly. Different color emitting quantum dots of CdTe can be obtained easily by changing the reflux time whereas it is hard to change the emission color of CdS with one variable. Another advantage of CdTe is the higher QY when compared with the CdS nanoparticles. When the optimized conditions of CdS is chosen for CdTe, the quantum yield obtained was 53% which is almost three times the QY of CdS (19%). Notably, the other importance of CdTe is the low FWHM value around 40nm when compared with CdS around 120nm.

In an effort to prepare magnetic luminescent hybrid nanoparticles with CdTe, we have utilized not only L-cysteine but also 2-MPA which is proven as a very effective

coating for QDs in our group (unpublished data) and PAA/MAA mixture as was studied and proven effective by Serdar Celebi (in press) [144].

4.3.5 CdTe/2-MPA/Iron oxide

The knowledge obtained from chapter 2 was adapted to the procedure for the synthesis of magnetic luminescent nanoparticles with CdTe. The trials to obtain colloidal solutions of magnetic luminescent nanoparticles can be summarized in Table 4. 2. Nevertheless, most of the trials were resulted in the precipitation of luminescent-magnetic material when the stabilizer was 2-MPA In case of 2-MPA such a result is understandable. In 2-MPA, the molecule has thiol and carboxylate functional group where thiol binding to CdTe is confirmed. The free carboxylate group has to stabilize the newly formed iron oxide. Such occupation of functional groups leaves behind insufficient amount of functionality to sustain colloidal form. Use of carboxylates for iron oxide stabilization causes the loss of steric repulsion between the particles which was an advantage for the initial CdTe NPs. So, the hybrid nanoparticles aggregate and can not resist to the gravitational forces and precipitate.

4.3.6 CdTe/L-cysteine/Iron oxide

L-cysteine has an additional functional group, amine, when compared with 2-MPA. The iron oxide NPs can be coordinated both from amine and carboxylate units of L-cysteine, in any case leaving the other group exposed to water for stability. However,

colloidal stability was not achieved with this surfactant neither with NaHTe approach nor Na_2Te approach (Table 4. 2).

Table 4. 2 Summary of the hybrid study with 2-MPA and L-cysteine.

Sample name	Cd concentration [mM]	Fe concentration [mM]	Luminescent / Magnetic	Coating	Method
SSO16I	1mM	3mM	N/Yppt	2-MPA	H_2Te
SSO16J	1mM	3mM	Ysol/Yppt	2-MPA	NaHTe
SSO17B	1mM	3mM	Yppt/Yppt	L-cysteine	NaHTe
SSO17C	1mM	3mM	Yppt/Yppt	L-cysteine	NaHTe
SSO17E	1mM	3mM	Yppt/Yppt	L-cysteine	Na_2Te
SSO17F4Fe	1mM	3mM	Nppt/Nppt	L-cysteine	Na_2Te
SSO17FeI	1mM	3mM	Ysol/Nppt	L-cysteine	Na_2Te
SSO17FeG	1mM	9mM	Ysol/Yppt	L-cysteine	Na_2Te
SSO17FeH	1mM	1.5mM	Yppt/Nppt	L-cysteine	Na_2Te
SSO18A	1mM	3mM	N/Yppt	L-cysteine	Na_2Te
SSO18B	0.25mM	3mM	Nl/Yppt	L-cysteine	Na_2Te

4.3.7 CdTe/PAA-MAA/iron oxide

CdS coated with PAA/MAA at 40/60 mole ratios were stable and highly stable (Celebi thesis) [144]. We have adapted this coating composition to CdTe nanoparticles. Reaction was performed at the optimized ratios derived for CdS: total COOH/Cd ratio = 2 and the reaction pH = 7.5. CdTe QDs obtained with these ratios had a QY of 41% without any post-synthesis treatments. As prepared quantum dots were used to synthesize magnetic nanoparticles within the same pot without having further purifications. The work has been summarized in Table 4. 3. The colloidal stability was achieved with PAA/MAA coating

where the absorption calibrated quantum yield of the hybrid NP was calculated as 0.5%. The low quantum yield originates from the absorption of the photons emitted by the green luminescing quantum dots (used for the hybrid synthesis) by the iron oxide NPs.

Table 4. 3 Synthesis of PAA-MAA stabilized hybrid nanoparticles.

Sample name	Cd concentration [mM]	Fe concentration [mM]	Luminescent / Magnetic	NH_4OH (mL)	Method	Luminescence
SSOSC4205FeG1	0.5mM	3mM	Y/Y	1	Na_2Te	Green
SSOSC4205FeG2	0.2mM	3mM	Y/Y	0.5	Na_2Te	Green
SSSC4205FeR1	1mM	3mM	Y/Y	0.5	Na_2Te	Red
SSSC4204FeMG	1mM	7mM	Y/Y	3.25	Na_2Te	Green

In the characterization of PAA-MAA stabilized magnetic luminescent nanoparticles, FT-IR (Figure 4. 17) and XRD (Figure 4. 18) data were utilized. The absence of S-H vibration around 2550cm^{-1} confirms the thiol binding to the surface of the particles. The carboxylic acid C=O stretching mode at 1720cm^{-1} disappeared and replaced by anti-symmetric and symmetric stretching vibrations of carboxylate at 1558cm^{-1} and 1398^{-1}, respectively. Relatively weak peaks showed at 1455cm^{-1} and 1338cm^{-1} corresponds to the CH_2 bending and wagging modes. The asymmetrical stretching of CH_2 peak was observed at 2955$cm^{-1.}$

The XRD data revealed the existence of nanoparticles with broad and relatively low intensity peaks. The observed and calculated peak powder patterns were very practical in the structural determination. The theoretical magnetite structure well matched with the pattern with peak positions at 18.3°, 21.2°, 30.1°, 35.4° and 62.5° which are the

corresponding peaks positions of (111), (200), (220), (311) and (440) planes, respectively. The superparamagnetic nanoparticles are crystallized in cubic structure like CdTe nanoparticles. The intense peak positions of cubic CdTe structure observed at 24° (111) and 39.7° (220).

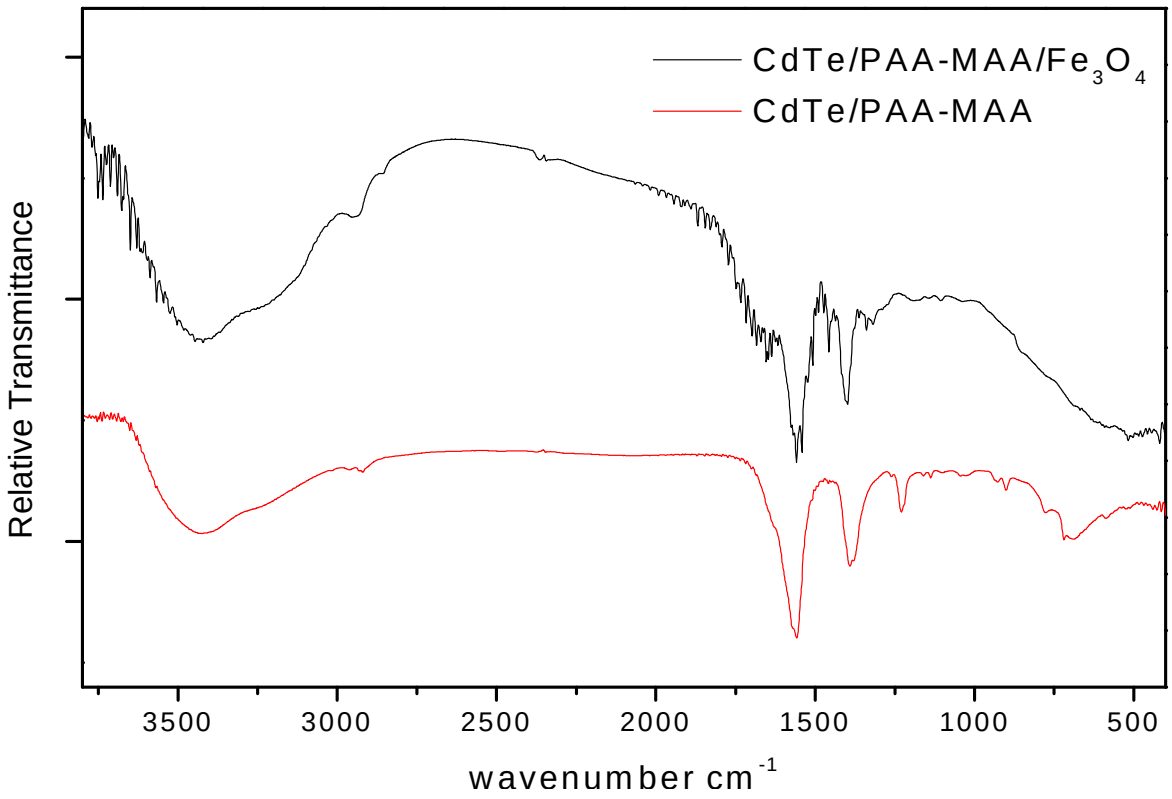

Figure 4. 17 FT-IR spectra of PAA-MAA/CdTe and CdTe/PAA-MAA/Fe_3O_4 hybrid nanoparticles

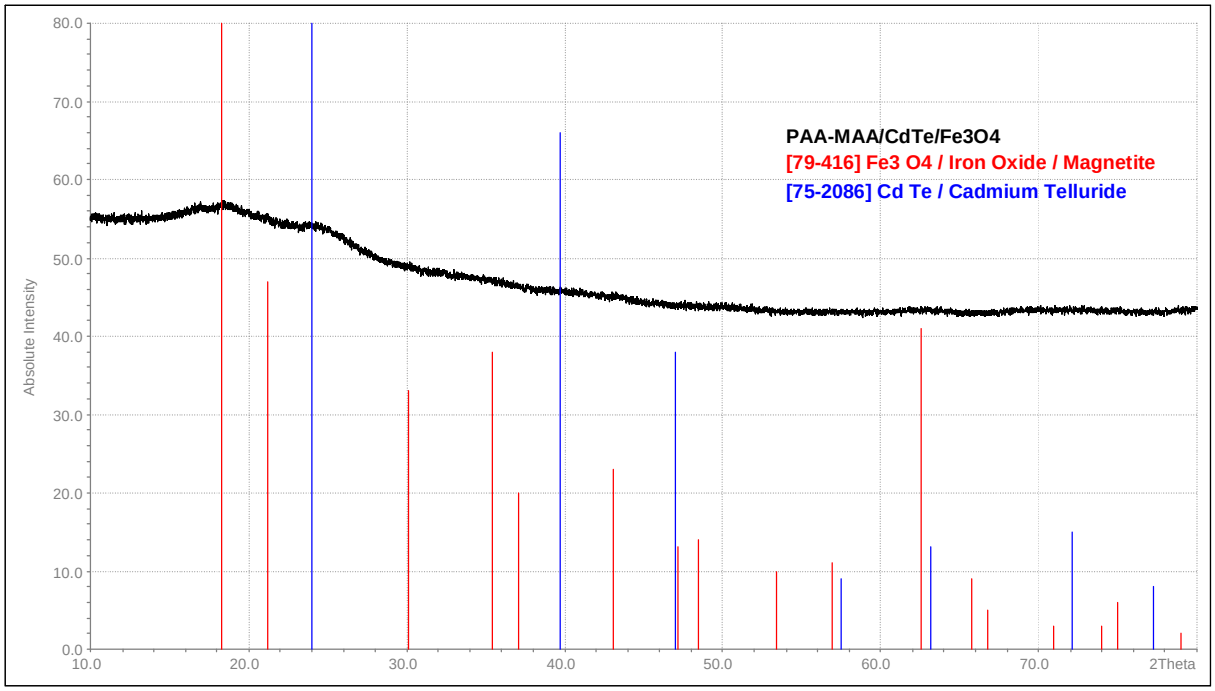

Figure 4. 18 p-XRD pattern of PAA-MAA/CdTe/Fe_3O_4

The quantum yield of the nanocomposite can be increased by changing reaction parameters like the reaction pH which plays an important factor in the stabilization of both species. Another improvement can be obtained by providing a shell with larger band gap material like CdS or ZnS over CdTe core which will increase the quantum yield.

Another improvement in the QY can be achieved by providing a shell protection on the surface. Hereby, the number of dangling atoms will be reduced and also their interaction with iron oxide molecules will be reduced. Telluride atoms on the surface have high affinity to iron ions. Like sulfide, telluride is a soft base which forms FeTe easily which was mentioned previously in chapter 2. The formation of FeTe plays an important role in the reduction of quantum yield.

4.4 Conclusions

Syntheses of CdTe QDs were performed in our laboratory for the first time. Aqueous CdTe quantum dots with L-cysteine, 2-MPA and PAA/MAA coatings were demonstrated successfully. The reaction method to obtain telluride with a simple, less-toxic and non-expensive approach was adapted for CdTe synthesis. The crystal growth of CdTe was investigated by absorption and PL spectra. Sufficient knowledge was obtained to tune the size of the nanoparticles with reflux time. The highest QY of 53% was achieved in 90 minutes of reflux when the particle size was relatively small and crystallinity was improved sufficiently. The optimum surface capping that decrease the surface defect sites and passivates the surface traps improves the QY.

Synthesized CdTe QDs were used to create magnetic luminescent nanocomposites in a simple one-pot synthesis approach. Major drawback of the system was maintaining colloidal stability. With 2-MPA and L-cysteine which are small molecules with close contact of both particles with relatively limited number of functional groups available for suspension fail to yield stable colloidal solutions of the hybrid structures. However, a stable hybrid system was achieved by the polymeric PAA/MAA coating. The method can be used to obtain various color emitting nanocomposites. Also, use of red luminescing QDs may provide better QY for the hybrids. Another drawback of the system was the high affinity of telluride atoms on the iron atoms. These phenomena can be prevented by capping the core of CdTe with larger band gap materials like CdS or ZnS.

Chapter 5

CONCLUSIONS

In order to achieve high colloidal stability and biocompatibility, L-cysteine was chosen as the stabilizer in our approach. The initial goal of the thesis was to synthesize CdS quantum dots in a simple, safe and non-expensive one-pot method with controllable particle size, narrow size distribution with high quantum efficiency in high reaction yields. The reaction parameters that influence the stability, quantum efficiency and crystal growth were investigated by varying cysteine:Cd^{2+}:S^{2-} molar ratios, pH and reaction temperature as described in Chapter 2. Optimum conditions for the best QY was determined with cysteine:Cd^{2+}:S^{2-} ratio of 5:2.5:1, final reaction pH of 10.5 and room temperature. Yet, better quantum yields up to 55% percent, which is the highest QY reported for L-cysteine, can be achieved by redispersing the optimized aliquot in pH 7 buffer. The emission color of the QDs was tuned from bluish-green to red by changing the reaction temperature which was not reported before. The toxicology studies revealed that L-cysteine coated QDs are biocompatible and besides have preferential cell uptake for MCF-7 more than HeLa cell which can be advantageous as a natural selection for medical applications.

These L-cysteine coated quantum dots were used to prepare magnetic luminescent hybrid nanoparticles in a one pot all aqueous synthetic method. This is the first report in the literature for such a system and was the final and main goal of this thesis. Number of CdS-QDs per iron oxide, pH of the medium, and the reaction procedures were varied to achieve colloidal stability and high quantum efficiency for the hybrid nanoparticles. The main drawback of the system was the low quantum efficiency due to the absorption of emitted photons from QDs by the iron oxide.

The knowledge gained from the described research was used to adopt the approach to CdTe QDs. CdTe QDs emitting in different colors from 481 nm to 700 nm were obtained by changing the reflux time of the reaction. The growth mechanism of L-cysteine capped CdTe was investigated by using absorption and fluorescence spectra.

In Chapter 4, CdTe QDs were exploited for the development of magnetic luminescent nanoparticles. Along with CdTe different coating materials, 2MPA and PAA/MAA mixture was also evaluated. When compared with 2-MPA and L-cysteine, PAA-MAA mixture improved the colloidal stability of the hybrid nanoparticles. Luminescent magnetic nanoparticles were achieved. The problems of the hybrid system and plausible solutions were stated. In the future studies, capping QDs with larger band gap material and tuning the emission wavelength of the luminescing entity to longer wavelengths to avoid the absorption of iron oxide particles can be adopted to increase the QY of the hybrid system.

BIIBLIOGRAPHY

[1] K. Sasaki and H. Saka, "Insitu High-Resolution Electron-Microscopy Observation of the Melting Process of in Particles Embedded in an Al Matrix," *Philosophical Magazine a-Physics of Condensed Matter Structure Defects and Mechanical Properties*, vol. 63, pp. 1207-1220, 1991.

[2] T. Ohashi, K. Kuroda, and H. Saka, "Insitu Electron-Microscopy of Melting and Solidification of in Particles Embedded in an Fe Matrix," *Philosophical Magazine B-Physics of Condensed Matter Statistical Mechanics Electronic Optical and Magnetic Properties*, vol. 65, pp. 1041-1052, 1992.

[3] S. Deki, K. Sayo, A. Yamada, K. Akamatsu, and S. Hayashi, "Novel preparation method for nano-sized gold particles by using NH2-terminated polyethyleneoxide," *Journal of Colloid and Interface Science*, vol. 214, pp. 123-125, 1999.

[4] P. W. Atkins and J. d. Paula, "Physical Chemistry," *7th ed.*, vol. New York, NY: Oxford University Press, 2002.

[5] D. Wang, "CdSe Quantum Dots and Luminescent/Magnetic Particles for Biological Applications " *Thesis submission*, vol. Graduate Faculty of the University of New Orleans, pp. 6, 2004.

[6] G. Chen and A. Shakouri, "Heat transfer in nanostructures for solid-state energy conversion," *Journal of Heat Transfer-Transactions of the Asme*, vol. 124, pp. 242-252, 2002.

[7] I. Ouchi, R. Miyamura, M. Sakoguchi, S. Hosaka, and M. Kitagawa, "Excitation and emission spectra of polyethylene terephthalate and polyethylene 2,6-naphthalate films," *Polymers for Advanced Technologies*, vol. 10, pp. 195-198, 1999.

[8] P. R. Hammond, "Comparison of Experimental and Theoretical Excited-State Spectra for Rhodamine-6G," *Ieee Journal of Quantum Electronics*, vol. 16, pp. 1157-1160, 1980.

[9] T. W. Kang and J. E. Oh, "Abnormal temperature-dependent photoluminescence characteristics of stacked InAs self-assembled quantum dot structures grown by molecular beam epitaxy," *Journal of Crystal Growth*, vol. 227, pp. 1039-1043, 2001.

[10] L. E. Brus, "Electron-electron and electron-hole interactions in small semiconductor crystallites: The size dependence of the lowest excited electronic state," *J. Chem. Phys.*, vol. 80, pp. 4403-4409, 1984.

[11] Y. Wang, N. Herron, W. Mahler, and A. Suna, "Linear-Optical and Nonlinear-Optical Properties of Semiconductor Clusters," *Journal of the Optical Society of America B-Optical Physics*, vol. 6, pp. 808-813, 1989.

[12] E. F. Hilinski, P. A. Lucas, and Y. Wang, "A Picosecond Bleaching Study of Quantum-Confined Cadmium-Sulfide Microcrystallites in a Polymer Film," *Journal of Chemical Physics*, vol. 89, pp. 3435-3441, 1988.

[13] Y. Wang, A. Suna, J. Mchugh, E. F. Hilinski, P. A. Lucas, and R. D. Johnson, "Optical Transient Bleaching of Quantum-Confined Cds Clusters - the Effects of Surface-Trapped Electron-Hole Pairs," *Journal of Chemical Physics*, vol. 92, pp. 6927-6939, 1990.

[14] M. F. Bertino, R. R. Gadipalli, L. A. Martin, L. E. Rich, A. Yamilov, B. R. Heckman, N. Leventis, S. Guha, J. Katsoudas, R. Divan, and D. C. Mancini, "Quantum dots by ultraviolet and x-ray lithography," *Nanotechnology*, vol. 18, pp. - , 2007.

[15] A. Schuler, M. Python, M. V. del Olmo, and E. de Chambrier, "Quantum dot containing nanocomposite thin films for photoluminescent solar concentrators," *Solar Energy*, vol. 81, pp. 1159-1165, 2007.

[16] P. K. Ghosh, M. K. Mitra, and K. K. Chattopadhyay, "ZnS nanobelts grown in a polymer matrix by chemical bath deposition," *Nanotechnology*, vol. 16, pp. 107-112, 2005.

[17] S. Ohkouchi, Y. Sugimoto, N. Ozaki, H. Ishikawa, and K. Asakawa, "Molecular beam epitaxial growth of site-controlled InAs quantum dot arrays using templates fabricated by the Nano-Jet Probe method," *Physica E-Low-Dimensional Systems & Nanostructures*, vol. 40, pp. 1794-1796, 2008.

[18] C. B. Murray and D. J. Norris, "Synthesis and characterization of nearly monodisperse CdE (E=S, Se, Te) semiconductor," *Journal of the American Chemical Society*, vol. 115, pp. 8706, 1993.

[19] C. B. Murray, C. R. Kagan, and M. G. Bawendi, "Synthesis and characterization of monodisperse nanocrystals and close-packed nanocrystal assemblies," *Annual Review of Materials Science*, vol. 30, pp. 545-610, 2000.

[20] O. Masala and R. Seshadri, "Synthesis routes for large volumes of nanoparticles," *Annual Review of Materials Research*, vol. 34, pp. 41-81, 2004.

[21] Z. A. Peng and X. G. Peng, "Formation of high-quality CdTe, CdSe, and CdS nanocrystals using CdO as precursor," *Journal of the American Chemical Society*, vol. 123, pp. 183-184, 2001.

[22] M. A. Hines and P. Guyot-Sionnest, "Synthesis and characterization of strongly luminescing ZnS-Capped CdSe nanocrystals," *Journal of Physical Chemistry*, vol. 100, pp. 468-471, 1996.

[23] G. Kalyuzhny and R. W. Murray, "Ligand effects on optical properties of CdSe nanocrystals," *Journal of Physical Chemistry B*, vol. 109, pp. 7012-7021, 2005.

[24] S. W. Kim, S. Kim, J. B. Tracy, A. Jasanoff, and M. G. Bawendi, "Phosphine oxide polymer for water-soluble nanoparticles," *Journal of the American Chemical Society*, vol. 127, pp. 4556-4557, 2005.

[25] H. T. Uyeda, I. L. Medintz, J. K. Jaiswal, S. M. Simon, and H. Mattoussi, "Synthesis of compact multidentate ligands to prepare stable hydrophilic quantum dot fluorophores," *Journal of the American Chemical Society*, vol. 127, pp. 3870-3878, 2005.

[26] E. C. Kang, A. Ogura, K. Kataoka, and Y. Nagasaki, "Preparation of water-soluble PEGylated semiconductor nanocrystals," *Chemistry Letters*, vol. 33, pp. 840-841, 2004.

[27] S. K. Mandal, N. Lequeux, B. Rotenberg, M. Tramier, J. Fattaccioli, J. Bibette, and B. Dubertret, "Encapsulation of magnetic and fluorescent nanoparticles in emulsion droplets," *Langmuir*, vol. 21, pp. 4175-4179, 2005.

[28] W. J. Parak, D. Gerion, D. Zanchet, A. S. Woerz, T. Pellegrino, C. Micheel, S. C. Williams, M. Seitz, R. E. Bruehl, Z. Bryant, C. Bustamante, C. R. Bertozzi, and A. P. Alivisatos, "Conjugation of DNA to silanized colloidal semiconductor nanocrystalline quantum dots," *Chemistry of Materials*, vol. 14, pp. 2113-2119, 2002.

[29] H. Y. Fan, E. W. Leve, C. Scullin, J. Gabaldon, D. Tallant, S. Bunge, T. Boyle, M. C. Wilson, and C. J. Brinker, "Surfactant-assisted synthesis of water-soluble and biocompatible semiconductor quantum dot micelles," *Nano Letters*, vol. 5, pp. 645-648, 2005.

[30] E. R. Goldman, E. D. Balighian, H. Mattoussi, M. K. Kuno, J. M. Mauro, P. T. Tran, and G. P. Anderson, "Avidin: A natural bridge for quantum dot-antibody conjugates," *Journal of the American Chemical Society*, vol. 124, pp. 6378-6382, 2002.

[31] D. V. Talapin, A. L. Rogach, A. Kornowski, M. Haase, and H. Weller, "Highly luminescent monodisperse CdSe and CdSe/ZnS nanocrystals synthesized in a hexadecylamine-trioctylphosphine oxide-trioctylphospine mixture," *Nano Letters*, vol. 1, pp. 207-211, 2001.

[32] O. Schmelz, A. Mews, T. Basche, A. Herrmann, and K. Mullen, "Supramolecular complexes from CdSe nanocrystals and organic fluorophors," *Langmuir*, vol. 17, pp. 2861-2865, 2001.

[33] M. Y. Li, Y. X. Ge, Q. F. Chen, S. K. Xu, N. Z. Wang, and X. J. Zhang, "Hydrothermal synthesis of highly luminescent CdTe quantum dots by adjusting precursors' concentration and their conjunction with BSA as biological fluorescent probes," *Talanta*, vol. 72, pp. 89-94, 2007.

[34] O. Palchik, R. Kerner, A. Gedanken, A. M. Weiss, M. A. Slifkin, and V. Palchik, "Microwave-assisted polyol method for the preparation of CdSe "nanoballs"," *Journal of Materials Chemistry*, vol. 11, pp. 874-878, 2001.

[35] M. Y. Gao, S. Kirstein, H. Mohwald, A. L. Rogach, A. Kornowski, A. Eychmuller, and H. Weller, "Strongly photoluminescent CdTe nanocrystals by proper surface modification," *Journal of Physical Chemistry B*, vol. 102, pp. 8360-8363, 1998.

[36] N. Gaponik, D. V. Talapin, A. L. Rogach, K. Hoppe, E. V. Shevchenko, A. Kornowski, A. Eychmuller, and H. Weller, "Thiol-capping of CdTe nanocrystals: An alternative to organometallic synthetic routes," *Journal of Physical Chemistry B*, vol. 106, pp. 7177-7185, 2002.

[37] A. Priyam, A. Chatterjee, S. K. Das, and A. Saha, "Synthesis and spectral studies of cysteine-capped CdS nanoparticles," *Research on Chemical Intermediates*, vol. 31, pp. 691-702, 2005.

[38] A. Chatterjee, A. Priyam, S. K. Das, and A. Saha, "Size tunable synthesis of cysteine-capped CdS nanoparticles by gamma-irradiation," *Journal of Colloid and Interface Science*, vol. 294, pp. 334-342, 2006.

[39] H. Zhang, Z. Zhou, B. Yang, and M. Y. Gao, "The influence of carboxyl groups on the photoluminescence of mercaptocarboxylic acid-stabilized CdTe nanoparticles," *Journal of Physical Chemistry B*, vol. 107, pp. 8-13, 2003.

[40] A. G. Young, D. P. Green, and A. J. McQuillan, "Infrared spectroscopic studies of monothiol ligand adsorption on CdS nanocrystal films in aqueous solutions," *Langmuir*, vol. 22, pp. 11106-11112, 2006.

[41] P. Zhong, Y. Yu, J. Z. Wu, Z. Y. Long, and C. S. Liang, "Synthesis of mercaptoethylamine-coated CdSe/CdS nanocrystals and their use for DNA probe," *Analytical Sciences*, vol. 23, pp. 1085-1089, 2007.

[42] C. Q. Hu, Z. H. Gao, and X. R. Yang, "One-pot low temperature synthesis of MFe2O4 (M = Co, Ni, Zn) superparamagnetic nanocrystals," *Journal of Magnetism and Magnetic Materials*, vol. 320, pp. L70-L73, 2008.

[43] G. Guo, W. Liu, J. Liang, H. Xu, Z. He, and X. Yang, "Preparation and characterization of novel CdSe quantum dots modified with poly (d, l-lactide) nanoparticles," *Materials Letters*, vol. 60, pp. 2565, 2006.

[44] N. Feltin and M. P. Pileni, "New technique for synthesizing iron ferrite magnetic nanosized particles," *Langmuir*, vol. 13, pp. 3927-3933, 1997.

[45] H. Mattoussi, J. M. Mauro, E. R. Goldman, G. P. Anderson, V. C. Sundar, F. V. Mikulec, and M. G. Bawendi, "Self-assembly of CdSe-ZnS quantum dot bioconjugates using an engineered recombinant protein," *Journal of the American Chemical Society*, vol. 122, pp. 12142-12150, 2000.

[46] V. Pillai, P. Kumar, M. J. Hou, P. Ayyub, and D. O. Shah, "Preparation of Nanoparticles of Silver-Halides, Superconductors and Magnetic-Materials Using Water-in-Oil Microemulsions as Nano-Reactors," *Advances in Colloid and Interface Science*, vol. 55, pp. 241-269, 1995.

[47] K. V. P. M. Shafi, A. Ulman, A. Dyal, X. Z. Yan, N. L. Yang, C. Estournes, L. Fournes, A. Wattiaux, H. White, and M. Rafailovich, "Magnetic enhancement of gamma-Fe2O3 nanoparticles by sonochemical coating," *Chemistry of Materials*, vol. 14, pp. 1778-1787, 2002.

[48] G. L. Messing, S. C. Zhang, and G. V. Jayanthi, "Ceramic Powder Synthesis by Spray-Pyrolysis," *Journal of the American Ceramic Society*, vol. 76, pp. 2707-2726, 1993.

[49] S. W. Kamau, P. O. Hassa, B. Steitz, A. Petri-Fink, H. Hofmann, M. Hofmann-Amtenbrink, B. von Rechenberg, and M. O. Hottiger, "Enhancement of the efficiency of non-viral gene delivery by application of pulsed magnetic field," *Nucleic Acids Research*, vol. 34, pp. -, 2006.

[50] A. K. Gupta and M. Gupta, "Synthesis and surface engineering of iron oxide nanoparticles for biomedical applications," *Biomaterials*, vol. 26, pp. 3995-4021, 2005.

[51] A. J. M. D'Souza, R. L. Schowen, and E. M. Topp, "Polyvinylpyrrolidone-drug conjugate: Synthesis and release mechanism," *Journal of Controlled Release*, vol. 94, pp. 91-100, 2004.

[52] K. Burugapalli, V. Koul, and A. K. Dinda, "Effect of composition of interpenetrating polymer network hydrogels based on poly(acrylic acid) and gelatin on tissue response: A quantitative in vivo study," *Journal of Biomedical Materials Research Part A*, vol. 68A, pp. 210-218, 2004.

[53] A. K. Gupta and A. S. G. Curtis, "Surface modified superparamagnetic nanoparticles for drug delivery: Interaction studies with human fibroblasts in culture," *Journal of Materials Science-Materials in Medicine*, vol. 15, pp. 493-496, 2004.

[54] X. Zhao and J. M. Harris, "Novel degradable poly(ethylene glycol) hydrogels for controlled release of protein," *Journal of Pharmaceutical Sciences*, vol. 87, pp. 1450-1458, 1998.

[55] G. A. Martínez-Castañón, M. G. Sánchez-Loredo, J. R. Martínez-Mendoza, and F. Ruiz, "Synthesis of CdS Nanoparticles: a Simple Method in Aqueous Media," *Journal of Materials online*, vol. 1, 2005.

[56] Y. I. Jeong, J. W. Nah, H. K. Na, K. Na, I. S. Kim, C. S. Cho, and S. H. Kim, "Self-assembling nanospheres of hydrophobized pullulans in water," *Drug Development and Industrial Pharmacy*, vol. 25, pp. 917-927, 1999.

[57] E. S. Miller, N. A. Peppas, and D. N. Winslow, "Morphological-Changes of Ethylene Vinyl Acetate-Based Controlled Delivery Systems during Release of Water-Soluble Solutes," *Journal of Membrane Science*, vol. 14, pp. 79-92, 1983.

[58] Y. Lu, Y. D. Yin, B. T. Mayers, and Y. N. Xia, "Modifying the surface properties of superparamagnetic iron oxide nanoparticles through a sol-gel approach," *Nano Letters*, vol. 2, pp. 183-186, 2002.

[59] J. Kim, J. E. Lee, J. Lee, J. H. Yu, B. C. Kim, K. An, Y. Hwang, C. H. Shin, J. G. Park, J. Kim, and T. Hyeon, "Magnetic fluorescent delivery vehicle using uniform mesoporous silica spheres embedded with monodisperse magnetic and semiconductor nanocrystals," *Journal of the American Chemical Society*, vol. 128, pp. 688-689, 2006.

[60] Y. H. Ni, H. J. Liu, F. Wang, Y. Y. Liang, J. M. Hong, X. Ma, and Z. Xu, "Shape controllable preparation of PbS crystals by a simple aqueous phase route," *Crystal Growth & Design*, vol. 4, pp. 759-764, 2004.

[61] N. Gaponik, I. L. Radtchenko, G. B. Sukhorukov, and A. L. Rogach, "Luminescent polymer microcapsules addressable by a magnetic field," *Langmuir*, vol. 20, pp. 1449-1452, 2004.

[62] Y. Okamoto, F. Kitagawa, and K. Otsuka, "Online concentration and affinity separation of biomolecules using multifunctional particles in capillary electrophoresis under magnetic field," *Analytical Chemistry*, vol. 79, pp. 3041-3047, 2007.

[63] D. S. Wang, J. B. He, N. Rosenzweig, and Z. Rosenzweig, "Superparamagnetic Fe2O3 Beads-CdSe/ZnS quantum dots core-shell nanocomposite particles for cell separation," *Nano Letters*, vol. 4, pp. 409-413, 2004.

[64] S. A. Corr, A. O' Byrne, Y. K. Gun'ko, S. Ghosh, D. F. Brougham, S. Mitchell, Y. Volkov, and A. Prina-Mello, "Magnetic-fluorescent nanocomposites for biomedical multitasking," *Chemical Communications*, pp. 4474-4476, 2006.

[65] C. Becker, M. Hodenius, G. Blendinger, A. Sechi, T. Hieronymus, D. Muller-Schulte, T. Schmitz-Rode, and M. Zenke, "Uptake of magnetic nanoparticles into cells for cell tracking," *Journal of Magnetism and Magnetic Materials*, vol. 311, pp. 234-237, 2007.

[66] X. Z. Li, L. Wang, C. Zhou, T. T. Guan, J. Li, and Y. H. Zhang, "Preliminary studies of application of CdTe nanocrystals and dextran-Fe3O4 magnetic nanoparticles in sandwich immunoassay," *Clinica Chimica Acta*, vol. 378, pp. 168-174, 2007.

[67] H. Gu, R. Zheng, X. Zhang, and B. Xu, "Facile One-Pot Synthesis of Bifunctional Heterodimers of Nanoparticles: A Conjugate of Quantum Dot and Magnetic Nanoparticles," *J. Am. Chem. Soc.*, vol. 126, pp. 5664-5665, 2004.

[68] G. H. Du, Z. L. Liu, Q. H. Lu, X. Xia, L. H. Jia, K. L. Yao, Q. Chu, and S. M. Zhang, "Fe3O4/CdSe/ZnS magnetic fluorescent bifunctional nanocomposites," *Nanotechnology*, vol. 17, pp. 2850-2854, 2006.

[69] A. Quarta, R. Di Corato, L. Manna, A. Ragusa, and T. Pellegrino, "Fluorescent-magnetic hybrid nanostructures: Preparation, properties, and applications in biology," *Ieee Transactions on Nanobioscience*, vol. 6, pp. 298-308, 2007.

[70] A. P. Alivisatos, "Semiconductor clusters, nanocrystals, and quantum dots," *Science*, vol. 271, pp. 933-937, 1996.

[71] L. Brus, "Electronic Wave-Functions in Semiconductor Clusters - Experiment and Theory," *Journal of Physical Chemistry*, vol. 90, pp. 2555-2560, 1986.

[72] J. M. Costa-Fernandez, R. Pereiro, and A. Sanz-Medel, "The use of luminescent quantum dots for optical sensing," *Trends in Analytical Chemistry: TRAC*, vol. 25, pp. 207, 2006.

[73] Y. Zhang, D. G. Fu, X. Wang, J. Z. Liu, and Z. H. Lu, "Optical and nonlinear optical properties of surface-modified CdS nanoparticles," *Colloids and Surfaces a-Physicochemical and Engineering Aspects*, vol. 181, pp. 145-149, 2001.

[74] X. H. Gao, W. C. W. Chan, and S. M. Nie, "Quantum-dot nanocrystals for ultrasensitive biological labeling and multicolor optical encoding," *Journal of Biomedical Optics*, vol. 7, pp. 532-537, 2002.

[75] M. Nirmal and L. Brus, "Luminescence photophysics in semiconductor nanocrystals," *Accounts of Chemical Research*, vol. 32, pp. 407-414, 1999.

[76] S. P. Mulvaney, H. M. Mattoussi, and L. J. Whitman, "Incorporating fluorescent dyes and quantum dots into magnetic microbeads for immunoassays," *Biotechniques*, vol. 36, pp. 602-+, 2004.

[77] V. C. Sundar, H. J. Eisler, and M. G. Bawendi, "Room-temperature, tunable gain media from novel II-VI nanocrystal-titania composite matrices," *Advanced Materials*, vol. 14, pp. 739-+, 2002.

[78] S. Gunes, K. P. Fritz, H. Neugebauer, N. S. Sariciftci, S. Kumar, and G. D. Scholes, "Hybrid solar cells using PbS nanoparticles," *Solar Energy Materials and Solar Cells*, vol. 91, pp. 420-423, 2007.

[79] A. A. Mamedov, A. Belov, M. Giersig, N. N. Mamedova, and N. A. Kotov, "Nanorainbows: Graded semiconductor films from quantum dots," *Journal of the American Chemical Society*, vol. 123, pp. 7738-7739, 2001.

[80] F. Wang, W. B. Tan, Y. Zhang, X. P. Fan, and M. Q. Wang, "Luminescent nanomaterials for biological labelling," *Nanotechnology*, vol. 17, pp. R1-R13, 2006.

[81] E. M. Goldys, K. Drozdowicz-Tomsia, G. Zhu, H. Yu, S. Jinjun, M. Motlan, and M. Godlewski, "Fluorescence labelling," *Optica Applicata*, vol. 36, pp. 217-224, 2006.

[82] D. W. Deng, J. S. Yu, and Y. Pan, "Water-soluble CdSe and CdSe/CdS nanocrystals: A greener synthetic route," *Journal of Colloid and Interface Science*, vol. 299, pp. 225-232, 2006.

[83] R. Yang, Y. X. Yan, Y. Mu, W. Ji, X. W. Li, M. Q. Zou, Q. Fei, and Q. H. Jin, "A rapid and facile method for hydrothermal synthesis of CdTe nanocrystals under mild conditions," *Journal of Nanoscience and Nanotechnology*, vol. 6, pp. 215-220, 2006.

[84] D. Gerion, F. Pinaud, S. C. Williams, W. J. Parak, D. Zanchet, S. Weiss, and A. P. Alivisatos, "Synthesis and properties of biocompatible water-soluble silica-coated CdSe/ZnS semiconductor quantum dots," *Journal of Physical Chemistry B*, vol. 105, pp. 8861-8871, 2001.

[85] W. C. W. Chan and S. M. Nie, "Quantum dot bioconjugates for ultrasensitive nonisotopic detection," *Science*, vol. 281, pp. 2016-2018, 1998.

[86] M. Bruchez, M. Moronne, P. Gin, S. Weiss, and A. P. Alivisatos, "Semiconductor nanocrystals as fluorescent biological labels," *Science*, vol. 281, pp. 2013-2016, 1998.

[87] J. Aldana, Y. A. Wang, and X. G. Peng, "Photochemical instability of CdSe nanocrystals coated by hydrophilic thiols," *Journal of the American Chemical Society*, vol. 123, pp. 8844-8850, 2001.

[88] G. P. Mitchell, C. A. Mirkin, and R. L. Letsinger, "Programmed assembly of DNA functionalized quantum dots," *Journal of the American Chemical Society*, vol. 121, pp. 8122-8123, 1999.

[89] A. L. Rogach, D. Nagesha, J. W. Ostrander, M. Giersig, and N. A. Kotov, ""Raisin bun"-type composite spheres of silica and semiconductor nanocrystals," *Chemistry of Materials*, vol. 12, pp. 2676-2685, 2000.

[90] D. V. Talapin, A. L. Rogach, I. Mekis, S. Haubold, A. Kornowski, M. Haase, and H. Weller, "Synthesis and surface modification of amino-stabilized CdSe, CdTe and InP nanocrystals," *Colloids and Surfaces a-Physicochemical and Engineering Aspects*, vol. 202, pp. 145-154, 2002.

[91] H. F. Qian, L. Li, and J. C. Ren, "One-step and rapid synthesis of high quality alloyed quantum dots (CdSe-CdS) in aqueous phase by microwave irradiation with controllable temperature," *Materials Research Bulletin*, vol. 40, pp. 1726-1736, 2005.

[92] A. L. Rogach, A. Kornowski, M. Y. Gao, A. Eychmuller, and H. Weller, "Synthesis and characterization of a size series of extremely small thiol-stabilized CdSe nanocrystals," *Journal of Physical Chemistry B*, vol. 103, pp. 3065-3069, 1999.

[93] A. Chatterjee, A. Priyam, S. C. Bhattacharya, and A. Saha, "Differential growth and photoluminescence of ZnS nanocrystals with variation of surfactant molecules," *Colloids and Surfaces a-Physicochemical and Engineering Aspects*, vol. 297, pp. 258-266, 2007.

[94] Z. X. Cai, H. Yang, Y. Zhang, and X. P. Yan, "Preparation, characterization and evaluation of water-soluble L-cysteine-capped-CdS nanoparticles as fluorescence probe for detection of Hg(II) in aqueous solution," *Analytica Chimica Acta*, vol. 559, pp. 234-239, 2006.

[95] W. H. Liu, H. S. Choi, J. P. Zimmer, E. Tanaka, J. V. Frangioni, and M. Bawendi, "Compact cysteine-coated CdSe(ZnCdS) quantum dots for in vivo applications," *Journal of the American Chemical Society*, vol. 129, pp. 14530-+, 2007.

[96] X. D. Cao, C. M. Li, H. F. Bao, Q. L. Bao, and H. Dong, "Fabrication of strongly fluorescent quantum dot-polymer composite in aqueous solution," *Chemistry of Materials*, vol. 19, pp. 3773-3779, 2007.

[97] B. Feng, F. Teng, A. W. Tang, Y. Wang, Y. B. Hou, and Y. S. Wang, "Synthesis and optical properties of L-cysteine hydrochloride-stabilized CdSe nanocrystals in a new alkali system," *Journal of Nanoscience and Nanotechnology*, vol. 8, pp. 1178-1182, 2008.

[98] Y. X. Yan, Y. Mu, G. D. Feng, L. Zhang, L. L. Zhu, L. Xu, R. Yang, and Q. H. Jin, "Novel strategy for synthesis of high quality CdTe nanocrystals in aqueous solution," *Chemical Research in Chinese Universities*, vol. 24, pp. 8-14, 2008.

[99] S. O. Oluwafemi, N. Revaprasadu, and A. J. Ramirez, "A novel one-pot route for the synthesis of water-soluble cadmium selenide nanoparticles," *Journal of Crystal Growth*, vol. 310, pp. 3230-3234, 2008.

[100] S. Celebi, A. K. Erdamar, A. Sennaroglu, A. Kurt, and H. Y. Acar, "Synthesis and characterization of poly(acrylic acid) stabilized cadmium sulfide quantum dots," *Journal of Physical Chemistry B*, vol. 111, pp. 12668-12675, 2007.

[101] H. Li, W. Y. Shih, and W. H. Shih, "Synthesis and characterization of aqueous carboxyl-capped CdS quantum dots for bioapplications," *Industrial & Engineering Chemistry Research*, vol. 46, pp. 2013-2019, 2007.

[102] A. Cervellino, C. Giannini, A. Guagliardi, and M. Ladisa, "Nanoparticle size distribution estimation by a full-pattern powder diffraction analysis," *Physical Review B*, vol. 72, pp. -, 2005.

[103] H. Weller, "Colloidal Semiconductor Q-Particles - Chemistry in the Transition Region between Solid-State and Molecules," *Angewandte Chemie-International Edition in English*, vol. 32, pp. 41-53, 1993.

[104] A. Priyam, A. Chatterjee, S. C. Bhattacharya, and A. Saha, "Surface-functionalized cadmium chalcogenide nanocrystals: A spectroscopic investigation of growth and photoluminescence," *Journal of Crystal Growth*, vol. 304, pp. 416-424, 2007.

[105] A. Creti, M. Anni, M. Z. Rossi, G. Lanzani, G. Leo, F. Della Sala, L. Manna, and M. Lomascolo, "Ultrafast carrier dynamics in core and core/shell CdSe quantum rods: Role of the surface and interface defects," *Physical Review B*, vol. 72, pp. -, 2005.

[106] J. O. Winter, N. Gomez, S. Gatzert, C. E. Schmidt, and B. A. Korgel, "Variation of cadmium sulfide nanoparticle size and photoluminescence intensity with altered aqueous synthesis conditions," *Colloids and Surfaces a-Physicochemical and Engineering Aspects*, vol. 254, pp. 147-157, 2005.

[107] Y. Nosaka, H. Shigeno, and T. Ikeuchi, "Formation of Polynuclear Cadmium-Thiolate Complexes and Cds Clusters in Aqueous-Solution Studied by Means of Stopped-Flow and Nmr Spectroscopies," *Journal of Physical Chemistry*, vol. 99, pp. 8317-8322, 1995.

[108] S. F. Wuister, F. van Driel, and A. Meijerink, "Luminescence and growth of CdTe quantum dots and clusters," *Physical Chemistry Chemical Physics*, vol. 5, pp. 1253-1258, 2003.

[109] H. Zhang, D. Y. Wang, and H. Mohwald, "Ligand-selective aqueous synthesis of one-dimensional CdTe nanostructures," *Angewandte Chemie-International Edition*, vol. 45, pp. 748-751, 2006.

[110] B. Fischer, B. Muller, K. G. Fischer, N. Baur, and W. Kreutz, "Acidic pH inhibits non-MHC-restricted killer cell functions," *Clinical Immunology*, vol. 96, pp. 252-263, 2000.

[111] Y. Yin and A. P. Alivisatos, "Colloidal nanocrystal synthesis and the organic-inorganic interface," *Nature*, vol. 437, pp. 664-670, 2005.

[112] R. Hardman, "A toxicologic review of quantum dots: Toxicity depends on physicochemical and environmental factors," *Environmental Health Perspectives*, vol. 114, pp. 165-172, 2006.

[113] A. M. Derfus, W. C. W. Chan, and S. N. Bhatia, "Probing the cytotoxicity of semiconductor quantum dots," *Nano Letters*, vol. 4, pp. 11-18, 2004.

[114] A. M. Smith, H. Duan, A. M. Mohs, and S. Nie, "Bioconjugated quantum dots for in vivo molecular and cellular imaging," *Advanced Drug Delivery Reviews*, vol. In Press, Corrected Proof.

[115] H. Li, W. Y. Shih, and W. H. Shih, "Non-heavy-metal ZnS quantum dots with bright blue photoluminescence by a one-step aqueous synthesis," *Nanotechnology*, vol. 18, pp. -, 2007.

[116] R. E. Bailey, A. M. Smith, and S. Nie, "Quantum dots in biology and medicine (review)," *Physica E*, vol. 25, pp. 1-12, 2004.

[117] A. Sukhanova, M. Devy, L. Venteo, H. Kaplan, M. Artemyev, V. Oleinikov, D. Klinov, M. Pluot, J. H. M. Cohen, and I. Nabiev, "Biocompatible fluorescent nanocrystals for immunolabeling of membrane proteins and cells," *Analytical Biochemistry*, vol. 324, pp. 60-67, 2004.

[118] L. Josephson, M. F. Kircher, U. Mahmood, Y. Tang, and R. Weissleder, "Near-infrared fluorescent nanoparticles as combined MR/optical imaging probes," *Bioconjugate Chemistry*, vol. 13, pp. 554-560, 2002.

[119] G. W. Poling, "Infrared reflection studies of the oxidation of copper and iron," *Journal of Electrochemical Society: Solid State Science*, vol. 116 pp. 958, 1969.

[120] J. T. Keiser, C. W. Brown, and R. H. Heidersbach, "The Electrochemical Reduction of Rust Films on Weathering Steel Surfaces," *Journal of the Electrochemical Society*, vol. 129, pp. 2686-2689, 1982.

[121] R. Mikami, M. Taguchi, K. Yamada, K. Suzuki, O. Sato, and Y. Einaga, "Reversible photo-switching of the magnetization of iron oxide nanoparticles at room temperature," *Angewandte Chemie-International Edition*, vol. 43, pp. 6135-6139, 2004.

[122] A. Bumb, M. W. Brechbiel, P. L. Choyke, L. Fugger, A. Eggeman, D. Prabhakaran, J. Hutchinson, and P. J. Dobson, "Synthesis and characterization of ultra-small superparamagnetic iron oxide nanoparticles thinly coated with silica," *Nanotechnology*, vol. 19, pp. -, 2008.

[123] F. Jimenez-Villacorta and C. Prieto, "Magnetic properties and interaction mechanisms of iron-based core-shell structures prepared by sputtering at low substrate temperatures," *Journal of Physics-Condensed Matter*, vol. 20, pp. -, 2008.

[124] T. Fujii, F. M. F. de Groot, G. A. Sawatzky, F. C. Voogt, T. Hibma, and K. Okada, "In situ XPS analysis of various iron oxide films grown by NO2-assisted molecular-beam epitaxy," *Physical Review B*, vol. 59, pp. 3195-3202, 1999.

[125] L. Wu, J. C. Yu, and X. Z. Fu, "Characterization and photocatalytic mechanism of nanosized CdS coupled TiO2 nanocrystals under visible light irradiation," *Journal of Molecular Catalysis a-Chemical*, vol. 244, pp. 25-32, 2006.

[126] M. Z. Rong, M. Q. Zhang, H. C. Liang, and H. M. Zeng, "Surface modification and particles size distribution control in nano-CdS/polystyrene composite film," *Chemical Physics*, vol. 286, pp. 267-276, 2003.

[127] A. L. Rogach, T. Franzl, T. A. Klar, J. Feldmann, N. Gaponik, V. Lesnyak, A. Shavel, A. Eychmuller, Y. P. Rakovich, and J. F. Donegan, "Aqueous synthesis of thiol-capped CdTe nanocrystals: State-of-the-art," *Journal of Physical Chemistry C*, vol. 111, pp. 14628-14637, 2007.

[128] J. F. Weng, X. T. Song, L. A. Li, H. F. Qian, K. Y. Chen, X. M. Xu, C. X. Cao, and J. C. Ren, "Highly luminescent CdTe quantum dots prepared in aqueous phase as an alternative fluorescent probe for cell imaging," *Talanta*, vol. 70, pp. 397-402, 2006.

[129] D. V. Talapin, A. L. Rogach, E. V. Shevchenko, A. Kornowski, M. Haase, and H. Weller, "Dynamic distribution of growth rates within the ensembles of colloidal II-

VI and III-V semiconductor nanocrystals as a factor governing their photoluminescence efficiency," *Journal of the American Chemical Society*, vol. 124, pp. 5782-5790, 2002.

[130] H. B. Bao, Y. J. Gong, Z. Li, and M. Y. Gao, "Enhancement effect of illumination on the photoluminescence of water-soluble CdTe nanocrystals: Toward highly fluorescent CdTe/CdS core-shell structure," *Chemistry of Materials*, vol. 16, pp. 3853-3859, 2004.

[131] C. Schulz-Drost, V. Sgobba, and D. M. Guldi, "Zero-versus one-dimensional water-soluble CdTe Nanocrystals - Synthesis and photophysical characterization," *Journal of Physical Chemistry C*, vol. 111, pp. 9694-9703, 2007.

[132] A. G. Joly, W. Chen, D. E. McCready, J. O. Malm, and J. O. Bovin, "Upconversion luminescence of CdTe nanoparticles," *Physical Review B*, vol. 71, pp. -, 2005.

[133] W. Klemm, H. Sodomann, and P. Langmesser, "Beitrage zur Kenntnis der Alkalimetallchalkogenide," *Z. Anorg. Allgem. Chemie* vol. 241, pp. 281 1939.

[134] M. Zelner, H. Minti, R. Reisfeld, H. Cohen, Y. Feldman, S. R. Cohen, and R. Tenne, "Preparation and characterization of CdTe nanoparticles in zirconia films prepared by the sol gel method," *Journal of Sol-Gel Science and Technology*, vol. 20, pp. 153-160, 2001.

[135] H. Peng, L. J. Zhang, C. Soeller, and J. Travas-Sejdic, "Preparation of water-soluble CdTe/CdS core/shell quantum dots with enhanced photostability," *Journal of Luminescence*, vol. 127, pp. 721-726, 2007.

[136] J. Lovric, S. J. Cho, F. M. Winnik, and D. Maysinger, "Unmodified cadmium telluride quantum dots induce reactive oxygen species formation leading to multiple organelle damage and cell death," *Chemistry & Biology*, vol. 12, pp. 1227-1234, 2005.

[137] X. G. Peng, J. Wickham, and A. P. Alivisatos, "Kinetics of II-VI and III-V colloidal semiconductor nanocrystal growth: "Focusing" of size distributions," *Journal of the American Chemical Society*, vol. 120, pp. 5343-5344, 1998.

[138] W. W. Yu, L. H. Qu, W. Z. Guo, and X. G. Peng, "Experimental determination of the extinction coefficient of CdTe, CdSe, and CdS nanocrystals," *Chemistry of Materials*, vol. 15, pp. 2854-2860, 2003.

[139] D. V. Talapin, A. L. Rogach, M. Haase, and H. Weller, "Evolution of an ensemble of nanoparticles in a colloidal solution: Theoretical study," *Journal of Physical Chemistry B*, vol. 105, pp. 12278-12285, 2001.

[140] M. Fischer and J. Georges, "Fluorescence quantum yield of rhodamine 6G in ethanol as a function of concentration using thermal lens spectrometry," *Chemical Physics Letters*, vol. 260, pp. 115-118, 1996.

[141] B. Schreder, T. Schmidt, V. Ptatschek, U. Winkler, A. Materny, E. Umbach, M. Lerch, G. Muller, W. Kiefer, and L. Spanhel, "CdTe/CdS clusters with "core-shell" structure in colloids and films: The path of formation and thermal breakup," *Journal of Physical Chemistry B*, vol. 104, pp. 1677-1685, 2000.

[142] P. T. K. Chin, J. W. Stouwdam, S. S. van Bavel, and R. A. J. Janssen, "Cluster synthesis of branched CdTe nanocrystals for use in light-emitting diodes," *Nanotechnology*, vol. 19, pp. -, 2008.

[143] L. Li, H. F. Qian, N. H. Fang, and H. C. Ren, "Significant enhancement of the quantum yield of CdTe nanocrystals synthesized in aqueous phase by controlling the pH and concentrations of precursor solutions," *Journal of Luminescence*, vol. 116, pp. 59-66, 2006.

[144] S. Celebi, "Design and Synthesis of CdS Quantum Dots and CdS-Fe3O4 Hybrid Nanoparticles in Aqueous Solution," *Thesis submission*, vol. Graduate School of Sciences and Engineering, Koc University, 2007.

VITA

Süleyman Sinan Öztürk was born in Bursa, Turkey in 1983. He completed his high school in Bursa Şükrü Şankaya Anatolian High School in 2001. He received his B.S. degree from the Department of Chemistry at Koç University, Istanbul, in 2006. The same year, he started his study M.S. degree in the Department of Materials Science and Engineering at Koç University. His research interests are colloidal fluorescent and magnetic nanoparticles and their magnetic, optical and electronic applications.